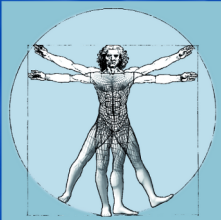


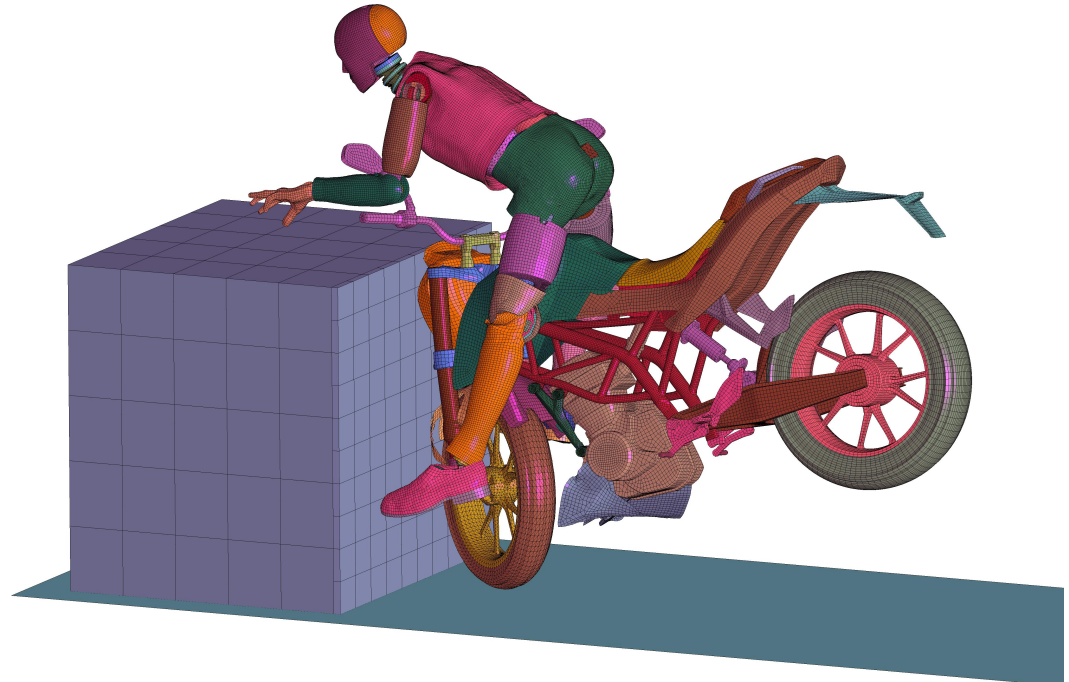
University of Stuttgart
Germany

Institute of Applied Mechanics
Chair of Continuum Mechanics
Prof.Dr.-Ing.W.Ehlers, Prof.O.Röhrle



Positioning and Validation of a Hybrid III FE Dummy for Motorcycle Crash Analysis

Julia Schaal (B.Sc.)



BOSCH

Robert Bosch GmbH - Campus Renningen
Corporate Research - Vehicle Safety and Automated Driving
Active/Passive Safety and Accident Research

Positioning and Validation of a Hybrid III FE Dummy for Motorcycle Crash Analysis

by Julia Schaal, B.Sc.

Supervised by

Prof. Oliver Röhrle, PhD (University of Stuttgart)
Florian Mayer, M.Sc. (Robert Bosch GmbH)
Harnoor Saini, M.Sc. (University of Stuttgart)

Master Thesis
for obtaining the academic degree
Master of Science (M.Sc.)

Robert Bosch GmbH
Campus Renningen



BOSCH

University of Stuttgart
Campus Vaihingen



University of Stuttgart
Germany

**Corporate Research - Vehicle
Safety and Automated Driving**
**Active/Passive Safety Systems and
Accident Research - Motorcycle Safety**

**The Institute of Applied Mechanics
- Chair of Continuum Mechanics**
**Continuum Biomechanics and
Mechanobiology Research Group**

Germany, April 2018

Report No.: CBM-2018-1
Institute of Applied Mechanics - Chair of Continuum Mechanics
Continuum Biomechanics and Mechanobiology Research Group
University of Stuttgart, Germany, 2018

Editor:
Prof. O. Röhrle, PhD

© Julia Schaal

Corporate Research - Vehicle Safety and Automated Driving
Active/Passive Safety Systems and Accident Research - Motorcycle Safety
Robert Bosch GmbH
Robert-Bosch-Campus 1
71272 Renningen, Germany

Institute of Applied Mechanics - Chair of Continuum Mechanics
Continuum Biomechanics and Machanobiology Research Group
University of Stuttgart
Pfaffenwaldring 5a
70569 Stuttgart, Germany

All rights reserved. No part of this publication may be reproduced, stored in a retrieval system, or transmitted, in any form or by any means, electronic, mechanical, photocopying, recording, scanning or otherwise, without the permission in writing of the author.

Confidentiality Clause

This master thesis is based on internal, confidential data and information of Robert Bosch GmbH.

This work may only be made available of the first, second and third reviewers and authorized members of the board of examiners. Any publication and duplication of this master thesis - even in part - is prohibited.

An inspection of this work by third parties requires the expressed permission of the author and the company.

Declaration of originality

I hereby declare that this thesis and the work reported herein was composed by and originated entirely from me. Information derived from the published and unpublished work of others has been acknowledged in the text and references are given in the list of sources.

Stuttgart, April 2018

Julia Schaal

Acknowledgements

At this point I would like to take the opportunity to thank everyone who supported me during my thesis work.

It is a pleasure to thank Florian Mayer for the opportunity to write this thesis for Corporate Research (CR) at Robert Bosch GmbH in Renningen. Additionally I would like to thank Prof. Oliver Röhrle for his support and for being the inspector of my thesis at the University of Stuttgart.

Beyond that I am heartily thankful to both of my supervisors, Florian Mayer and Harnoor Saini, whose encouragement, guidance and support from the initial to the final level enabled me to develop an understanding of the subject.

Lastly, I offer my regards and blessings to all of those who supported me in any respect during the completion of this project.

Abstract

The aim of this thesis was to rebuild real crash tests in FE simulations. Therefore, a dummy model was positioned and validated for motorcycle crash analysis in LS-DYNA. The Hybrid III FE dummy model and the KTM 125 Duke motorcycle model were used.

The two FE models were combined into one model, by adjusting the dummy position to sit on the motorcycle. Also the contact definitions between the models were included, more specifically the contact between the dummy hand and the handlebar was investigated. Afterwards, gravity simulations were run with the defined postures. The resulting positions and displacements were saved and used as the initial state for the crash simulations. Besides the new angles of the dummy posture and the displacement of the fork spring in the motorcycle was adapted for the new position. As a next step, three crash simulations with different velocities were performed. In those simulations, the pre-positioned models were driven forward against a wall. In the last step, the dummy position, kinematics and load were validated. The real crash tests served as the reference model. For the validation of the position, the reference specifications and pictures before the crash test were compared. The kinematics were analysed with the animation and video recordings in selected time steps, wherein only small differences could be seen. Furthermore, the load on the dummy in the simulation was validated with the sensor signals of the experimental crash tests. Additionally, head and neck injury criteria were considered and compared. The simulation results were comparable with the experimental signals.

The FE simulations of the motorcycle crash scenarios with the included dummy model, predicted the real crash tests well. However, the simulations showed some oscillations and deviations to the real crash data. Therefore, further investigations are necessary to use the FE model for research.

Contents

List of Figures	iii
List of Tables	v
List of abbreviations and terms	vi
1 Introduction	1
1.1 Finite-Element-Method	3
1.2 Motivation and Aim of the Thesis	3
2 Background and State of the Art	5
2.1 Biomechanics and Anatomy	5
2.1.1 Anatomical Basics	5
2.1.2 Head	5
2.1.3 Neck	7
2.2 Crash Tests	10
2.2.1 Vehicle Safety Tests	11
2.2.2 Motorcycle Industry	12
2.2.3 Performed Crash Tests at DEKRA	13
2.3 Crash Test Dummies	14
2.3.1 Definition and Composition	14
2.3.2 Dummy types	15
2.3.3 FE model of Hybrid III Dummy	16
2.3.4 Dummy Positioning	16
2.4 Validation	17
2.5 LS-DYNA	18
2.5.1 LS-DYNA input file	19
3 Model Setup	20
3.1 Model Description	20
3.1.1 Dummy Model	20
3.1.2 Motorcycle Model	21
3.2 Model Combination	23
3.3 Dummy Positioning	23
3.3.1 Geometrical Position	25
3.3.2 Dummy Positioning in LS-PrePost	25
3.3.3 Seating Position	27
3.4 Contact Implementation	29
3.4.1 Contact Definition	30
3.4.2 Tiebreak Contact	31
3.4.3 Friction	33

4 Simulation Setup	34
4.1 Simulation Environment	34
4.2 Gravity Simulation	35
4.2.1 Joint Stiffness	36
4.2.2 Model Position	36
4.3 Crash Simulation	37
4.3.1 Contact Settings	37
5 Results and Validation	39
5.1 Numerical Accuracy	39
5.2 Dummy Position	40
5.2.1 Validation with Reference Information	40
5.2.2 Validation with Reference Pictures	40
5.3 Dummy Kinematics	43
5.3.1 Gravity Kinematics	43
5.3.2 Crash Kinematics	43
5.4 Dummy Load	47
5.4.1 Data Post-Processing	47
5.4.2 Data Comparison	48
6 Discussion	69
6.1 Model	69
6.1.1 Dummy Model	69
6.1.2 Motorcycle Model	69
6.1.3 Contact Specifications	70
6.2 Validation Aspects	71
6.2.1 Position	71
6.2.2 Kinematics and Load	71
7 Conclusion and Outlook	72
A Appendix I: Extended Validation	74
Bibliography	76

List of Figures

1.1	Index of road fatalities by mode of transport	1
1.2	FEM Process	3
1.3	Procedure of Motorcycle Crash Test Simulation	4
2.1	Anatomical Planes and Directions	6
2.2	Anatomical head layers	6
2.3	Wayne State Tolerance Curve (WSTC)	7
2.4	Cervical Vertebra	8
2.5	Moving directions of the neck	8
2.6	Neck Shear Criterion	9
2.7	Neck Tension Criterion	10
2.8	Crash Simulation	10
2.9	Total HUman Model for Safety (THUMS)	12
2.10	Motorcycle Crash with Airbag from Namiki et al.	13
2.11	Crash Test Setup at DEKRA Crash Test Centre	13
2.12	Sensors on the Dummy wrist at Crash Test	14
2.13	Sitting and Standing Hybrid III Dummy	15
2.14	FE Hybrid III 50 th and 5 th percentile Dummy	17
3.1	LSTC Hybrid III Dummies	21
3.2	Motorcycle FE Model of the KTM 125 Duke	23
3.3	Calculation of the hip angle	25
3.4	Dummy position angles defined in the documentation picture	26
3.5	LS-PrePost Positioning Tool	28
3.6	The dummy hand grip and the handlebar	28
3.7	The positioned dummy on the motorcycle	29
3.8	Contact definition in LS-DYNA	30
3.9	Tiebreak contact between the hand and the handlebar	32
3.10	Schematic of the definition of friction	33
4.3	Crash Simulation Setup	37
4.1	Motorcycle and Dummy models before the gravity simulation	38
4.2	Motorcycle and Dummy models after the gravity simulation	38
5.1	Reference position of the dummy with lines, left side	41
5.2	Motorcycle and Dummy models before the gravity simulation with reference lines, left side	41
5.3	Motorcycle and Dummy models after the gravity simulation with reference lines, left side	41
5.4	Reference position of the dummy with lines, front view	42
5.5	Motorcycle and Dummy models before the gravity simulation with reference lines, front view	42
5.6	Motorcycle and Dummy models after the gravity simulation with reference lines, front view	42

5.7 Crash Test 9.5 $\frac{km}{h}$	44
5.8 Crash Simulation 9.5 $\frac{km}{h}$	44
5.9 Crash Test 12.8 $\frac{km}{h}$	45
5.10 Crash Simulation 12.8 $\frac{km}{h}$	45
5.11 Crash Test 47.8 $\frac{km}{h}$	46
5.12 Crash Simulation 47.8 $\frac{km}{h}$	46
5.13 Integrated Acceleration Signal as Quality Check	48
5.14 The calculation of the HIC in LS-PrePost	49
5.15 Head Acceleration at 9.5 $\frac{km}{h}$	50
5.16 Head Injury Criteria (HIC) at 9.5 $\frac{km}{h}$	51
5.17 Neck Force at 9.5 $\frac{km}{h}$	52
5.18 Neck Shear Force F_x at 9.5 $\frac{km}{h}$ with Threshold	53
5.19 Neck Tensile Force F_z at 9.5 $\frac{km}{h}$ with Threshold	53
5.20 Neck Moment at 9.5 $\frac{km}{h}$	54
5.21 Head Acceleration at 12.8 $\frac{km}{h}$	56
5.22 Head Injury Criteria (HIC) at 12.8 $\frac{km}{h}$	57
5.23 Neck Force at 12.8 $\frac{km}{h}$	58
5.24 Neck Shear Force F_x at 12.8 $\frac{km}{h}$ with Threshold	59
5.25 Neck Tensile Force F_z at 12.8 $\frac{km}{h}$ with Threshold	59
5.26 Neck Moment at 12.8 $\frac{km}{h}$	60
5.27 Head Acceleration at 47.8 $\frac{km}{h}$	62
5.28 Head Injury Criteria (HIC) at 47.8 $\frac{km}{h}$	63
5.29 Neck Force at 47.8 $\frac{km}{h}$	64
5.30 Neck Shear Force F_x at 47.8 $\frac{km}{h}$ with Threshold	65
5.31 Neck Tensile Force F_z at 47.8 $\frac{km}{h}$ with Threshold	65
5.32 Neck Moment at 47.8 $\frac{km}{h}$	66
5.33 Neck Movement at Crash with 47.8 $\frac{km}{h}$ in a frontal view	67
5.34 Experiment and Simulation Neck Moment at 47.8 $\frac{km}{h}$	67
A.1 Reference position of the dummy with lines, right side.	75
A.2 Motorcycle and Dummy models before the gravity simulation (0 ms) with reference lines, right side.	75
A.3 Motorcycle and Dummy models after the gravity simulation (725 ms) with reference lines, right side.	75

List of Tables

1.1	Severity Classification of the Abbreviated Injury Scale (AIS)	2
2.1	Reference values for the calculation of N_{ij}	9
2.2	Biomechanical load parameters on the dummy	18
3.1	50 th percentile male dummy and human in comparison	22
3.2	Information about the models according to ISO 13232	24
3.3	Dummy position of the 19 joints	27
4.1	Dummy position before and after the gravity simulation	36
5.1	Corridor Rate of the 9.5 $\frac{km}{h}$ Crash	53
5.2	NIC values of the 9.5 $\frac{km}{h}$ Crash	55
5.3	N_{ij} values of the 9.5 $\frac{km}{h}$ Crash	55
5.4	Corridor Rate of the 12.8 $\frac{km}{h}$ Crash	57
5.5	NIC values of the 12.8 $\frac{km}{h}$ Crash	59
5.6	N_{ij} values of the 12.8 $\frac{km}{h}$ Crash	61
5.7	Corridor Rate of the 47.8 $\frac{km}{h}$ Crash	63
5.8	NIC values of the 47.8 $\frac{km}{h}$ Crash	65
5.9	N_{ij} values of the 47.8 $\frac{km}{h}$ Crash	67

List of abbreviations and terms

Abbreviations

ABS	Antilock Braking System
AEB	Autonomous Braking System
AIS	Abbreviated Injury Scale
ATD	anthropometric test devices
BHCS	Bosch Healthcare Solutions
CAE	Computer-aided engineering
CFC	Channel Filter Class
CNS	central nervous system
ESP	Electronic Stability Program
FEM	finite element method
FEA	finite element analysis
FMVSS	Federal Motor Vehicle Safety Standard
GM	General Motors
HBM	Human Body Models
HIC	Head Injury Criterion
HPC	Head Protection Criterion
HUMOS	Human Model of Safety
LSTC	Livermore Software Technology Corporation
NIC	neck injury criterion
MATD	Motorcycle Anthropometric Test Device
MBS	multibody system
NHTSA	National Highway Traffic Safety Administration
pdb	Partnership for Dummy Technology and Biomechanics
PMHS	Post Mortem Human Subjects
SAE	Society of Automotive Engineers

THOR	Test device for Human Occupant Restraint
THUMS	Total Human Model for Safety
WSTC	Wayne State Tolerance Curve

Terms

LS-Dyna	program of simulation which works with Finite Element Method
LS-PrePost	an advanced pre and post-processor for LS-DYNA
Dummy	anthropometric doll for measurements
human body model	detailed model of a human (like THUMS)

1 Introduction

Safety is a state, when the risk is smaller than the greatest tolerable risk of a technical process or condition. Thereby a difference between active and passive safety is made. Active safety deals with the avoidance of accidents and with the decreasing of the number of collisions. Additionally road constructions or flow regulation are considered as well as the vehicle design with systems like ABS and ESP. Passive safety deals with accident-reducing provisions to limit the consequences of accidents. Besides the vehicle design, aspects like safety establishments and emergency services are in focus [45]. To reach the aim of passive safety it is necessary to gain a better understanding of the collision mechanism [62]. Different spheres of action are considered for passive safety: accidental research (accident statistics, accidental reconstruction, accidental analysis), safety provisions, experimental simulations, safety evaluation, computational simulations and biomechanics.

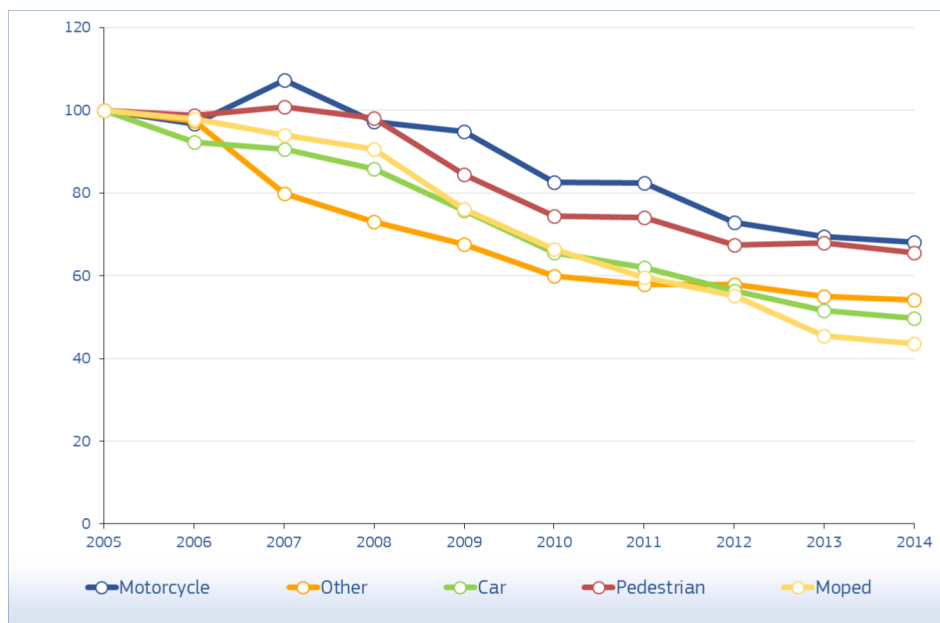


Figure 1.1: Index of road fatalities by mode of transport (2005 = 100 %), EU, 2005-2014 [64].

In 2016, over 26.000 EU citizens were killed in road accidents. About 17 % of these traffic fatalities were of motorcyclists and moped riders [64]. Studies from 2014 showed, that it is 27 times as likely for a motorcyclist to die in a vehicle accident, than for a car passenger, and injuries are six times as likely [61]. In the last few years the motorcycle fatalities were decreased by around 32 %. One of the reasons might be, that researchers advanced the driving conditions [64]. Wearing helmets while driving a motorcycle is essential, because in motorcycle accidents head or neck injuries often lead to disabilities or even to death. The efficiency of helmets is about 37 % in preventing motorcycle deaths, and about 67 % to protect the motorcyclists of brain injuries [34]. But still, the number of motorcycle fatalities decreased less compared to other modes of transport (see figure 1.1). Therefore it is still necessary to invest in safety research and in safety improvements.

To evaluate situations and its consequences, the knowledge of the reaction of different body parts in extreme loads is necessary. In 1947, Colonel John P. Stapp tested the limit of the human body by increasing the speed of a sled, thereby he survived a load of 35 G. Through these tests helmets, seats, positioning techniques and some other systems could be improved [24]. Another pioneer in impact biomechanics research was Lawrence M. Patrick. His approach was to improve automotive safety systems [78].

Nowadays there is still one of the most famous conferences for impact biomechanics named after Stapp, the Stapp Car Crash Conference. Other important international conferences on biomechanics and investigations in safety improvements are the *IRCOBI* and *carhs* [8, 35, 76]. To licence a vehicle, several regulations are necessary. The first regulations on vehicle safety were defined by the National Highway Traffic Safety Administration (NHTSA), but the standards in Europe are almost the same. For motorcycle test and analysis the norm ISO 13232 is regulating the research evaluation of rider crash protective devices [36, 61].

To allow a comparison between the consequences on occupants in different accident situations, the categories to evaluate the technical accident severity were insufficient. Thus, the Abbreviated Injury Scale (AIS) was developed over 50 years ago to describe the injury severity in accidents objectively. Every relevant considered injury is categorized by its lethality and thereby rated. The classification specifies the probability of survival and only describes the injury, not its type of treatment. The severity is scaled from minor to maximum, see table 1.1 [29].

Table 1.1: Severity Classification of the Abbreviated Injury Scale (AIS) [29]

AIS-Code	AIS injury severity	evaluation of the injury
1	minor	
2	moderate	
3	serious	
4	severe	probably survive
5	critical	survive insecure
6	maximum	not survivable according to the current state of medical art
9	NFS ("not further specified")	injury and severity unknown

For safety research, especially crash tests are used to analyse the loads and risks of the situations. There are five different types of test models, that are used for crash test analyses. First of all there are tests with human volunteers. These tests are highly realistic, but of course they are limited in loads and in voluntary people. As a second model human cadavers are used, but their availability is also limited. The advantage of the Post Mortem Human Subjects (PMHS) are the almost alike behaviour to humans, except for the muscle action, the blood pressure and some biochemical reactions. With the PMHS more load can be tested, but there is always a limit because of ethical aspects. Another way of crash test modelling is the usage of animal cadavers to test the loads with defined boundary conditions. As a forth type anthropometric test devices (ATD) or also called dummies are available for crash test analyses. The dummies are unlimited in availability and almost without limit in test usage. The fifth version of test models are Human Body Models (HBM). These are the most recent used models with improved biofidelity (human-likeness) [26, 77].

Besides the accident investigations and the crash test transactions with test models like

dummies, simulations of the crash tests are a good way to analyse and thereby enhance crash situations. By using computational simulations there will be neither ethical concerns nor broken motorcycles.

1.1 Finite-Element-Method

For this work the computational simulations to position the dummy on a motorcycle and the crash simulations with this model, are based on the finite element method (FEM). The FEM is a numerical method to approximate to initial value problems. It is typically used to analyse a complex technical or physical problem in various fields. The procedure of a finite element analysis (FEA) is categorized in three parts: Pre-Processing, Solver and Post-Processing (as shown in figure 1.2).

The first step, *Pre-Processing*, is to build a model according to the mechanical behaviour. The analysis depends on the quality of this model. Afterwards the geometry gets meshed into finite elements, which is mostly done by a Pre-Processor. For these elements an approximation function can be defined. If the approximation function is of higher order, the solution will be more precise. Also, if the mesh is finer, the analysis will be more precise, but also more CPU-intensive. As a last step of the Pre-Processing the boundary conditions and forces have to be defined. Thereby the joints and the moving directions of the displacements are determined. The next part is the *solver*. The linear algebraic system of equations for the displacements has to be solved. There are many different FEM universal programs which automatically compute the numerical solution. *Post-Processing* is the third part of FEA. After the calculation the solution is outputted and can be represented graphically in a Post-Processor. Additionally the FE program computes the distortion and strain [44, 68].

In this thesis the program LS-DYNA is used as FE solver and LS-PrePost as Pre- and Post-Processor, the program is described in chapter 2.5.



Figure 1.2: A schematic graphic of the FEM Process.

Compared with multibody systems (MBS) the FEM might have a higher computational cost and modelling is more complicated. But with FEM the simulation is more detailed and flexible. Furthermore it is possible to consider the material behaviour [63].

1.2 Motivation and Aim of the Thesis

The aim of this work is to position the Hybrid-III FE 50th percentile Dummy on a motorcycle model in LS-DYNA and to validate the dummy position and load with real crash test data (see the frame of figure 1.3). The positioning of the dummy and the implementation of the holding of the dummy was the main investigation to simulate collisions. With the simulations of the crash tests, the signals of acceleration, moments and loads of the head and neck of the dummy will be compared to the physical crash tests in the DEKRA Test Centre in Neumünster, Germany. Thereby a validation of the dummy in the crash simulation can be done. Validated models can be used for further investigations and research on motorcycle safety.

With the FE simulations, the load on every part of the model can be calculated. Thereby the passive safety can be improved, for example by testing airbag constructions and safety belts.

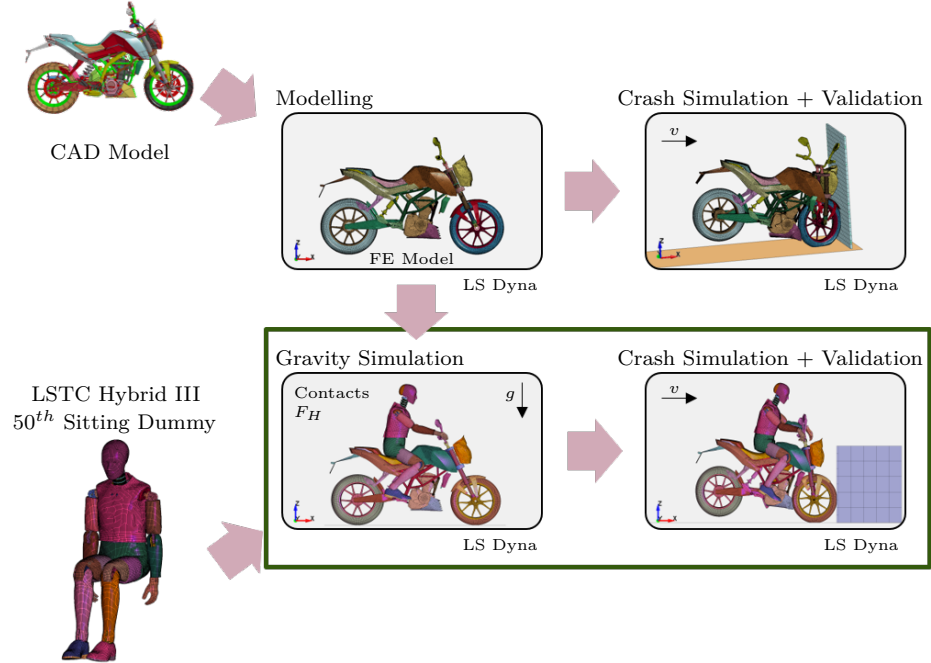


Figure 1.3: Procedure of Motorcycle Crash Test Simulation in LS-DYNA (the frame shows the implementation in this work).

In this thesis some basic knowledge and information on biomechanics and crash tests will be presented. Afterwards there will be a part about the model and the simulation setup. Herein the positioning process of the dummy, the contact implementation and the simulations will be described. Afterwards there will be a chapter on the test results and the validation of the simulations. The thesis will end with a discussion of the work and with a brief summary and outlook.

2 Background and State of the Art

For a better understanding of this thesis, some basic information is necessary. First of all there will be a definition of biomechanics and the basic anatomy which is needed for this thesis. Furthermore an overview on crash simulations in general and on the used crash test data from DEKRA will be given. Additionally different crash test dummies are introduced and the validation methods are described briefly. The program LS-DYNA is playing a main role in this work, thus there will be a brief overview on it.

2.1 Biomechanics and Anatomy

Biomechanics is a multidisciplinary subject with many characteristics and specializations. A general definition of biomechanics by Richard and Kullmer [68] is:

"Biomechanics is the adaptation of mechanical principles on biological systems, biological tissue and medical problems."

In active safety for vehicles, biomechanics considers ergometrical (executable work) and dynamometrical (raised forces) aspects. For passive safety the focus of biomechanics lays on the mechanical load capacity of the living body or parts of the body. By this, injury mechanics in accidents are analysed and objective criteria for reversible and irreversible injuries are determined. Therefore biomechanics is also defined as the occupation on mechanical behaviour and reaction of the human body on mechanical loads [45, 46].

2.1.1 Anatomical Basics

The anatomical description of axes and planes is independent from the Cartesian coordinate system (x,y,z). This enables a precise denotation which is shown in figure 2.1. The coronal plane, divides the human body into a front and a back part. The direction to the front (stomach) is called ventral or anterior and the contrary direction is described as dorsal or posterior. The sagittal plane passes vertical to the body surface, it separates the left and the right side. Directions to the middle (medial) and outwards to a side (lateral) are differenced. The transversal plane is parallel to the standing plane, thus it divides the body into upper and lower segments. Parts that are in higher direction are superior and the ones lower than the transversal plane are inferior. There is also a differentiation between the parts near the trunk (proximal) and the parts that are more distant to the trunk (distal) [42].

2.1.2 Head

The anatomical structure of the human head is subdivided into several layers (figure 2.2): the scalp, the skull or cranium, the meninges and the brain. The scalp itself has a multilayered skin, existing of hypodermic tissue and muscles with a thickness of about 5 mm to 7 mm. Underneath a loose connective tissue (the periost or bone skin) is the skull, which consists of connected bones. The skull is divided into facial bones with eyeholes, the nasal cavity and the oral cavity with teeth, a skullcap and the base of the skull. To protect the brain, there are three meninges that isolate the brain and spinal cord from the bones (dura mater,

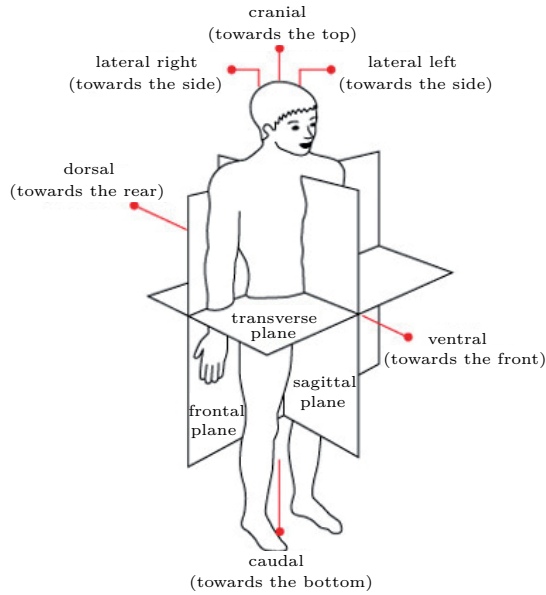


Figure 2.1: Anatomical Planes and Directions [73].

arachnoidea and pia mater). In between there are ventricles and a transparent liquid called liquor, that supplies the brain with nutritions and damps concussion. The brain is located inside the cranium and meninges. Together with the spinal cord it forms the central nervous system (CNS). Structurally and functional there are five different areas in the brain [42, 45, 71].

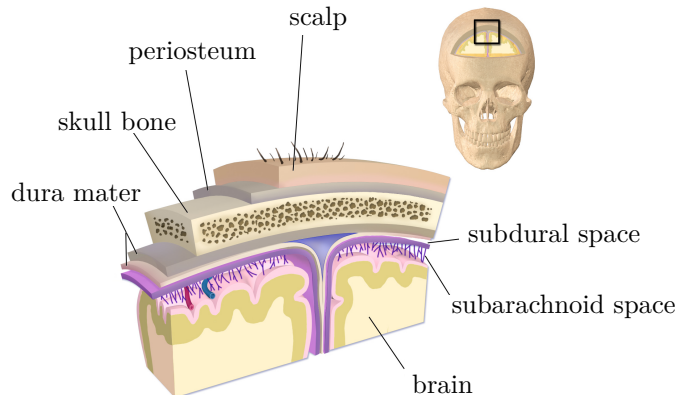


Figure 2.2: Anatomical head layers [6].

Head Injuries

Head injuries in accidents often cause permanent bodily damages or even lead to death. Although research and provisions reduced the amount and severity of injuries, the head is still the most endangered part of the body. Analysing head injuries is quite difficult, because only the types of injuries are well known, but mainly not their appearance and mechanical loads. Craniocerebral injuries are either with hurt meninges ("open") or without ("closed") and grouped into:

- bruises, contusions and lacerations,
- fractures of the facial bones and skull fractures and

- brain injuries, mainly affected by mechanical load.

Lesions of the soft tissue of the skull or face are very common, they are classified as light injuries AIS1 or AIS2. Skull fractures are divided into fractures of the skullcap or of the base of the skull. If there wasn't a clash with the head on hard structure, skull fractures can be excluded. Injuries of the brain are clinically categorized into diffuse and focal injuries. Diffuse brain injuries are about 75 % of the head injuries in accidents and include turgors and mild contrusions to the point of injuries of the white brain substance. The most common type is the concussion with short reduced consciousness. The focal injuries are traumatically caused hemorrhages, big effusions in the brain through skull fractures and contrusions. Contrusions are observed on the side of the impact (coup contrusion) and on the opposite side (contre-coup contrusion). The main injuries are hemorrhages in between the meninges and diffuse injuries [42, 45, 71].

The most commonly used criteria for head injuries is the Head Injury Criterion (HIC) or the European counterpart Head Protection Criterion (HPC). They are based on the Wayne State Tolerance Curve (WSTC) as well as the 3 ms criteria a_{3ms} . The WSTC is a head acceleration curve based on detailed tests with cadavers (figure 2.3).

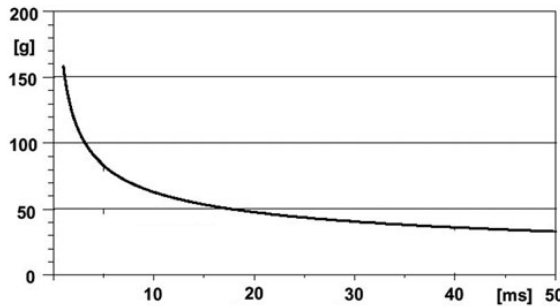


Figure 2.3: The Wayne State Tolerance Curve (WSTC) (acceleration vs. duration of the acceleration impulse) [71].

These criteria consider the head acceleration and define acceptable threshold values, but they are not useful to rate the risk of fractures. The instruction of the HIC is determined by the US NHTSA. It is calculated in a maximum time interval ($t_2 - t_1$) of 36 ms:

$$HIC = \max \left[\frac{1}{t_2 - t_1} \int_{t_1}^{t_2} a(t) dt \right]^{2.5} \cdot (t_2 - t_1), \quad (2.1)$$

while the acceleration $a(t)$ is measured in g and the time in seconds. Its threshold for the commonly used HIC_{15} in frontal and side collisions is 700. The a_{3ms} criterion is defined as a 3 ms acceleration on the head, which should not exceed 80 g. There are also European and international rules like ECE R94 and R95 and the FMVSS 208 that need to be observed and which contain for example the HIC and the a_{3ms} criteria. Other criteria consider the kinetic energy in the head through collision to analyse the shear strain of the brain. These criteria need extended modelling and calculations after a crash test, which is quite sophisticated [71]. In this work the results will be compared to the HIC and the a_{3ms} to analyse the injury risk, according to the measured sensor signals in the related crash test documentation.

2.1.3 Neck

Often loads on the head include loads on the neck, because the head and the neck form a functional unit. Heavy injuries of the cervical spine in the road traffic are common for

motorcycle accidents. The three main parts of the spine are the cervical spine, the thoracic spine and the lumbar column. The spine is dominantly affected by accidents in the region of the cervical spine, which reaches from the base of the skull to the first rib. Therefore the focus here is laid on this part of the spine, the cervical vertebra. The cervical vertebra is numbered from C1 as atlas, C2 as axis unto C7 as vertebrae prominens (figure 2.4). This part functions as support of the head and enables its movement. It also connects the head and face with the chest and pelvis and contains supply organs. Additionally it includes muscles, the oesophagus, the trachea and the thyroid gland as well as the bloodvessels [42, 45, 71].

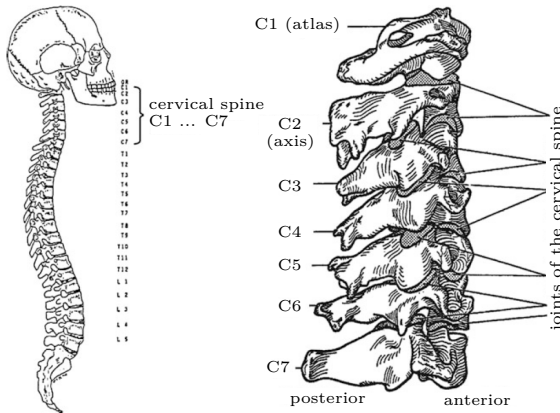


Figure 2.4: The spine and the cervical vertebra [45].

The moving directions of the neck are differed into four basic movements: the inclination to the front (flexion), the inclination to the back (extension), the bending to one side (lateral bend) and the axial rotation (see figure 2.5) [45, 71].

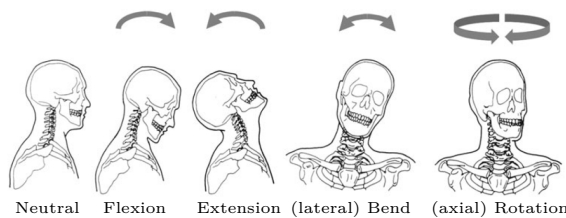


Figure 2.5: The four basic moving directions of the head and neck [71].

Neck Injuries

Injuries of the cervical vertebra are counted more serious and life-threatening than the ones further down the spine. The classification of neck injuries are distinguished from the possible moving directions and the mechanical loads. Dislocations of the atlas joint is the consequence of shear stress to the ventral or dorsal direction and axial torsion. High compressions can lead to a broken atlas (C1) and with an extension of the cervical vertebra to a fracture of C2. The main loads which can affect the neck are from a collision of the head or from a bend with axial or shear forces. It is assumed that an acceleration of the head with only tensile load can cause injuries of the upper cervical vertebra [71]. With a collision of the head, which is observed often, the main loads on the neck are compression-flexion, compression-extension, tensile-flexion, tensile-extension and side bends. The injury of the soft parts of the cervical vertebra, unspecified called whiplash, are the most frequent form of spine injuries of the road traffic. These injuries are the consequences of soft rear collisions or frontal/angular-frontal

collisions. Whiplash is categorized as light injury (AIS1) and the persons concerned are typically complaining about neck and head pain, vertigo and more.

To categorize the neck injuries, there are rules with allowable forces and more complex criteria for analysing especially the whiplash. The neck injury criterion (NIC) was developed to estimate the injury category by considering the change of the pressure. Another criterion N_{ij} considers the risk of getting a heavy cervical vertebra injury. Prasad and Daniel developed this criterion by describing a combination of the axial force F_z and the sagittal bend moment M_y , which are normalized with reference values [67]. The N_{ij} is also recorded in the Federal Motor Vehicle Safety Standard (FMVSS) 208 [21]. Calculating this probability was realized by the equation

$$N_{ij} = \frac{F_z}{F_{ref}} + \frac{M_y}{M_{ref}}, \quad (2.2)$$

wherein the critical reference values are scaled factors, which were determined for a three year old child. By considering all four load cases, the threshold for injury in each case is 1.0. Thus, there are four values, N_{te} for tension and extension, N_{tf} for tension and flexion and the analogue values for compression N_{ce} and N_{cf} . The reference values are shown in table 2.1

Table 2.1: Reference values for the calculation of N_{ij} [71]

reference values	load case	Hybrid III 50 th percentile	unit
M_y	Flexion	310	Nm
M_y	Extension	135	Nm
F_z	Compression	6,160	N
F_z	Tension	6,806	N

Furthermore, the regulations of the maximal loads in a frontal collision are specified by ECE R94 and FMVSS 208 [18, 21]. For the axial tensile neck force the total maximum value has to be under 3.3 kN, for a duration of 35 ms the value has to be under 2.9 kN and for a load with 60 ms or more it shouldn't exceed 1.1 kN. The neck shear criterion allows a maximum force of 3.1 kN, 1.5 kN for a load duration between 25 to 35 ms and 1.1 kN for a load with a duration of 45 ms or more (compared to the figures 2.6 and 2.7). While the extension of the neck, the bending moment shouldn't be above 57 Nm [18].

The N_{ij} criteria and the ECE R94 regulations with the tension and shear criteria will be considered for the *neck injury criteria* in this thesis.

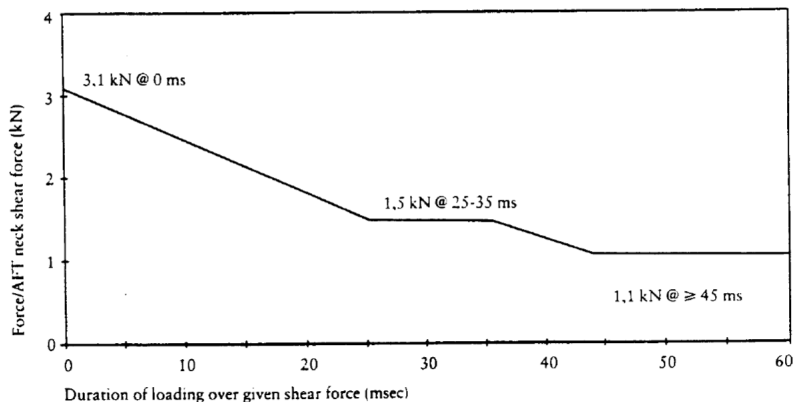


Figure 2.6: Neck Shear Criterion [18].

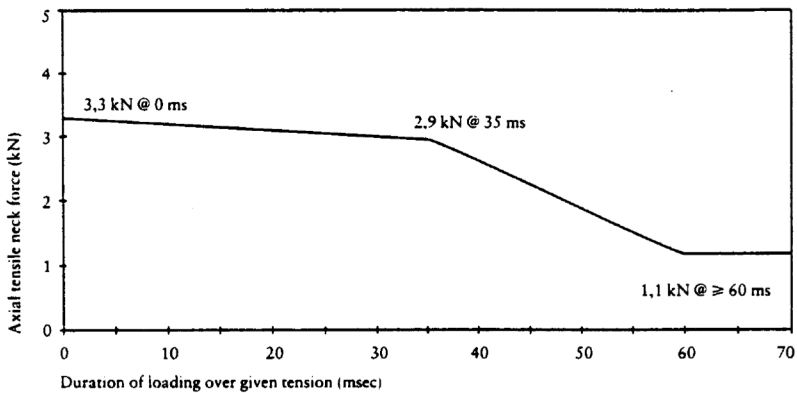


Figure 2.7: Neck Tension Criterion [18].

2.2 Crash Tests

Considering the passive safety of a vehicle, crash simulations are used to rebuild safety arrangements in the most realistic way possible. Furthermore the behaviour of the system can be analysed and information about the deformation of the vehicle, the damage of the occupant safety structure and the forces and accelerations on the dummy can be inspected. Since it is impossible to reconstruct every kind of accident, there are international agreements to categorize the accidents in groups like frontal crashes, side impacts, tail collisions and roll-over scenarios. As mentioned in the chart in figure 2.8 there are crash constructions to rebuild the crash situation. The results of a test are measurement data and video records, to analyse the structure and deformation behaviour and the load on the dummy [45].

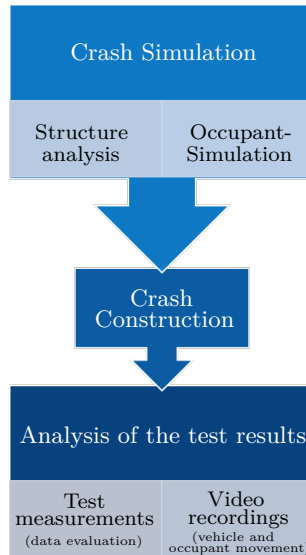


Figure 2.8: Crash Simulation and its aim (chart according to [45]).

In the experimental tests, test objects of the systems are needed as model. This contains immense costs and an enormous amount of preparation and execution time which collide with the short development times available. Computational simulations on the contrary offer a quicker developing method. The results are reliable and exact from the conceptual phase to the series production. Dependent on the focus of the investigation either finite element

method (FEM) or multibody system (MBS) programs are used. The most common MBS program for crash simulations is MADYMO, which is first published in 1978 by Bacchetti and Maltha [1]. Since 1980 the state of the art of commercial FEM programs for crash analysis are three programs based on the DYNA program [45].

2.2.1 Vehicle Safety Tests

The investigation in vehicle safety started after the first car accident in 1869. In 1934 General Motors (GM) started the first car safety tests [10]. In the US the NHTSA began in 1978 to test and rate vehicles using crash test dummy data [61]. It is internationally mandatory and statutory to perform vehicle tests before a car gets a licence for road traffic. Therefore there are many providers with test equipment, mainly the automotive producers. But also some university institutes and the survey institutions like ADAC, DEKRA or TÜV provide the state of the art of safety test centres [45].

There are different crash types which are based on frequent car crashes.

First there are tests with the whole vehicle, called **full tests**. These tests are with frontal or side collisions and rear impact. With these tests, the best results are gained related to the kinematics and deformation behaviour.

The second type are **sled tests** for frontal or side crashes. The used sleds are distinguished into two different kinds. One is the acceleration sled, where the vehicle gets catapulted by a hydraulic system. The other one is a delay sled, which releases the vehicle by disconnecting the cable drive. The state of the art in measurement technology and servo sleds are provided for example by KISTLER and MILLBROOK [43, 55].

Tests with only components of the vehicle are the third type of crash tests, the **component tests**. The car body in white is sufficient to test for example the roof or door deformation. And for testing parts such as the seat belt, only subsystems are necessary [45].

Some of the test constructions are placed outdoor to collide cars with buses or utility vehicles. But most of the crash tests are made indoors in big halls. Besides the vehicle and sometimes the dummy, there are different things needed for a crash experiment. The crash lane is up to 160 m long and can be divided into a acceleration, slow-down, delay and crash compartment. The longest crash lane with over 200 m was recently inaugurated by DAIMLER AG in 2016 in their new Technology Centre for Vehicle Safety in Sindelfingen, Germany. This is the state of the art crash centre in the world [11]. At the end of the lane a crash block is installed, which can be modified with various constructions for different impact angles or collision elements. The actuation of the sled is mostly a steel rope with a hydraulic, electro or combustion engine [45].

The **computational simulations** are also well developed. There are different models for reconstruction of accidents, for calculation of the structure, models of occupants and pedestrians and models for biomechanical researches. The first computational crash simulations were made for military defence and planes, but in 1981 Eberhard Haug used this knowledge for the first simulation of destructive car crash tests [30, 31].

As already mentioned, in the crash simulations also the behaviour and load on the occupants are valued. Thus, there are FE simulations with small female dummies and big male dummies, but also with little children dummies and even with a pregnant crash test dummy [66]. Furthermore there are simulations with pedestrians and traffic simulation models [80]. Most recent car crash simulations are simulations with human body models. These models rebuild humans with bones, muscles and ligaments and have mechanical characteristics of human tissues. The available models are from a Brite/Euram project, called HUMOS (Human Model of Safety) or developments in cooperation with Toyota Central R&D Labs called Total Human Model for Safety (THUMS) (see figure 2.9). Human models enable more accurate analysis of

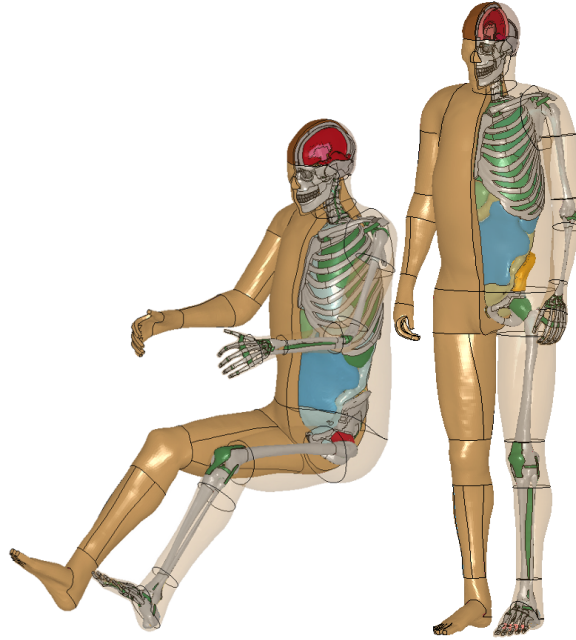


Figure 2.9: Total HUMAN Model for Safety (THUMS) occupant and pedestrian [16].

injuries. Different tools and techniques are used in the latest developments on the topic of positioning human models for crash tests [7, 13, 23, 32].

2.2.2 Motorcycle Industry

In the motorcycle industry crash simulations are still necessary to evaluate protective devices. But the possibilities of testing are more limited than in the automotive industry. The international standard ISO 13232 is defined specifically for motorcycle protective devices: "Motorcycles - Test and analysis procedures for research evaluation of rider protective devices fitted to motorcycles". In this standard, definitions for crash simulations with motorcycles like the impact conditions, the special motorcycle anthropometric impact dummy, computer simulations, documentation and more. There are also many patents for motorcycle simulations, like a patent for the test dummy in accident simulations [79].

The crash equipment for motorcycle tests are related to the ones used for cars. For the frontal impact there is a sled which accelerates the motorcycle and the dummy to the defined velocity and releases the system of motorcycle and dummy right before the crash object.

In the computational simulations, motorcycles were first modelled as lumped masses or multibody systems. Nieboer et al. [62] and Deguchi et al. [12] modelled simple motorcycles with MADYMO for crash test analysis. For testing the components, different impact and load tests were realized with a prescribed motion and the contacts between the motorcycle and the dummy/barrier were validated [12]. The first FE models used to analyse motorcycle crashes were developed around 2000. Mukherjee et al. [58, 59] and Namiki et al. [60] are known researchers in groups for motorcycle crash analysis. Their investigation was mostly aimed for the development of an airbag system for motorcycles and the prediction of the injury state of the motorcyclist in different accidental situations. Figure 2.10 shows a motorcycle-car side impact scenario with an airbag.

Normally the motorcyclist models are multibody models [45], but some research groups which were working with FEM are also considering the dummy behaviour and describe their

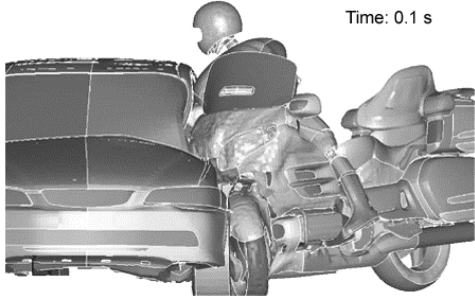


Figure 2.10: Motorcycle Crash with Airbag from Namiki et al. [60].

investigations, so for example Mukherjee et al. [59]. Contacts between the dummy and the motorcycle are defined and also the grip on the handle bar is described. In these simulations the hand encircles the handle bar with a force of 200 N and stays attached to the bar for 100 ms. There is no interaction in this simulation, but the results show, that the point of release is important to the rising height of the dummy [59].

2.2.3 Performed Crash Tests at DEKRA

The crash tests considered for validation in this work were recorded in June 2017 in the DEKRA Crash Test Centre in Neumünster, Germany. Within three days several crash tests were realized with different motorcycles. In figure 2.11 one of the crash test setups is shown.



Figure 2.11: Crash Test Setup at the DEKRA Crash Test Centre. [DEKRA]

In this work the focus lays on the crash tests with the motorcycle KTM 125 Duke. The tests were realized with three different velocities:

- $9.5 \frac{km}{h}$
- $12.8 \frac{km}{h}$
- $47.8 \frac{km}{h}$

One very slow velocity was realized, which should be as far as possible under $10 \frac{km}{h}$. Another slow velocity crash, without a damage of the motorcycle was tested. Thus, a third crash test could be driven with a higher velocity. In this work, the two slow velocities are quite important to analyse the deceleration for the grip release of the dummy hands from the motorcycle handlebar. The dummy within the test setting was the Hybrid III 50th percentile male which is standing and normally used as pedestrian with a modified head and neck. The dummy was wearing protective clothing including a helmet. To measure the kinematics and the loads on the dummy, it was equipped with a piezoresistive accelerometer (Endevco model 7264C) on the head and a cell with six channels to measure the neck load (force and moments). Additionally eight to ten evaluation sensor kits from the Bosch Healthcare Solutions (BHCS) were fixed on different parts of the dummy. Four to six of them were put on the wrists, two on the chest and two on the helmet, always two right next to each other (figure 2.12).



Figure 2.12: Sensors on the right Dummy wrist in a Crash Test Scenario. [DEKRA]

The sensor data from DEKRA, which is used in this thesis, was prepared according to the "Regulations for Bosch Two-Wheeler Manoeuvre Database". The dummies used for motorcycle crash simulations are often modified dummies which are developed for automotive crash tests. In the following section there will be an overview on crash test dummies.

2.3 Crash Test Dummies

The most famous test device for vehicle safety is the crash test dummy. It is the robust and ethically correct alternative for human test subjects. Further the repeatability of such tests is increased by using this dummies. Therefore the crash test dummy is a safe and repeatable device for investigations on transport safety and on reducing injury risks to occupants [56]. Results from real crash tests are used to position and validate the dummy in the FE test setup. This section will give an overview on the composition of a dummy, the different dummy types and on the dummy which is used for the crash test analysis.

2.3.1 Definition and Composition

Crash test dummies as they are shown in figure 2.13 are full-scale antropometric test devices (ATD), which are mainly used to test the accidental behaviour and loads of an occupant or passenger within a crash situation. Anthropometry is defined as the measurements of the size and proportions of the human body [14]. This indicates, that the geometry, weight, inertia, joint stiffness and energy absorption of the dummy is comparable with human bodies [56, 63]. For the analysis, the dummy can be equipped with different sensors, which are depending on

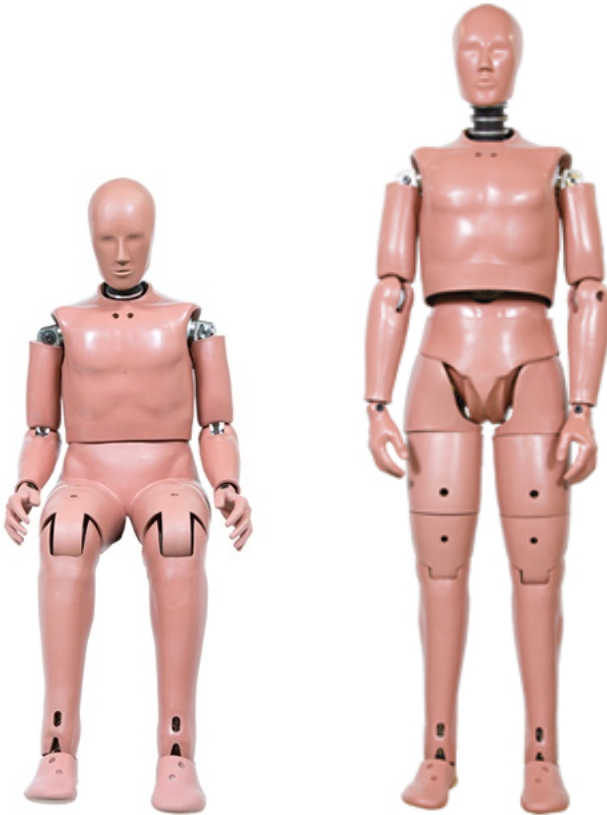


Figure 2.13: Hybrid III Sitting Dummy (left), Hybrid III Standing Dummy (right) [40]

the use case. The acceleration, forces, displacements and joint moments are measured in all relevant locations. By this, the actual load on the body can be measured and the predicted severity of injury can be identified [45, 63].

The problem in using the dummies is that they need to model the complicated human body and thereby be biofidelic but also provide simple reproducible results [45].

2.3.2 Dummy types

There are many different types of dummies. Over 50 years ago the first dummy was developed and since then dummy technology is steadily improving. The Hybrid III ATD family which was introduced in 1978 is commonly used for frontal impact tests [56]. The forth generation of Hybrid dummies is now in development [33]. The Hybrid IV or Test device for Human Occupant Restraint (THOR) is an advanced Hybrid III dummy with improved biofidelic features and expanded instrumentation. Besides the generation development, the dummies can also be categorized by their intended purpose. There are test devices of occupants for different kinds of vehicle crashes like frontal impacts, side impacts or rear impacts. But there are also dummies representing pedestrians, which are standing instead of sitting or for aerospace and military use. Other categorizations are the sex, age, size and weight of the dummy. There are dummies for children of three different ages and even pregnant dummies. The female and male dummies are available in different sizes and weights: 5th percentile female, 50th percentile male and 95th percentile male. This means that either 5 %, 50 % or 95 % of the population is smaller and lighter than the proportions of the dummy. The most common

dummy for frontal impact is the sitting Hybrid III 50th percentile male dummy [33, 72]. In 2009 Ghajari et al. [25] published their developments for motorcyclists in LS-DYNA. They invested in modelling a suitable dummy for motorcycles to improve the safety analysis. Since head injuries are a frequently mentioned consequence of accidents, they added a helmet to a modified Hybrid III dummy head. But because the Hybrid III dummy was developed for car rear impacts, its neck is too stiff for direct impact investigations. For motorcycle crash tests a dummy needs to have modified parts.

St. Laurent et al. [74] described in 1989 the first Motorcycle Anthropometric Test Device (MATD) which is a modified Hybrid III pedestrian dummy. The MATD is also specified in part 3 of ISO 13232 where many changes of the Hybrid III dummy are recommended to make the dummy usable for motorcycle crash tests [37]. The MATD has a different joint stiffness compared to the Hybrid III dummy [59] and some other modified features which are partly listed below [75]:

- The head was changed to make it compatible to a helmet.
- The neck was renewed to suit the different motorcyclist positions with upright head.
- The pelvis was changed to allow positioning of the dummy on the motorcycle.
- The hands were modified to wrap around the handlebars.
- The leg compartments and the abdomen were made frangible.

2.3.3 FE model of Hybrid III Dummy

Nowadays it is not possible to carry out crash test simulations without Computer-aided engineering (CAE) product developments, even finite element dummies are standard, especially in the automotive industry. Therefore Livermore Software Technology Corporation (LSTC) and others are developing accurate, detailed and robust LS-DYNA FE models of crash test dummies. In 2010 the 50th percentile male, 5th percentile female and 95th percentile male FE models were developed according to the Hybrid III ATD family. In figure 2.14 the fully assembled FE models of the Hybrid III 50th and 5th percentile dummy are pictured. They exist out of the six main assemblies head, neck, torso, pelvis, arms and legs with 200000-255000 elements and a global mesh size of 6 mm. The FE models are calibrated by validation to Head Drop Test, Neck Extension and Flexion Test and Thorax Impact Test [56]. The used FE dummy model is described in chapter 3.1.

2.3.4 Dummy Positioning

The position of a dummy or human body model in a crash test analysis is very important. Since a body has many degrees of freedom, the position can significantly affect the results. Slight differences in the position can cause different kinematics or injuries [49, 58].

In the FE environment there are many different tools for the positioning of dummy or human body models. It is possible to position the FE model by either simulations, geometric smoothing procedures or the geometrical deformation approach [23, 41]. To position a human body model the two last methods are more important because the model is more detailed and soft tissues have to be taken care of [13].

FEM programs have different tools to help the user to position a dummy. The application in LS-PrePost that is used in this work is called *Dummy Positioning*. There are also similar and more powerful tools like PIPER, the positioning tool from HyperWorks and the tool in ANSA [5, 7, 41]. Since the tool in LS-PrePost is sufficient to position a dummy, this was used in this thesis.



Figure 2.14: FE model of the Hybrid III 50th percentile male (left) and 5th percentile female (right) Dummy [56].

In 2006, Mukherjee et al. developed a positioning program in MATLAB for the motorcyclist dummy MATD. Dummies have a multi-jointed body, therefore it is a difficult task to match the position of experimental data [58]. The inverse kinematics problem was solved by a program, which computes the necessary joint angles by the coordinates from experiments. The thereby calculated error function was optimized with the MATLAB optimization tool function 'fmincon' [58].

In 2014, A. Gromer from DYNAmore showed in a workshop several possibilities to position a dummy in a car using LS-DYNA. On the one hand they provide a pre-simulation template where the modified angles have to be adjusted. On the other hand a procedure for positioning was demonstrated and the PRIMER tool was introduced. To seat the dummy either a prescribed motion or gravity simulations can be used [28]. In this work the positioning was done with the Tool in LS-PrePost. The seating simulation was done with gravity load, wherein the end position is unknown. This simulation type takes longer than by a prescribed motion, but it might be more accurate [28].

2.4 Validation

The validation of this work was done for several different aspects. First of all, the numerical accuracy will be proved to be sure, that the simulation results are numerical valid. Afterwards the position of the dummy was validated by comparing the sitting posture to pictures from the documentation. Also given specifications like distances and angles which determine the posture are compared to the positioned FE model.

Furthermore the kinematics of the dummy is validated in relation to the video data from three different crash tests. For this, frames with a distance of 25 ms were made and compared to each other.

The last validation aspect is the evaluation of the load data from the sensors and the simulation. The focus in this work lays on the acceleration data of the head and the force and moment

data from the neck of the dummy. In a first step, the load data from the physical test and the computational model are compared to each other. For rating the biofidelity of a dummy, in ISO 18571 the corridor method is described to calculate the level of correlation between two signals [38]. The software CORA, which is provided by the Partnership for Dummy Technology and Biomechanics (pdb), helps to evaluate time-history signals by combining two independent methods, the corridor rating and the cross-correlation rating. The corridor method evaluates the fitting of a curve into an inner and an outer corridor, which are either user-defined or automatically calculated. By using the cross-correlation method, the phase shift, shape and area of the curves are evaluated. The values in the CORA software are related to the ISO 9790 for lateral impacts [65]. In this work, the corridor method was used to validate the simulation signals to the sensor signals of the crash test. The function for the analysis was implemented in MATLAB according to the evaluation in the CORA software. The coefficients for the corridor rating values were taken from ISO 18571 [38]. Additionally, the acceleration data of the head is evaluated with the HIC and the a_{3ms} criteria. Thereby the values of the simulation data is compared to the sensor data. Furthermore, the load of the dummy neck was checked against the N_{ij} criteria and the acceptable maximal values. These injury criteria comparison was also made with MATLAB by using the maximal values for injury criteria which are listed in table 2.2.

Table 2.2: Biomechanical load parameters on the dummy [18]

Load Case Parameter	Threshold Values
Head Load	
HIC	700
resultant head acceleration (a_{3ms})	80.0 g
Neck Load	
axial neck force F_z at 0 ms	3.3 kN
axial neck force F_z at 35 ms	2.9 kN
axial neck force F_z at 60 ms	1.1 kN
neck shear force F_x at 0 ms	3.1 kN
neck shear force F_x at 25-35 ms	1.5 kN
neck shear force F_x at 45 ms	1.1 kN
neck bending moment M_y	57.0 Nm

In general, the sensor data was prepared with the tool UNIview, which was developed by ROBERT BOSCH GmbH. The simulation data was prepared in LS-PrePost V4.2.5 and the validation of this work was done with self-implemented functions in MATLAB R2013b.

2.5 LS-DYNA

LS-DYNA, which is based on the finite element method (FEM), is a computing program of the developer Livermore Software Technology Corporation (LSTC). With this program it is possible to simulate and analyse non-linear physical processes with a computer [17].

Important applications are crash simulations for the automotive industry, structural component production for vehicle construction and biomedical researches. For crash simulations and safety analysis, models of humans or dummies are necessary. Toyota Motor Corporation and

Toyota Central R&D Labs developed a human model called THUMS. This model combines multi-body-systems and finite element models and contains not just the shapes but also bones, muscles, ligaments and inner organs [17]. There are also various dummy models which are available for crash test analysis. The Hybrid III 50th percentile male dummy, which is used in this work, was implemented by LSTC.

Typical LS-DYNA versions for crash simulations are R7.2.0 or R9.1.1. This work was done with the available MPP version R8.0.0 and calculated with 8 or 16 cores. For the preparation of the model and the post simulation work, the LS-PrePost versions 4.3.20 and 4.5.2 are used. For modelling with LS-DYNA several input files are necessary and specific contacts are defined.

2.5.1 LS-DYNA input file

In the beginning of the simulation with LS-DYNA an input file has to be set up. With a program like LS-PrePost the models can be modified or created and saved in a keyword file (.k-file). This file contains all the information about the model and the simulation. The geometry of the model is defined by rigid bodies, beams or shells with a specified amount of NODES and ELEMENTS. The .k-file can be extended with all necessary keywords (below in capital letters) and the corresponding cards, where the parameters of the simulation are defined. First of all, there are CONTROL cards which define among other things the time of simulation, the type of integration (explicit or implicit) and the type of analysis (static or dynamic). Furthermore the DATABASE cards specify the output data. Depending on the model and the aim of research different parameters can be displayed for different segments and materials. There are extra cards to save the user-defined BOUNDARY conditions and INERTIAL options like velocities. The model elements and nodes can be combined to PARTS and SECTIONS and connected to the fitting MATERIAL. In between parts, sections or nodes certain CONTACTS can be defined to avoid penetrations. Additionally functions (CURVE) and forces or displacements (LOAD) on the body, for example gravity load, can be specified. All the cards are related with IDs to declare which elements, parts, materials etc. belong together.

The results of the simulation can be displayed per animation and diagrams for all of the parts, elements or nodes. For further utilization and visualization in convenient programs like *MATLAB* the results can be extracted into tables.

3 Model Setup

Before the simulation of the crash scenarios can be done, the models have to be prepared. The dummy model in this work is the 50th percentile Hybrid III FE sitting male dummy, which has to be seated on the motorcycle model. These used models are described in the section below.

To set up the combined model, the implementation of both models and their specifications is necessary. Additionally a barrier model has to be prepared. Further steps are the positioning of the dummy in a seating posture on the motorcycle model and the connections between the two models, that need to be defined.

3.1 Model Description

The model used in this thesis is made up of a dummy model from LSTC and an in-house developed motorcycle model. The model's coordinate system is defined so that the x-axis points to the front, the y-axis to the left and the z-axis to the top. All the specifications and values, which are used in this model, are made with a consistent unity system: millimetres (mm), kilograms (kg), milliseconds (ms) and kilo-newtons (kN).

3.1.1 Dummy Model

At the beginning, the Hybrid III 50th percentile male dummy, which is upright standing in its primary function as pedestrian, was used. The reason for using the standing Hybrid III dummy first was the different shape of the pelvis [62]. But because of numerical instabilities of the dummy in calculations with the whole motorcycle model and the inefficient possibility of re-meshing as well as the intense reduce of the time step, the more detailed dummy model of the sitting Hybrid III 50th percentile male was used further on (figure 3.1). The finite element models for the calculations in LS-DYNA are provided by LSTC. The MATD was not used because the crash tests which are available for validation of the simulation are made with a Hybrid III dummy. Other reasons are the availability of this modified dummy and its acquisition and simulation costs [4].

The sitting FE-Hybrid III dummy has a weight of 79.62 kg and its joints are arranged for the positioning tool in LS-PrePost. Actually the model is used for automotive crash simulations. Therefore it is prepared with a seatbelt accelerometer and a sitting pelvis. The whole model consist of around 450,000 finite elements with about 280,000 nodes. The element size is globally between 5 and 8 mm and it has a warpage angle of 10 and smaller. The Jacobian factor is mostly higher than 0.6, which can be indicated with a good element quality.

The body is fragmented into 367 inner and outer parts. The head on its own, for example, is composed with 19 different parts and the neck with 16 parts. A detailed description of the material used in this model would go beyond the scope of this work. Thus, only the most important material for this thesis is described. The outer parts of the dummy are realized partly with viscoelastic material (head, neck and torso), with low density foam (limbs), with elastic material (neck and shoes) and with Blatz-Ko rubber (pelvis and hands).

The validation of the dummy kinematics and load is done for the head and neck, hence these parts were described more detailed. The dummy head is modeled with an viscoelastic skin

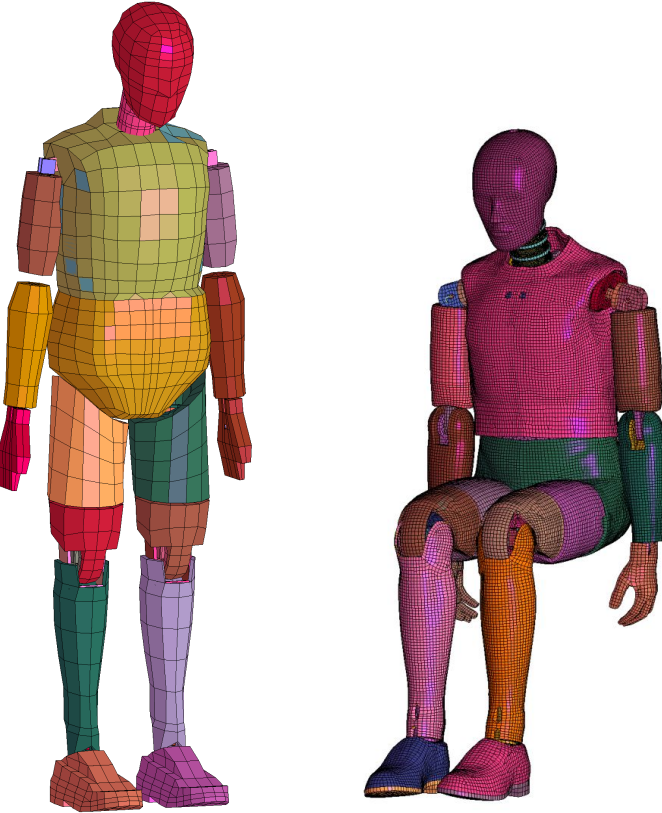


Figure 3.1: LSTC 50th percentile FE Hybrid III Standing and Sitting Dummy.

and an elastic skull. Inside the skull there is an elastic base on which rigid ballast parts and the rigid accelerometer are located. The neck is built up with viscoelastic rubber elements and in between there are elastic discs. The construction has an included elastic cable and is based on an elastic bracket.

For the realization of the holding grip, the dummy hands are important and therefore they are also described in more detail. The inner and outer parts of hands are realized with a Blatz-Ko rubber material, which describes a nearly incompressible continuum rubber. Inside the hand-shaped parts, there are two plates with elastic material for stabilization of the part which displays the wrist joint.

In table 3.1 some of the proportions of a 50th percentile male sitting dummy are listed and compared to the dimensions of a 50th percentile male human.

3.1.2 Motorcycle Model

The motorcycle model, which is used in this work, was constructed by Dinesh Loganathan in his master thesis. The finite element model was made with HyperMesh and consists of 43 parts with about 150,000 elements and 110,000 nodes (figure 3.2). The global element size is 5 to 10 mm and the centre of gravity is near the engine. The warpage is smaller than 15 for deformable elements and its Jacobian is greater than 0.5.

The weight of this model amounts to 127 kg, this correlates to the value for the real motorcycle [57]. In the documentation of the crash tests from DEKRA the weight with the measurement instruments is denoted with 145.5 kg.

Table 3.1: 50th percentile male dummy and human in comparison [15, 33]

proportions	Hybrid III dummy	German 50 th percentile male
weight [kg]	79.62	79
total sitting height [mm]	883.9	910
shoulder pivot height [mm]	513.1	625
thigh clearance [mm]	147.3	150
elbow to wrist pivot [mm]	297.2	350 (elbow to grip axis)
shoulder to elbow [mm]	337.8	365
elbow rest height [mm]	200.7	240
buttock to knee [mm]	591.8	610
popliteal height [mm]	442.0	450
knee pivot to floor [mm]	492.8	535
buttock popliteal length [mm]	464.8	495
chest depth [mm]	221.0	225
foot length [mm]	259.1	265
foot width [mm]	99.1	101
shoulder width [mm]	429.3	405
chest circumference [mm]	985.5	975
waist circumference [mm]	850.9	875

For this model a validation with the video data from the high speed crash test with 48 $\frac{km}{h}$ was done. Additionally a validation of the acceleration data in the centre of gravity was made, wherein the deceleration peak matched between the real and the simulated data. Thus, the behaviour of the motorcycle is assumed to be acceptable for further crash tests analysis in this work.

The part of major interaction between the dummy and the motorcycle are the handlebar, because of the holding grip, and the seat. The handlebar is realized as rigid shell and therefore the structure of the handlebar stays the same when it gets in contact with the dummy. The seat was implemented as well as rigid shell, thus the behaviour when the dummy is sitting on it is minimal and disregarded in this work.

At the beginning of this work, the motorcycle was reduced to its main components to position the dummy. These components were the handlebar, the two parts of the seat, the footrest and the fuel tank cover. Using these parts of the motorcycle reduced the calculation time, which made the simulations more economical and cost-efficient.

The motorcycle model was modified to suit this application. First of all, the control and database cards had to be adjusted for the whole model. The material curve for plastic was put in a right order, since there was a number disorder. Furthermore, the gravity load, the mass elements, which should demonstrate the dummy weight, and the wall were disabled from this model.



Figure 3.2: Motorcycle FE Model of the KTM 125 Duke.

3.2 Model Combination

The model was combined in an including file where all the CONTROL and DATABASE cards were defined. The initial velocity and gravity load cards were disabled in the single model files, because they were defined for the whole model. In addition, the wall for the crash test simulations was constructed. This wall was realized with a solid cube and a plate in front of it. The plate consists of solid and shell elements. The material of the wall parts is a combination of rigid and null material. The shell elements with null material are for a better contact definition. The material has the properties of steel, therefore it is a very stable construction, which wasn't moved within the crash tests.

In the table listed below (table 3.2) a general overview on the models and their characteristics is given. In total the motorcycle and the dummy weighted 230 kg in the crash test, the simulation model weights totally 207,5 kg.

After the preparation of the models, the dummy was positioned to sit on the motorcycle.

3.3 Dummy Positioning

The initial position of the dummy is important, because it influences the results of the simulations [58]. The dummy model has nineteen joints that have to be adapted to the right posture with one to three degrees of freedom.

For an uniform nomination some nomenclature is defined. For the angles the nomenclature is taken from the manual for LS-DYNA, the rotation around the x-axis is named ϕ , the one around the y-axis θ and ψ is called the rotation around the z-axis. Distances are named with d and lengths with l and the corresponding index.

In the documentation of the crash tests, some specifications about the position were defined. The mean values of the three crash tests are listed below:

- The distance of the knee joints: $d_{knee} = 673.67 \text{ mm}$
- The distance from the nose to the key: $d_{nk} = 588.67 \text{ mm}$
- The distance from the nose to the fairing: $d_{nf} = 651.67 \text{ mm}$
- The torso angle of inclination: $\theta_{torso} = 85.67^\circ$

Table 3.2: Information about the models according to ISO 13232

Parameter	Dummy	Motorcycle	Barrier	Model Combination (without barrier)
model, manufacturer, year	Hybrid III 50 th percentile sitting male, LSTC, 2013	KTM Duke 125, Dinesh Loganathan, 01/2018	wall, Julia Schaal, 2018	model combination, Julia Schaal, 2018
total mass	79.62 kg	127 kg	6000 kg	207.49 kg
element size (average)	5-8 mm	5-10 mm	50-95 mm	5-8 mm
centre of gravity	x: 110.25 mm, y: -0.15 mm, z: 101.87 mm	x: -266.82 mm, y: 0.33 mm, z: 579.74 mm	x: 394.45 mm, y: 0 mm, z: 462.50 mm	x: -307.28 mm, y: 0.28 mm, z: 744.10 mm
contact surface types	automatic single surface (3), automatic surface to surface (6), tied nodes to surface (18), tied nodes to surface offset (2)	automatic surface to surface (5)	-	additionally: automatic surface to surface (1 + 2 with wall), automatic surface to surface tiebreak (1)
rigid bodies and associated joint types	cylindrical joint (1), revolute joint (21), spherical joint (6), translational joint (4), nodal rigid body (179), rigid bodies (27)	revolute joints (3), nodal rigid body (202), rigid bodies (17)	-	no additional joints
type and numbers of finite elements	total: 451779 (beam (256), discrete (1), seatbelt accelerometer (10), shell (225910), solid (225602))	total: 148510 (discrete (2), shell (98250), solid (50258))	total: 365 (shell (140), solid (225))	total: 600289 (beam (256), discrete (3), seatbelt accelerometer (10), shell (324160), solid (275860))

Additionally, in the documentation, there are pictures of the motorcycle with the positioned dummy before the crash tests. Unfortunately, the dummy doesn't have any markers or coordinate information. Thus, finding the right posture is very challenging. First of all, the geometrical position is defined by the reference pictures and some placement parameters. Afterwards the angles are adjusted to fit the motorcycle model and to be compatible for a numerically stable calculation.

3.3.1 Geometrical Position

The geometrical position of the dummy is analysed with the help of the pictures of the documentation from DEKRA and the parameters of the distance between the knee joints and the torso angle of inclination. It is assumed, that the joints of the dummy are axially symmetric to the sagittal axis.

For the calculation of the hip angle, the distance between the hip joints was measured in LS-PrePost as $d_{hip} = 180.54 \text{ mm}$. From the documentation the target distance of the knee joints is given as $d_{knee} = 673.67 \text{ mm}$. Also the femur length with $l_{femur} = 362.55 \text{ mm}$ was taken from the FE model. Figure 3.3 shows the geometrical relation of the described parameters. It shows the front view of the lower body part between the hip and the knee joints.

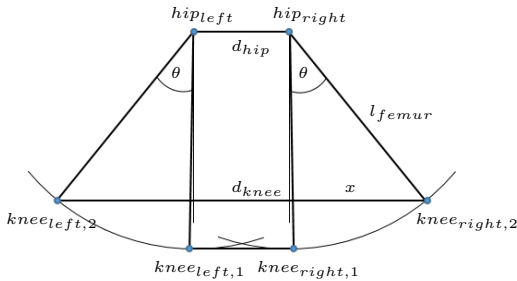


Figure 3.3: Calculation of the hip angle.

For the calculation of the hip angle θ , first the length between the knee joint and the vertical line to the hip joint has to be determined: $x = \frac{d_{knee} - d_{hip}}{2} = 246.57 \text{ mm}$. Afterwards θ can be computed with the trigonometrical equation $\sin(\theta) = \frac{x}{l_{femur}}$. Thus, the hip angle was identified as $\theta = 42.85^\circ$.

The other angles were measured from picture 3.4. The joint positions were assumed in certain locations and the angles are labelled in the local coordinate systems, which are located in the joints. For the definition of the hip and shoulder joint locations, the torso angle of inclination $\theta_{torso} = 86^\circ$ was considered. All the angles were measured in frontal view, thus the global coordinate system was placed according to the pictures edges. The angles were calculated from this picture according to the angles in the FE dummy model. Some angles couldn't be defined from this picture. Afterwards the FE model of the dummy was adjusted to the measured angles in LS-PrePost.

3.3.2 Dummy Positioning in LS-PrePost

In LS-PrePost there is a special application, which helps to move a dummy model, the *Dummy Positioning Tool* (figure 3.5). After loading a dummy file, LS-PrePost recognizes the dummy and the joints itself. First of all, the H-point or hip-point of the dummy can be translated and rotated into a basic position. The H-point is defined at the lateral height of the hip, but is actually the pivot point between the torso and the upper leg portions. It is an important

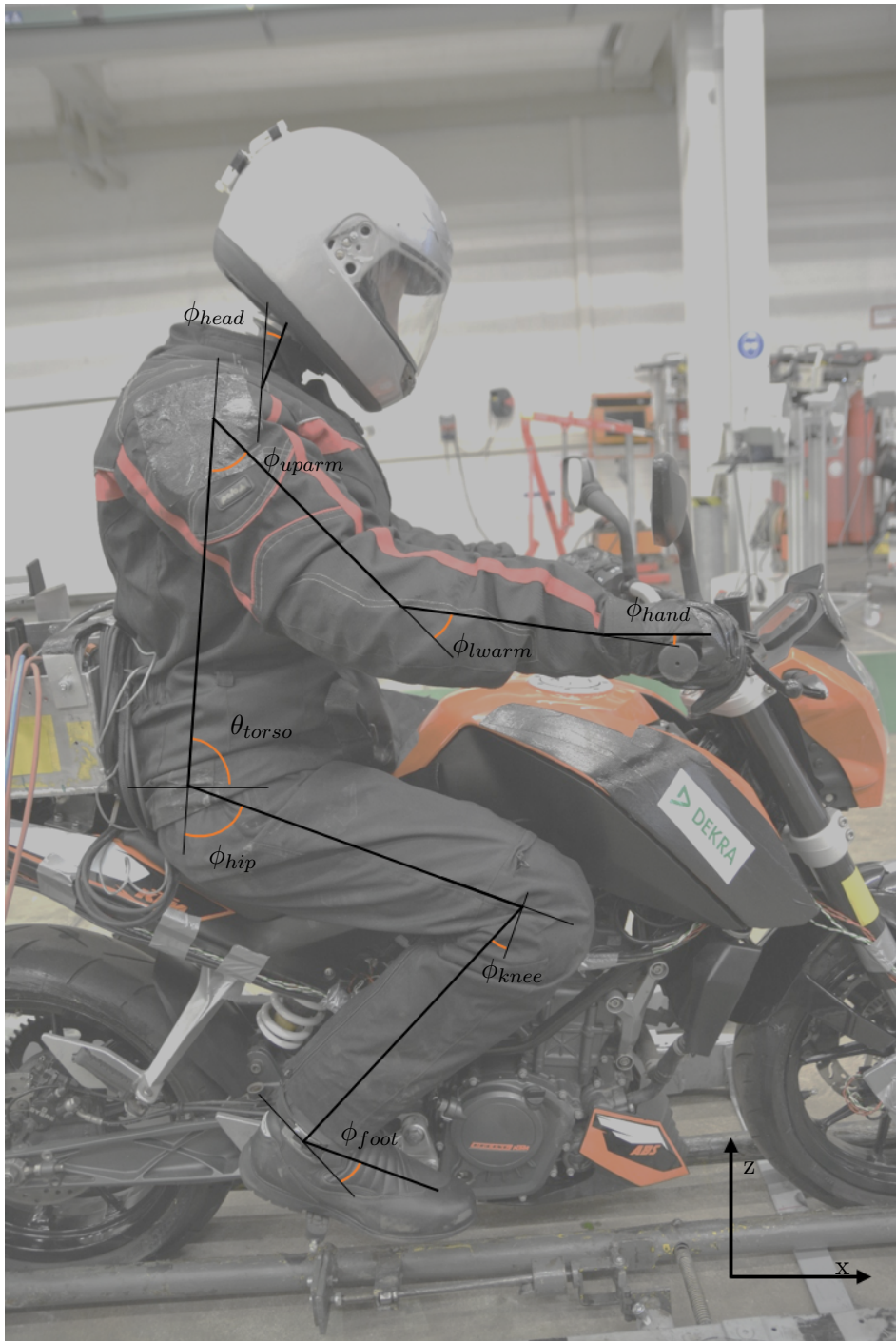


Figure 3.4: Dummy position angles defined in the documentation picture.

Table 3.3: Dummy position of the 19 joints, absolute angles in [°]

Angular Parameters	Nomination	Values from picture	Values in the FE model
torso	ψ_{torso}		0
	θ_{torso}		0
	ϕ_{torso}	86	4.33 (from vertical line)
neck-head	ϕ_{head}	21	6.98
upper leg	ψ_{upleg}		15.43
	θ_{upleg}	45.85	24.95
	ϕ_{upleg}	20	30.27
lower leg	ϕ_{lwleg}	23	23.06
	ψ_{foot}		24.33
foot	θ_{foot}		22.23
	ϕ_{foot}	23	36.30
	$\phi_{shoulder}$	41	57.5
upper arm	ϕ_{uparm}		0.8
elbow	ϕ_{elbow}		1.36
lower arm	ϕ_{lwarm}	37	23.5
wrist	ϕ_{wrist}		79.27
hand	ϕ_{hand}	8	0.21

feature in international standards of vehicle design [3]. Afterwards, the limbs can be rotated with the CARDAN angles (first around the z-axis, second around the new y-axis and third around the new x-axis). The joints have defined stop angles and a stiffness that can be modified in the *CONSTRAINED_JOINT_STIFFNESS card, while the physiological constraints need to be respected. In this work, the stop angle ψ of the upper legs were modified for a greater movement around the z-axis. The anatomical values for the external rotation is restricted with 40° and the internal rotation with 25°. With a bended hip even an external rotation of 60° is possible [42]. Also the stop angles of the feet were adjusted with additional 2° for ψ , to enable the adduction of the foot, which is a rotation of the foot around the z-axis towards the sagittal axis. In the literature, the maximum of this angle is given as 35°, thus the changed value with $\psi = 25^\circ$ lays in the anatomical range [42].

3.3.3 Seating Position

As a next step, the positioned dummy was seated on the motorcycle. This was done by defining the coordinates of the H-point. The H-point in this work was set to $x = -458\text{ mm}$, $y = 0.329\text{ mm}$ and $z = 919.997\text{ mm}$. The y value was set to the same value as the centre of gravity of the motorcycle. For the z value, the closest distance possible to the seat was chosen, thereby the dummy doesn't move too far when the gravity load is acting. The x coordinate was set in a way the pelvis of the dummy didn't touch the motorcycle.

Since with the first posture of the dummy, the limbs didn't fit to the motorcycle parts, some adaptations had to be done. The neck has a more upright position, because the distances from

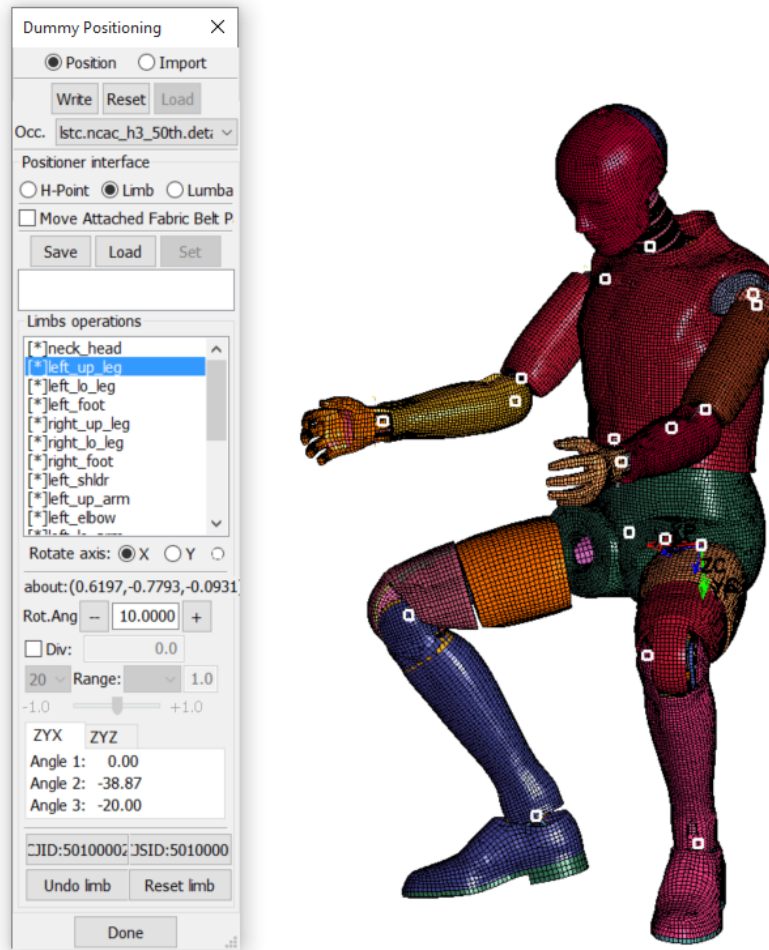


Figure 3.5: LS-PrePost Positioning Tool with the FE Hybrid III Sitting Dummy in his first position.

the nose to the key and the fairing were approximated and the neck angle was constrained for further motion.

The settings of the leg and foot angles were changed in a way, that the shoes of the dummy fitted on the footrest of the motorcycle. It was very difficult to find these settings. The angles of the legs and feet had to be re-positioned several times, because of unexpected foot movements. The left foot didn't stay on the footrest in every time step. Furthermore, numerical instabilities of the calculation occurred within the gravity simulations.

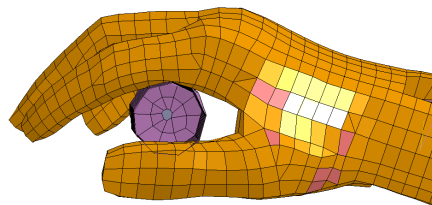


Figure 3.6: The dummy hand grip and the handlebar.

Additionally, the arms were moved to a different position. As the grip of the hand doesn't fit around the handlebar (see figure 3.6). The palm of the hand was positioned to lay on the handlebar with more than one close contact point. To realize this posture, the wrist was turned around and the arms were moved to slightly different positions. By moving the upper arm joint and the elbow joint, the arm was moved in y-direction. This way the hand was placed in the middle of the handlebar grip. For a new position in x- and z-direction, the other joints had to be adapted.

The new position and its angle values are registered in the third column of table 3.3. With this posture of the dummy (see figure 3.7), the simulations were done. But before the simulations could run, the contacts between the models had to be defined.



Figure 3.7: The positioned dummy on the motorcycle.

3.4 Contact Implementation

In the combined model, there are interactions between the dummy model, the motorcycle and the wall. Therefore, contacts are used to define the correlation between different parts. Thus, there will be a definition of contacts in general and of the used contacts in this model. Furthermore, the holding of the dummy's hand to the handlebar was modelled with a tiebreak contact. Additionally the friction coefficients between every correlated part had to be determined. These values are set in the contact definition.

3.4.1 Contact Definition

Contact definitions allow interactions between unmerged Lagrangian elements. This is important when parts correlate with each other for example by impact, push, sliding or similar and when parts should be tied together. In LS-DYNA many different contact types are available. In a contact setting, defined locations (segments, nodes, parts or sets of it) are checked for potential penetrations of slave nodes through master segments (figure 3.8). The contact point must lie within the master segment and is calculated at every time step except for some TIE or TIEBREAK definitions. In a one way contact definition, it is important, that the slave segment needs a finer mesh than the master segment. When it is a non-automatic contact card, the segment orientation plays also an important role.

A penetration is detected, if the projection distance d , is negative $d < 0$. With positive values of the projection distance $d > 0$, the slave node has an offset. Is the projection distance zero, $d = 0$, the slave is ON the master segment surface. The contact force calculation of the slave node f_S is dependant on the contact stiffness K_C and the penetration depth δ : $f_S = K_C \cdot \delta$. In the master segment the force, which each segment node receives, depends on the location of the contact point [2, 52].

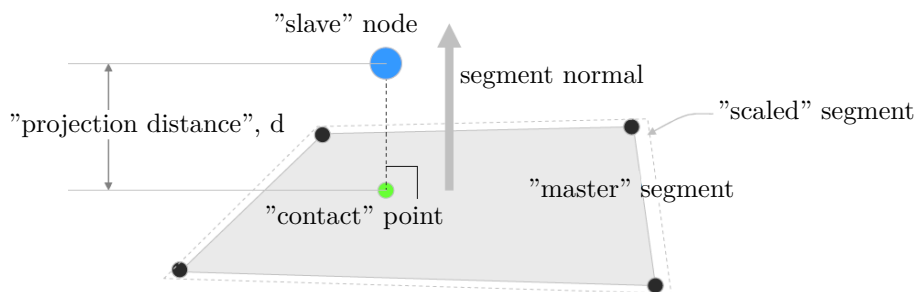


Figure 3.8: Contact definition in LS-DYNA [2].

For the contact definition in occupant models several recommendations were made, some of them are described here. One suggestion is the usage of the SOFT constrained option, which might be necessary if the contacted surfaces have wide variation in their elasticity. Another point is, that the user does not need to reduce the amount of elements in the contact definition to get a shorter simulation time, this is done by the algorithm. Large penetrations and redundant contacts should be avoided because they might cause numerical instabilities. It is also recommended to use as little contact definitions as possible to make the model clearer and to improve the simulation time [28].

Therefore, the contact definitions that were added for the model integration were of the type *CONTACT_AUTOMATIC_SURFACE_TO_SURFACE. In this work, three additional contacts of this type were defined. The first one was added between the dummy parts and the motorcycle:

```
*CONTACT_AUTOMATIC_SURFACE_TO_SURFACE_MPP_ID
$#      cid                               title
      1005dummy and motorcycle
$#  ignore   bucket  lcbucket  ns2track  inititer  parmax  unused  cparm8
      1       200          0           3         2     1.0005        0
```

```

$#    ssid      msid      sstyp      mstyp      sboxid      mboxid      spr      mpr
    100004      1000      2          2          0          0          1          1
$#    fs        fd        dc        vc        vdc        penchk      bt        dt
    -2.0      1000.0     0.0      0.0      0.0      0.0      0.01.00000E20
$#    sfs       sfm       sst       mst       sfst       sfmt       fsf       vsf
    1.0        1.0      0.0      0.0      1.0      1.0      1.0      1.0
$#    soft      sofscl   lcidab   maxpar   sbopt      depth      bsort      frcfrq
    1         0.1        0       1.025      2.0        2          0          1

```

The parameter IGNORE = 1 activates the ignorance of initial penetrations. SSID and MSID are the IDs of the slave and master segments. The SOFT option with 1 is for a soft constraint formulation, which could be necessary, as outlined above, because of different material parameters.

The contacts between the wall and the two models are defined in a similar way. The friction coefficient for this contact was set to 0.1.

```

*CONTACT_AUTOMATIC_SURFACE_TO_SURFACE_MPP_ID
$#      cid                               title
      1006dummy and wall
$#    ignore    bucket    lcbucket    ns2track    inititer    parmax    unused    cparm8
        1        200        0            3            2        1.0005      0
$#    ssid      msid      sstyp      mstyp      sboxid      mboxid      spr      mpr
    1000000      1000      2          2          0          0          1          1
$#    fs        fd        dc        vc        vdc        penchk      bt        dt
    0.1        0.0      0.0      0.0      0.0      0.0      0.01.00000E20
$#    sfs       sfm       sst       mst       sfst       sfmt       fsf       vsf
    1.0        1.0      0.0      0.0      1.0      1.0      1.0      1.0
$#    soft      sofscl   lcidab   maxpar   sbopt      depth      bsort      frcfrq
    1         0.1        0       1.025      2.0        2          0          1

*CONTACT_AUTOMATIC_SURFACE_TO_SURFACE_MPP_ID
$#      cid                               title
      1007motorcycle and wall
$#    ignore    bucket    lcbucket    ns2track    inititer    parmax    unused    cparm8
        1        200        0            3            2        1.0005      0
$#    ssid      msid      sstyp      mstyp      sboxid      mboxid      spr      mpr
    1000000      100004     2          2          0          0          0          0
$#    fs        fd        dc        vc        vdc        penchk      bt        dt
    0.1        0.0      0.0      0.0      0.0      0.0      0.01.00000E20
$#    sfs       sfm       sst       mst       sfst       sfmt       fsf       vsf
    1.0        1.0      0.0      0.0      1.0      1.0      1.0      1.0
$#    soft      sofscl   lcidab   maxpar   sbopt      depth      bsort      frcfrq
    1         0.1        0       1.025      2.0        2          0          1

```

3.4.2 Tiebreak Contact

The holding force of the dummy hand to the motorcycle handlebar has to be implemented, because otherwise, even only with gravity load, the dummy hands wouldn't stay attached to the handlebar. To realize this behaviour, there are several options available. The parts could be bound together with a spring element, a beam element could be defined in between the parts or the holding force could be realized with a time limit, like in the publication by Mukherjee et al. [59]. In this work, a special contact definition with an included failure criterion was used, the tiebreak contact.

The tiebreak contact in general transmits compressive and tensile forces and acts like a glue. The tie part, ties all the slave nodes to the master segments with a linear spring, when a contact

point can be found. The failure option is modelled by the break part, with high tensile forces or stress, the spring decouples and the slave nodes can move independently. In the automatic definition of this contact *CONTACT_AUTOMATIC_SURFACE_TO_SURFACE_TIEBREAK, which was applied in this thesis, there are several different options for the calculation. In general all slave nodes are tied to the master segments. The different options can be looked up in the LS-DYNA manual [51]. With option 1 and 3, all nodes that are initially in contact or come into contact while calculating are tied. The difference between these options is the failure realization after sticking in option 3. Therefore, option 3 is chosen for the tiebreak contact, which is shown below. Since the surface to surface contact is a two-way contact, it is concerned with a stress based failure. The equation of the failure criterion is given by

$$\left(\frac{|\sigma_n|}{NFLS} \right)^2 + \left(\frac{|\sigma_s|}{SFLS} \right)^2 \geq 1 \quad (3.1)$$

with NFLS as normal failure stress and SFLS as shear failure stress. To assume failure, the normalized and squared stresses have to be equal or greater than 1. When this is the case, the tensile spring is deactivated.

```
*CONTACT_AUTOMATIC_SURFACE_TO_SURFACE_TIEBREAK_MPP_ID
$#      cid                               title
      1000hand to handlebar auto tiebreak
$#  ignore   bucket   lcbucket   ns2track   inititer   parmax   unused   cparm8
      1       200          0           3           2     1.0005      0
$#  ssid     msid     sstyp      mstyp      sboxid     mboxid    spr      mpr
      1001     1001        0           2           0         0       1       1
$#  fs       fd       dc       vc       vdc     penchk    bt      dt
      0.3      0.0      0.0      0.0      0.0       0     0.0  1.00E20
$#  sfs      sfm      sst       mst      sfst      sfmt     fsf      vsf
      1.0      1.0      0.0      0.0      0.0       0.0     1.0     1.0
$#  option   nfls     sfsls     param     eraten    erates   ct2cn   cn
      3      0.05    0.0035      0.0      0.0       0.0     0.0     0.0
$#  soft     sofscl   lcidab   maxpar   sbopt     depth    bsort   frcfrq
      1       0.1        0       1.025     2.0       2       0       1
```

The values, which are used in this work, are empirical, since there wasn't any comparable literature available. In the chapter 4 the method for determining the failure stress values is stated.

The tiebreak contact is defined between the hand and the surface of the grasp of the handlebar (see figure 3.9).

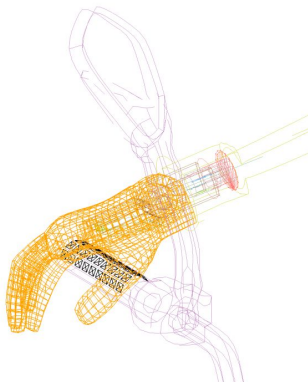


Figure 3.9: Tiebreak contact between the hand and the handlebar.

3.4.3 Friction

The friction between the parts of the model, were defined in relation to literature values and the empirical values from DYNAmore for crash simulations.

In this work, the coulomb friction was considered which is defined as $F^T \leq \mu \cdot F^N$ (see figure 3.10). Herein the friction coefficient is calculated as

$$\mu = \mu_d + (\mu_s - \mu_d) \cdot e^{(-d_c \cdot |v_{rel}|)}, \quad (3.2)$$

with μ_s as the static coefficient of friction, μ_d as the dynamic coefficient of friction and d_c as the exponential decay factor. The coefficient of friction used in this work are values for μ .

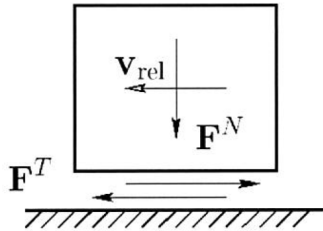


Figure 3.10: Schematic of the definition of friction [27].

Since the advice from DYNAmore was a friction coefficient of $\mu_{all} = 0.2$ for all parts in a contact between the dummy and the surrounding, this value was set as a general friction coefficient. To define the friction coefficient between the rubber sole of the shoe and the footrest, the values for rubber on dry asphalt are stated in the literature as $\mu_{stat} = 0.7..0.8$ and $\mu_{dyn} = 0.5..0.6$ [22]. These values were adjusted to the suggestion given by the DYNAmore support with $\mu = 0.5$. Thus, the static and dynamic friction coefficients for the shoes and the footrest were defined as $\mu_{shoe} = 0.6$ in this work.

These friction values are set in the contact definition between the dummy and the motorcycle. Since the coefficients vary for the combination of different materials, the friction is set in a separate *DEFINE_FRICTION card, which is declared by the value $FS = -2$ and $FD = 1000$ sets the corresponding ID.

```
*DEFINE_FRICTION
$#      id      fs_d      fd_d      dc_d      vc_d
      1000    0.2      0.0      0.0      0.0
$#  pid_i   pid_j   fs_ij   fd_ij   dc_ij   vc_ij   ptypei   ptypej
  100020  51100001    0.6      0.0      0.0      0.0
  100020  51200001    0.6      0.0      0.0      0.0
```

For the friction in the contact to the wall, the coefficient was defined as $\mu_{wall} = FS = 0.1$. Furthermore the friction coefficient between the hand and the handlebar was specified and set as $\mu_{hand} = 0.3$. This value equals the minimum data, which is given for friction with leather on a dry surface [22]. Thus, in the contact definition for the hand and the handlebar, the value FS is set to 0.3.

4 Simulation Setup

After the model preparation, the simulation environment had to be defined. Furthermore, the two different types of simulations were introduced. First, there was a gravity simulation, which was necessary to position the dummy on the motorcycle. As a second simulation type, the three different crash tests were calculated with the pre-positioned models.

4.1 Simulation Environment

The models were connected by including them into a new keyword file, wherein also the settings for the simulation environment were made.

In addition CONTROL and DATABASE cards had to be defined. The initial time step size of the simulations was determined by LS-DYNA (DTINIT=0.0). Since the simulations were run with mass scaling, the scale factor was set to TSSFAC = 0.67 and the minimum time step size was defined by DT2MS = $-5.555 \cdot 10^{-4}$ ms. Mass scaling means, that nonphysical mass is added to some elements, if it is necessary to achieve the time step size criterion [53]. The maximal percentage change in the total mass was defined with the parameter ENDMAS, which was set to $1.0 \cdot 10^8$ in this work. The mass scaling values were chosen according to the initial settings in the dummy model from LSTC.

```
*CONTROL_TERMINATION
$# endtim    endcyc      dtmin     endeng     endmas      nosol
    1000.0        0        0.1        0.01.000000E8        0

*CONTROL_TIMESTEP
$           The following gives Natural Time-Step
$# dtinit      tssfac      isdo      tslimt      dt2ms      lctm      erode      ms1st
    0.0        0.67        0        0.0-5.5550E-4        0        0        0
$# dt2msf      dt2mslcl    imscl     unused     unused      rmscl
    0.0        0        0                      0.0
```

Since the simulations in this work were run by mass scaling, the MSSCL parameter in the *DATABASE_EXTENT_BINARY card was activated to localize the regions of the added mass. This database output was considered to ensure, that the additional mass was minor in the regions of interest.

Further important database cards for this use case were the contact outputs called NCFORC and RCFORC, that calculated the contact forces in the defined master and slave segments and their nodes. Additionally HISTORY_DISCRETE was a necessary database card to get the displacements of the springs in the motorcycle fork. For the analysis of the loads on the dummy, two other outputs were considered. On the one hand, the acceleration on the head is available in the NODOUT binout of the node number 52500001, which is the node of the head accelerometer. On the other hand, the neck load, with forces and moments, was calculated for the section 50100001 and is available in the SECFORC binout.

The simulations were run with LS-DYNA version R8.0.0. The gravity simulation was calculated with 8 CPUs. Because of instabilities of the calculations with 8 CPUs, the crash simulations were calculated with 16 CPUs.

4.2 Gravity Simulation

For the positioning of the dummy, a simulation with gravity load was run. The first simulations were made with the components of the motorcycle and the broadly defined standing dummy model. When the motorcycle model was replaced, numerical instabilities occurred. Thus, the dummy was changed to the finer meshed sitting dummy. The gravity was realized with a load in z-direction to the earth's centre with $x = 0 \text{ mm}$, $y = 0 \text{ mm}$ and $z = -6.37 \cdot 10^9 \text{ mm}$. A positive defined body load acts in negative direction, thus the $9.807 \cdot 10^{-3} \frac{\text{mm}}{\text{ms}^2}$ acted as gravitation force.

```
*LOAD_BODY_Z
$# lcid      sf      lciddr      xc      yc      zc      cid
      1000      1.0          0      0.0      0.0-6.37000E9      0
#
*DEFINE_CURVE
$# lcid      sidr      sfa      sfo      offa      offo      dattyp      lcint
      1000          0      0.0      0.0          0.0          0.0          0          0
$#           a1          o1
            0.0      0.009807
      10000.0      0.009807
```

With this simulation, the initial dummy and motorcycle postures for the following crash tests are calculated. The end time of the simulation was set to 1000 ms, with the aim to get the equilibrium state of the model.

After the simulation, the position of the dummy and the one of the motorcycle was extracted by saving their new node coordinates to a separate keyword files. It was important to save also the unreferenced node coordinates, otherwise, the models won't run properly anymore. In a next step, the node coordinates in the model files had to be replaced with the new values and the new positioned models are saved to new keyword files.

For the dummy model, the joints had to be redefined, because the nodes of the correlating parts were not coincident. There is a tool for this in LS-PrePost. Within the "Model Checking" window in the "Keyword Check" section, there is a button called "Snap", which snaps all joint nodes. The snapped dummy model had to be saved afterwards.

The motorcycle model in its positioned structure, was also snapped for a proper joint definition. Furthermore, the new motorcycle was loaded by the dummy, thereby the fork and its springs were also tensioned. The initial displacement of the springs had to be defined manually in the .k-file. The offset of -47.3 mm was set in the *ELEMENT_DISCRETE card.

```
*ELEMENT_DISCRETE
$# eid      pid      n1      n2      vid      s      pf      offset
  246537  100040  213108  213110      0      1.0      0      -47.3
  246538  100040  210151  213111      0      1.0      0      -47.3
```

The gravity simulation was done several times, with repositioned dummy models. One of the reasons was the numerical instability in the dummy model. They occurred mostly in simulations with higher velocities. Also the feet and shoes of the dummy caused instabilities and led to changes in the dummy position. Finding the right position of the feet on the footrests was challenging and time- and cost-intensive. With the wrong position, the heel of the shoe got stuck on the footrest within the crash, therefore negative volume occurred. Also, the feet moved a lot within the gravity simulation. One of the consequences to this was, that the feet weren't placed on the footrest in every time step.

For the initial models of the crash simulations, the right state of the simulation had to be chosen. In this work, the simulation state after 725 ms of gravity calculation was selected.

4.2.1 Joint Stiffness

A further setting that had to be done for the gravity simulation was the adaptation of some joint stiffness. In the CONSTRAINED_JOINT_STIFFNESS card, the stiffness for each joint is defined.

Since the original dummy was bending his arms and wrists in an unnatural way, the stiffness values of the arms and wrists were accommodated. A sitting motorcyclist is actively holding himself in an upright position. In this model, there aren't any active parts like muscles, thus the joint stiffness had to be adjusted. The stiffness of the lower arm was set from 3.13 Nm to 41.3 Nm , which is the stiffness value of the elbow for a shoulder angle of 30° and an elbow angle of 140° [20]. Furthermore the stiffness of the wrist joints were changed to the values used in the simple standing dummy model, thus it was set from 0.178 Nm to 0.4 Nm .

4.2.2 Model Position

After the gravity simulation, the dummy sat on the motorcycle in a new position. The settings of the H-point and angles changed (see table 4.1) and the models were prepared for the crash simulations. Also the motorcycle had a new position, especially the spring in the fork was displaced. Figures 4.1 and 4.2 show the model before and after the gravity simulation.

Table 4.1: Dummy position before and after the gravity simulation (left side) values in [mm] and [°]

Parameters	Nomination	Values of positioning	Values after gravity (725 ms)
h-point in [mm]	x	-458.000	-447.059
	y	0.329	-7.249
	z	919.997	893.694
torso angle in [°]	ψ_{torso}	0.0	-5.15
	θ_{torso}	0.0	-0.61
	ϕ_{torso}	4.33	-0.36
neck-head	ϕ_{head}	-6.98	-6.98
upper leg	ψ_{upleg}	15.43	16.25
	θ_{upleg}	-24.95	-24.31
	ϕ_{upleg}	-30.27	-30.68
lower leg	ϕ_{lwleg}	23.06	22.97
	ψ_{foot}	24.33	22.88
	θ_{foot}	22.23	22.85
foot	ϕ_{foot}	-36.30	10.20
shoulder	$\phi_{shoulder}$	57.50	57.41
upper arm	ϕ_{uparm}	0.80	0.88
elbow	ϕ_{elbow}	1.36	1.33
lower arm	ϕ_{lwarm}	-23.50	-23.48
wrist	ϕ_{wrist}	-79.27	-78.79
hand	ϕ_{hand}	-0.21	2.19

4.3 Crash Simulation

The crash simulations were calculated with the positioned models. For the velocity, the card *INITIAL_VELOCITY was included. According to the documentation of the three frontal crash tests with the KTM Duke 125, the velocities in x-direction were set to:

1. Crash: $v_1 = 9.5 \frac{km}{h} = 2.6388 \frac{mm}{ms}$
2. Crash: $v_2 = 12.8 \frac{km}{h} = 3.5556 \frac{mm}{ms}$
3. Crash: $v_3 = 47.8 \frac{km}{h} = 13.27778 \frac{mm}{ms}$

Furthermore, the wall model was included in the simulation. The distance between the wall and the motorcycle was set depending on the velocity, so that the crash took place after 100 ms. Also, the contacts between the dummy and the wall and between the motorcycle and the wall were included. In figure 4.3 the setup of the crash simulation is shown.

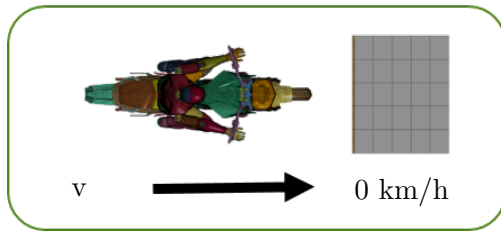


Figure 4.3: Crash Simulation Setup.

4.3.1 Contact Settings

As already mentioned, the holding force of the dummy was realized with a tiebreak contact. Since one of the available publications describes a time limited holding condition [59], the settings for the tiebreak contact were found by analysing the dummy behaviour in the real crash tests. The kinematics of the dummy hands was recreated according to the videos of the experiments. In the second crash test with $12.8 \frac{km}{h}$ the dummy lost contact to the handlebar, while it still stayed in contact in the first test scenario. In the experimental crash tests, the dummy hands were taped to the handlebar with a gaffer tape from Conrad Electronics [9]. Thus the tiebreak settings were made according to these observations.

The adhesion of the gaffer tape to the back of the tape is specified as $2.3 \frac{N}{cm}$. Since the width of the tape is 50 mm, the adhesion stress is given as $\sigma_{a,t} = 0.0046 \frac{N}{mm^2} = 4.6 \cdot 10^{-6} \frac{kN}{mm^2}$ [9]. In the experiments the tape was sticking on different material, therefore this value serves only as guideline for the tiebreak settings.

Using the determined value for the stress didn't lead to the expected results. Therefore the values NFLS and SFLS of the tiebreak contact were determined through empirical analysis. The normal failure stress was set to $NFLS = 0.05 \frac{kN}{mm^2}$ and the shear failure stress was defined as $SFLS = 0.0035 \frac{kN}{mm^2}$. The tied area was detected as $A = 733 mm^2$, thus the maximal normal force amounts $F_n = 36.65 kN$ and the maximal shear force is $F_s = 1.91 kN$. Compared to the crash test behaviour, these values fit well to replicate the holding force of the dummy hands to the handlebar. Thus it is assumed that these values are plausible to rebuild the crash tests.



Figure 4.1: Motorcycle and Dummy models before the gravity simulation (0 ms).

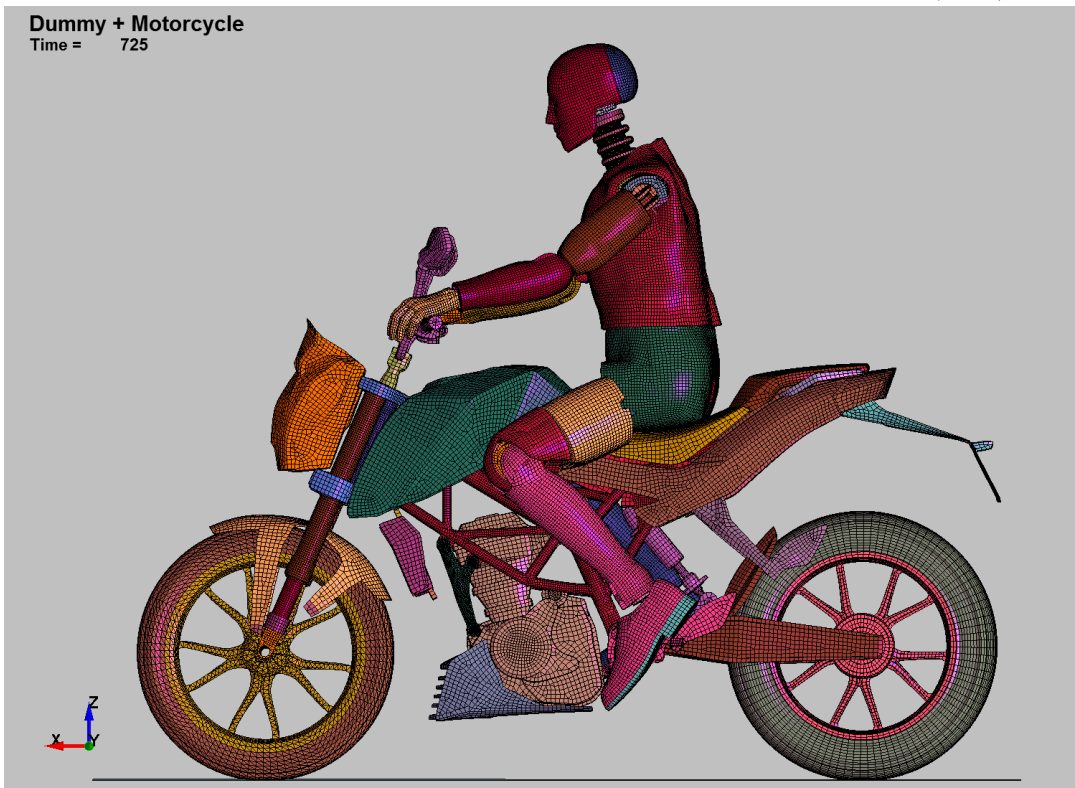


Figure 4.2: Motorcycle and Dummy models after the gravity simulation (725 ms).

5 Results and Validation

After the simulations were calculated, the post processing was done with LS-PrePost and MATLAB. At first, the numerical accuracy was proven and the regions of mass scaling were appointed. Afterwards, the position of the dummy after the gravity simulation was validated with the existing pictures and specifications. In a third part, the dummy kinematics was analysed and evaluated with the video documentation of the crash tests. In a final step, the load and acceleration of the dummy head and neck was compared to the measurement data and validated with the injury criteria.

5.1 Numerical Accuracy

To be sure that the simulations demonstrate plausible results, the numerical accuracy has to be verified. Additionally, the system energy was analysed.

The energy ratio has to be 1.0. It is calculated with the total energy, which is the sum of internal, kinetic, contact and hourglass energies, divided by the internal energy and the external work:

$$\text{energy ratio} = \frac{\text{total energy}}{\text{internal energy} + \text{external work}}. \quad (5.1)$$

For the gravity simulation, the energy ratio had a maximal value of 1.04 and a minimal value of 0.688 at the very beginning. Thus, the energy was in balance. The crash simulations had an energy ratio between 1.004 and 1.1. The energy ratio was regarded in balance, with a difference of 10 % from the optimal value.

Furthermore, the hourglass energy should not exceed 10 % of the stress energy, which is called internal energy in LS-DYNA. This was correct for the gravity simulation. Here, the hourglass energy was 0.72 % of the internal energy, with two exceptions at the beginning. For the crash simulation the difference between the hourglass energy and the internal energy was calculated with a maximal difference of 4.33 %. Thus it was less than the acceptable 10 %.

Since the simulations were made with mass scaling, the amount and regions of added mass have to be identified. In the gravity simulation a maximum mass of 1.11 kN was added. 1.06 kg of the mass was added to the motorcycle model. To the head and neck part of the dummy a maximum mass of 2 g were added, which is equal to 0.0025 % of the total mass of the dummy model. The remaining dummy had 53 g additional mass. The added mass in the crash simulations amounted a maximum of 1.17 kg. The dummy head and neck parts had an additionally mass of 2 g. Thus, the added mass to the regions of interest was very small.

In every regarded simulation, the energy was in balance. Also the added mass to the regions of interest was acceptable. Hence, the simulations with mass scaling produced numerically accurate results.

5.2 Dummy Position

Three different positional states of the dummy are compared to validate the position. The first state is the picture before the real crash test scenario (r). As a second state the model after the positioning in LS-PrePost is considered (p). The third position is the model after the gravity simulation (g). The picture and the specifications of the real position serve as a reference for the validation.

5.2.1 Validation with Reference Information

Primarily the averaged specification values from the three crash test documentations are compared with the measurements in the FE models. The distance of the knee joints in the positioned model is measured as $d_{knee,p} = 494.64 \text{ mm}$ and for the model after gravity simulation as $d_{knee,g} = 498.33 \text{ mm}$. Since the reference value is $d_{knee,r} = 673.67 \text{ mm}$, the positioned model aims 73.4 % and the gravity model 74 % of the reference distance. For the distance between the nose and the key, the node 50103415 from the dummy nose and 211933 for the motorcycle key hole are chosen. Thus, the distance in the positioned model amounts to $d_{nk,p} = 701.71 \text{ mm}$ and in the gravity model to $d_{nk,g} = 696.82 \text{ mm}$. The difference between the value of the reference model with $d_{nk,r} = 588.67 \text{ mm}$ and the simulations amounts to 19.2 % and 18.4 %. For the fairing the node 141899 is chosen to measure the distance between the nose and the fairing. For the positioned model, a distance of $d_{nf,p} = 705.47 \text{ mm}$ is determined. The gravity model has a distance of $d_{nf,g} = 704.60 \text{ mm}$. The reference value is given as $d_{nf,r} = 651.61 \text{ mm}$. Therefore the model values are set with a variation of 8.3 % and 8.1 %.

The torso angle is given as $\theta_{torso} = 85.67^\circ$. In the models the angle is measured according to the vertical line. Thus, the reference value is $\theta_{torso,r} = 4.33^\circ$. In the positioned model, this angle was set exactly to the given value, therefore it has a conformity of 100 %. The torso angle in the model after the gravity simulation is given as $\theta_{torso,g} = -0.89^\circ$. Herein, the value changes totally and additionally the dummy model turned around the z-axis with -5.66° . The deviation to the reference distances could be kept in an acceptable way. However, the torso angle couldn't be satisfied. The position of state p is closer to the reference state r. The position in state g has partly greater differences, especially for the torso angle.

5.2.2 Validation with Reference Pictures

The position of the dummy is also validated with the available pictures from the real crash test. Three different perspectives are chosen for the comparison, the frontal view and the two side views. The pictures are taken from the first crash test scenario with $9.5 \frac{\text{km}}{\text{h}}$. For a better comparison, the position is redrawn by lines. Thereby, the shapes of combined lines can be compared.

The comparison of the models from the left side clearly shows differences (see figures 5.1, 5.2 and 5.3). The arm in the reference picture has a greater bending angle than both of the FE models. The head in the simulation models is straighter than the one of the real dummy. For the foot position the model after the gravity simulation shows more correlating angles to the reference position than the model before the gravity simulation. Also the position of the legs are more similar between the real posture and the gravity model. The torso of the dummy looks more inclined in the simulation models than in the reference picture, where although the angle values show the opposite.

By comparing the right sides of the position, almost the same descriptions as for the left side can be made. Thus, the correlating figures are shown in appendix A.

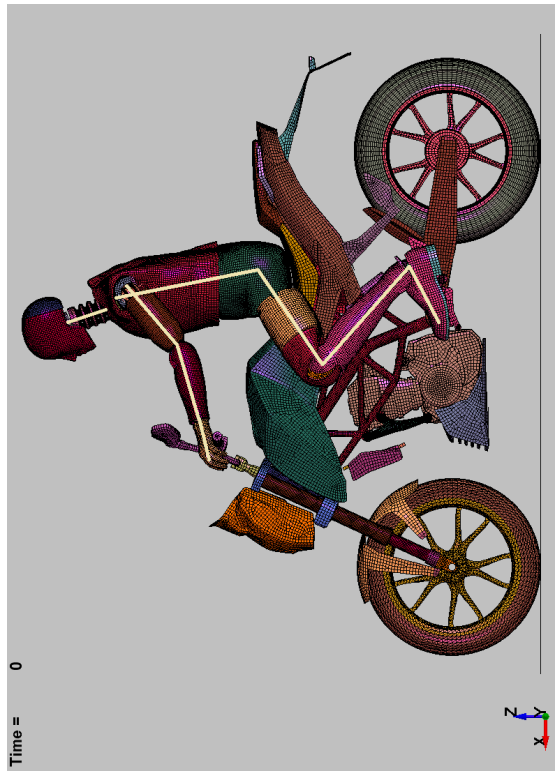


Figure 5.2: Motorcycle and Dummy models before the gravity simulation (0 ms, state p) with reference lines, left side.

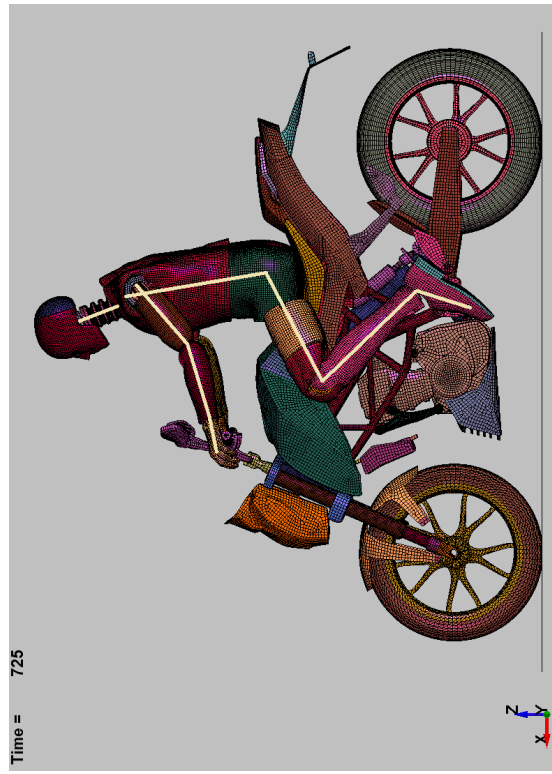


Figure 5.3: Motorcycle and Dummy models after the gravity simulation (725 ms, state g) with reference lines, left side.

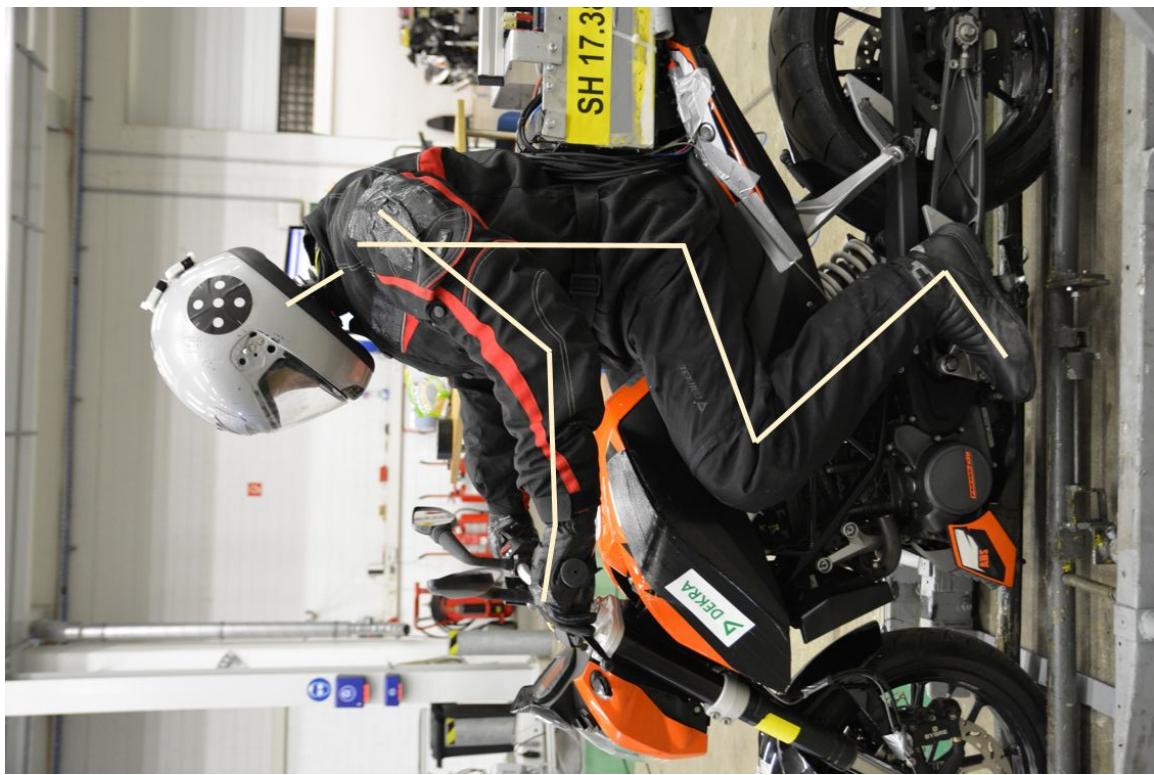


Figure 5.1: Reference position of the dummy with lines (state r), left side.



Figure 5.4: Reference position of the dummy with lines (state r), front view.

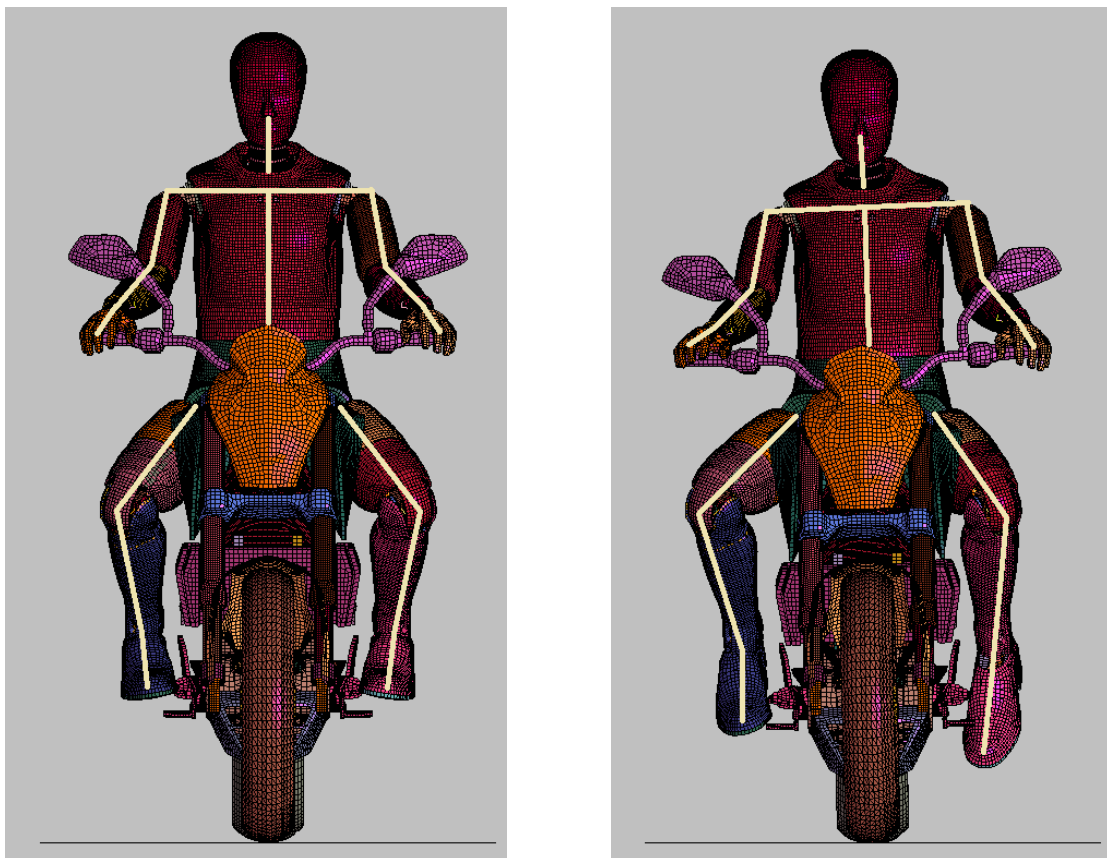


Figure 5.5: Motorcycle and Dummy models before the gravity simulation (0 ms, state p) with reference lines, front view.

Figure 5.6: Motorcycle and Dummy models after the gravity simulation (725 ms, state g) with reference lines, front view.

When the frontal view is considered, only the upper parts of the dummy can be compared to the reference dummy, because there is no picture of the whole front view available (see figures 5.4, 5.5 and 5.6). The reference dummy sits slightly bent to the left side. While the FE dummy model was positioned straightly on the motorcycle. After the gravity simulation, the dummy is leaning towards the right side. Moreover it is obvious, that the dummy position is not reflected anymore after the gravity simulation. Since there is no reference picture of the front view with the position of the knees and feet, there can't be made any statement on the knee distance or the foot position with the reference. The different foot positions of the models before and after the gravity are obviously visible. The left foot of the post gravity model is more stretched and rotated.

The position of state g was closer to the picture of the reference state. However, the dummy was leaning towards the other side. Also the unsymmetrical position after the gravity simulation matches more to the reference, than the position in state p.

In summary of the position validation can be said, that the positions of the FE models only correlate partly with the reference position. In spite of the differences, the position of state g provided an acceptable result, which was used for further simulations.

5.3 Dummy Kinematics

For the validation of the dummy kinematics, the gravity simulation and the crash simulations are considered. Additionally, the animations of the simulations are regarded and evaluated.

5.3.1 Gravity Kinematics

The gravity simulation was run from 0 to 1000 ms. Within this time, the dummy bounces several times off the seat. If there is a force acting on a human body in real life, the body would also bounce a little when he is hitting a seat. Also, the material of the dummy pelvis, causes the rebounding motion, because it is realized with rubber material. However, the z-acceleration data displays great oscillations. The absolute maximum of the acceleration for the motorcycle is $a_{z,m} = 177 \frac{m}{s^2}$ and for the dummy $a_{z,d} = 353 \frac{m}{s^2}$, although the only load on the dummy was the gravity.

After 1000 ms, the right foot of the dummy, was stuck on the footrest for a straight motion. Also, the motorcycle was bending more and more to the right side. That's why the position after 725 ms was chosen. Hereby, it was possible to run the crash simulations for the longest time.

5.3.2 Crash Kinematics

The kinematics of the crash simulation is shown for each test scenario in different time steps. The selected time steps are 0 ms, 25 ms, 50 ms, 75 ms and 100 ms after crash. In this way, the real crash test videos are compared to the animation.

Kinematics at $9.5 \frac{km}{h}$

The dummy kinematics in the first crash test scenario with $9.5 \frac{km}{h}$ is almost the same in the simulation and the experiment (see figures 5.7 and 5.8). The dummy remains sitting on the motorcycle and the feet stay close to the footrest. Also the hands are staying attached to the handlebar. Only the left foot is moving to a straighter position and the hands are grasping around the handlebar.



(a) 0 ms post Crash



(b) 25 ms post Crash



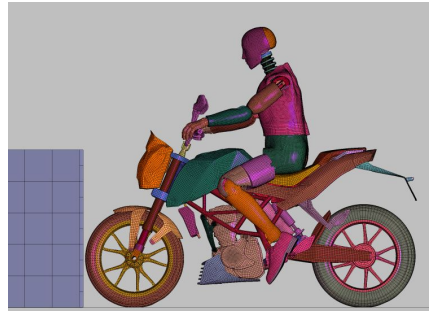
(c) 50 ms post Crash



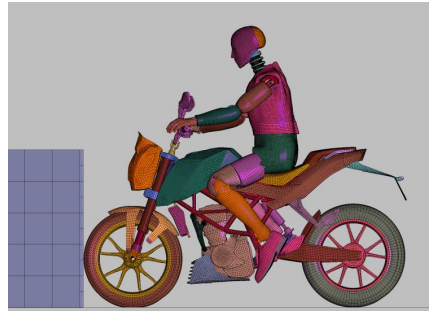
(d) 75 ms post Crash



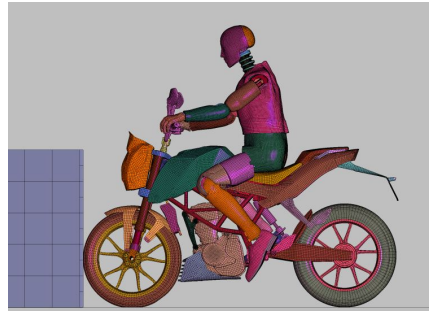
(e) 100 ms post Crash

Figure 5.7: Crash Test $9.5 \frac{km}{h}$.

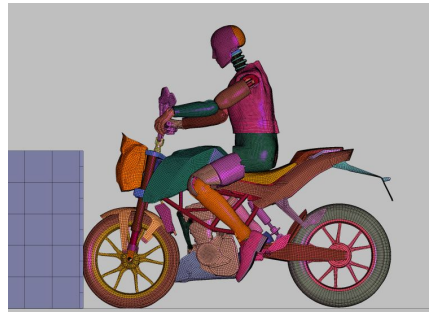
(a) 0 ms post Crash



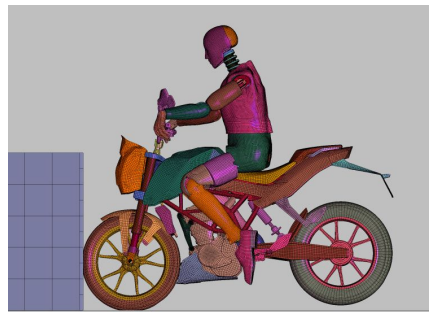
(b) 25 ms post Crash



(c) 50 ms post Crash



(d) 75 ms post Crash



(e) 100 ms post Crash

Figure 5.8: Crash Simulation $9.5 \frac{km}{h}$.



(a) 0 ms post Crash



(b) 25 ms post Crash



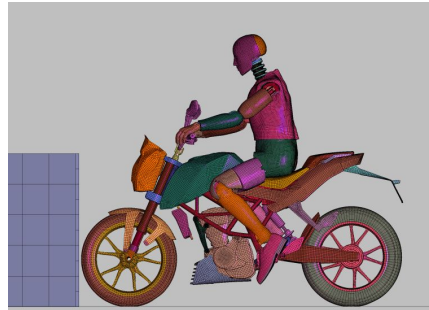
(c) 50 ms post Crash



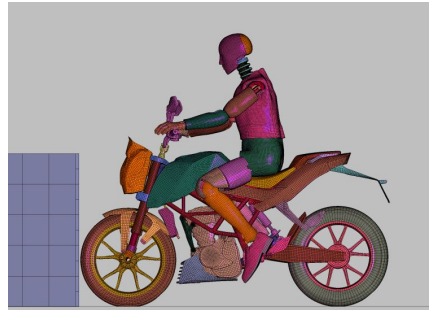
(d) 75 ms post Crash



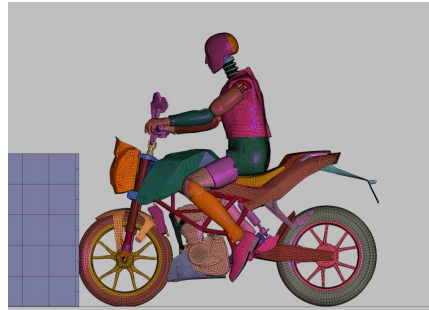
(e) 100 ms post Crash

Figure 5.9: Crash Test $12.8 \frac{km}{h}$.

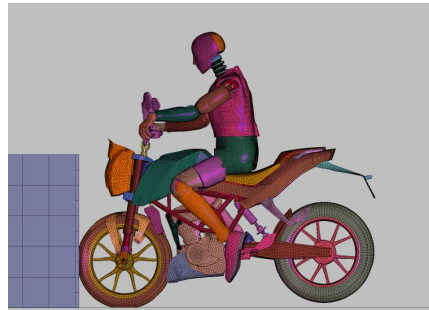
(a) 0 ms post Crash



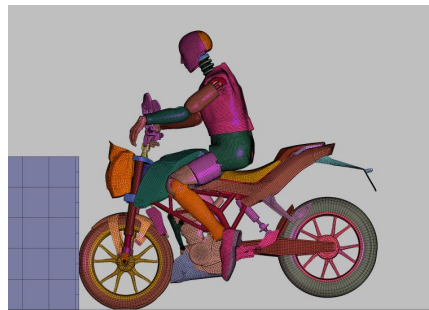
(b) 25 ms post Crash



(c) 50 ms post Crash



(d) 75 ms post Crash



(e) 100 ms post Crash

Figure 5.10: Crash Simulation $12.8 \frac{km}{h}$.



(a) 0 ms post Crash



(b) 25 ms post Crash



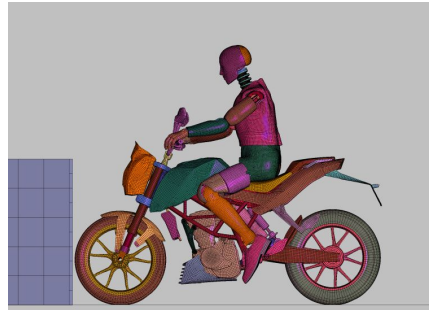
(c) 50 ms post Crash



(d) 75 ms post Crash



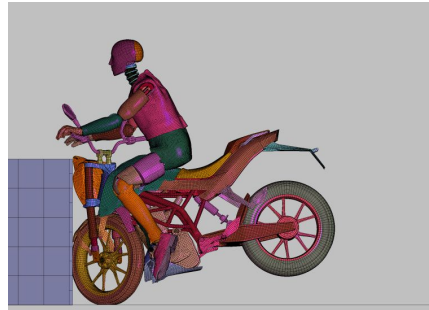
(e) 100 ms post Crash



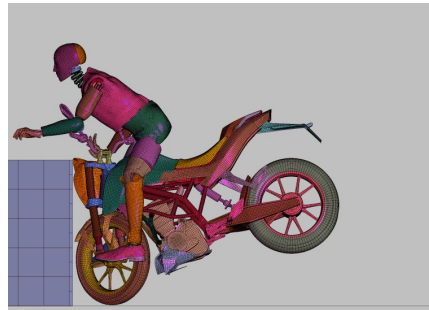
(a) 0 ms post Crash



(b) 25 ms post Crash



(c) 50 ms post Crash



(d) 75 ms post Crash



(e) 100 ms post Crash

Figure 5.11: Crash Test $47.8 \frac{km}{h}$.**Figure 5.12:** Crash Simulation $47.8 \frac{km}{h}$.

Kinematics at 12.8 $\frac{km}{h}$

Also the kinematics of the 12.8 $\frac{km}{h}$ crash scenario is comparable (figures 5.9 and 5.9). The dummy still remains on the motorcycle, but its pelvis lifts itself at 100 ms post crash. The same motion can be seen in the reference picture. Furthermore, in the real crash test, the left hand begins to lose contact to the handlebar at 75 ms. In the simulation, this procedure is also observable. After 100 ms, the left hand isn't in contact with the handlebar anymore.

Kinematics at 47.8 $\frac{km}{h}$

The third crash scenario with 47.8 $\frac{km}{h}$ is shown in the figures 5.11 and 5.12. Obviously, the last picture of the simulation is missing. This is due to the fact that the handlebar of the motorcycle turns to the right and causes negative volume in the arm of the dummy. Hence, for the selection of the gravity positioned dummy, the inclination of the motorcycle was also a big issue. After 50 ms, the rear wheel of the motorcycle lifts and the dummy rises up and moves over the handlebar. This observation is almost the same for the two compared crashes. Since the dummy was wearing a helmet in the experiment, it is difficult to make a statement on the movement of the head and neck. But it can be assumed, that the neck was bent more in the simulation at 75 ms after the crash.

The validation of the kinematics showed comparable results. The movements in the simulation model correlate to the experimental video sequences. Especially the contact of the dummy hands to the motorcycle handlebar was investigated in accordance to the experiment. Thus, the kinematics of the three crash test scenarios could be rebuild in a good way.

5.4 Dummy Load

To validate the acceleration and load on the dummy, the sensor data from the real crash tests are used as a reference. The used sensor data provided by DEKRA were already filtered in accordance to the Society of Automotive Engineers (SAE) standards. Crash test data is commonly filtered with a SAE Channel Filter Class (CFC) [19]. Thus, the acceleration data of the dummy head was filtered with the CFC 1000, which means a filtering with a 1000-Hz low-pass filter. The neck force was also filtered with the CFC 1000, whereas the neck moment was filtered with a CFC 600. Since the signals weren't recorded from a determined time, they had to be cut to a beginning of 50 ms before crash. The crash point was identified by the first deceleration signal of the fork crash sensor. Thus, for the first crash test, there was 96.65 ms data available before crash. For the second crash test 73.75 ms before the crash was available. The crash test with 47.8 $\frac{km}{h}$ had 77.25 ms recorded data before the crash. So, 50 ms data before crash and 100-200 ms after crash were considered.

5.4.1 Data Post-Processing

The post-processing of the simulation data was mainly done with LS-PrePost. In this program, the commonly used SAE CFC filters are already available. To filter crash test data, different filter frequencies are recommended. For the aircraft industry the NASA suggests a CFC 180 filter [39]. In the manual of the FE dummy model, the CFC 108 filter is recommended. To check the quality of the filtered data, the integrated signals should be compared. If there isn't any difference, the lowest checked filter can be used [19, 39].

Thus, a sample check for the simulation data of the x-acceleration signals at 47.8 $\frac{km}{h}$ with different filters (CFC 1000, CFC 600, CFC 300, CFC 180, CFC 108, CFC 60, CFC 50 and

CFC 20) was done. The CFC filter with a frequency of 108-Hz was chosen, because this is the lowest frequency with a good accordance to the raw signal. In figure 5.13 the integration check is shown with only the frequencies around 108-Hz for a clearer view. Therefore, in this work all simulation data was filtered uniformly with the CFC 108-Hz low-pass filter.

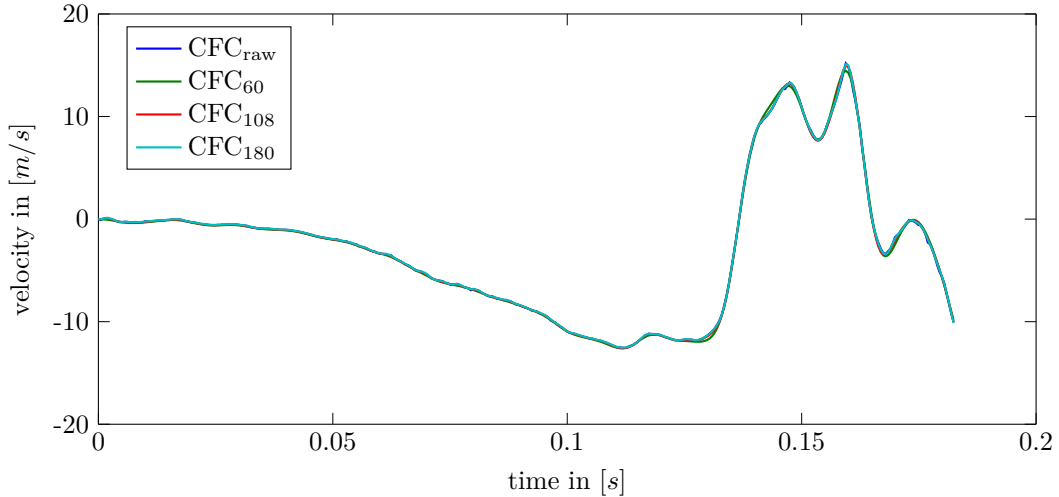


Figure 5.13: Integrated Acceleration Signal as Quality Check.

Additionally, the simulation data had to be prepared to have only 50 ms data before the crash. The simulation was calculated with 100 ms before the crash. Therefore, 50 ms of the simulation signals was cut from the beginning.

The coordinate systems of the head acceleration sensor and the upper neck load cell are equal to the defined coordinates in the FE dummy model. Thus, the x-axes show in ventral direction, the y-axes in lateral direction to the right side and the z-axes in caudal direction (the directions are described in figure 2.1) [69].

5.4.2 Data Comparison

For the validation of the crash simulations, the accelerations of the head, the forces on the neck and the moments on the neck are considered. These simulation results are compared to the experimental data.

As already mentioned in chapter 2, the data is compared according to the corridor method in the CORA software. For this, the corridor method was implemented in MATLAB. In the manual of the CORA software, this method is explained and two norms are mentioned for the rating parameters. Since ISO 9790 treats only lateral impacts, the rating in ISO 18571 was considered. Thus, the inner and outer corridor are defined depending on the absolute maximum of the sensor data and the parameters a_0 and b_0 , which are set to $a_0 = 0.05$ and $b_0 = 0.5$ according to ISO 18571:

$$\delta_i = a_0 * \max(|\text{data}_{\text{sensor}}|), \quad (5.2)$$

$$\delta_o = b_0 * \max(|\text{data}_{\text{sensor}}|). \quad (5.3)$$

For the calculation of the corridor rating, the sensor data and the simulation data are compared in each time step. When the simulation data lays within the inner corridor δ_i , it is rated with $c = 1$. For values that are outside of the outer corridor δ_o , the rating is set with $c = 0$. Is the

simulation data in between the outer and the inner corridor, the rate is calculated by

$$c_i = \left(\frac{\delta_o - |data_{simulation} - data_{sensor}|}{\delta_o - \delta_i} \right)^k, \quad (5.4)$$

wherein k is set to 2. The total rate C_{total} is calculated by taking the number of time steps (n) in account:

$$C_{total,loadcase} = \frac{\sum_{i=1}^n c_{i,loadcase}}{n}. \quad (5.5)$$

The corridor rating was calculated for each load case in every direction and for the resultant curve. The values of the corridor rate lay between 0, when the simulation data isn't in any corridor, and 1, if the simulation data is completely within the inner corridor.

Additionally, the corresponding injury criteria is considered. The values calculated with the simulation data are compared to the ones with the experimental data.

For the calculation of the HIC with the resultant of the head acceleration data, it is necessary to attend the units. The acceleration data need to be given in [g] ($9.807 \frac{m}{s^2}$) and the time in seconds [s]. Additionally, LS-PrePost has a description on how the HIC is calculated (see figure 5.14). This procedure was implemented with the filtered signals in MATLAB.

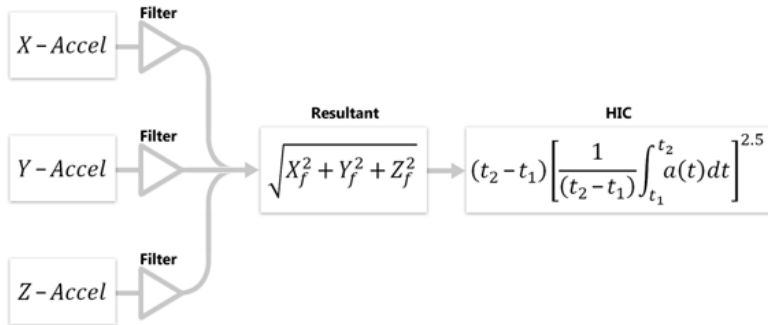


Figure 5.14: The calculation of the HIC in LS-PrePost [50].

Furthermore, the a_{3ms} criterion was calculated by identifying the maximal load for a duration of 3 ms.

For the neck injury criteria, the maximal force values of different load durations are calculated and the boundary conditions are compared to the load data. Besides this, the values of the N_{ij} criteria are calculated.

Load at 9.5 $\frac{km}{h}$

Firstly, the crash test scenario with 9.5 $\frac{km}{h}$ is considered and compared to the measured sensor signals. In all plots, the simulation curve is presented in blue colour and the experimental data was plotted in dark green. Also there is a black line at 50 ms in the plots to visualize the time of the crash impact. For the corridor method, the inner and outer corridors are shaded in green colours. Hereby, the differences between the simulation and the reality are clearly recognizable.

Head Acceleration

For the acceleration on the head, firstly the resultant curve and the results in the three directions x, y and z are observed (figure 5.15).

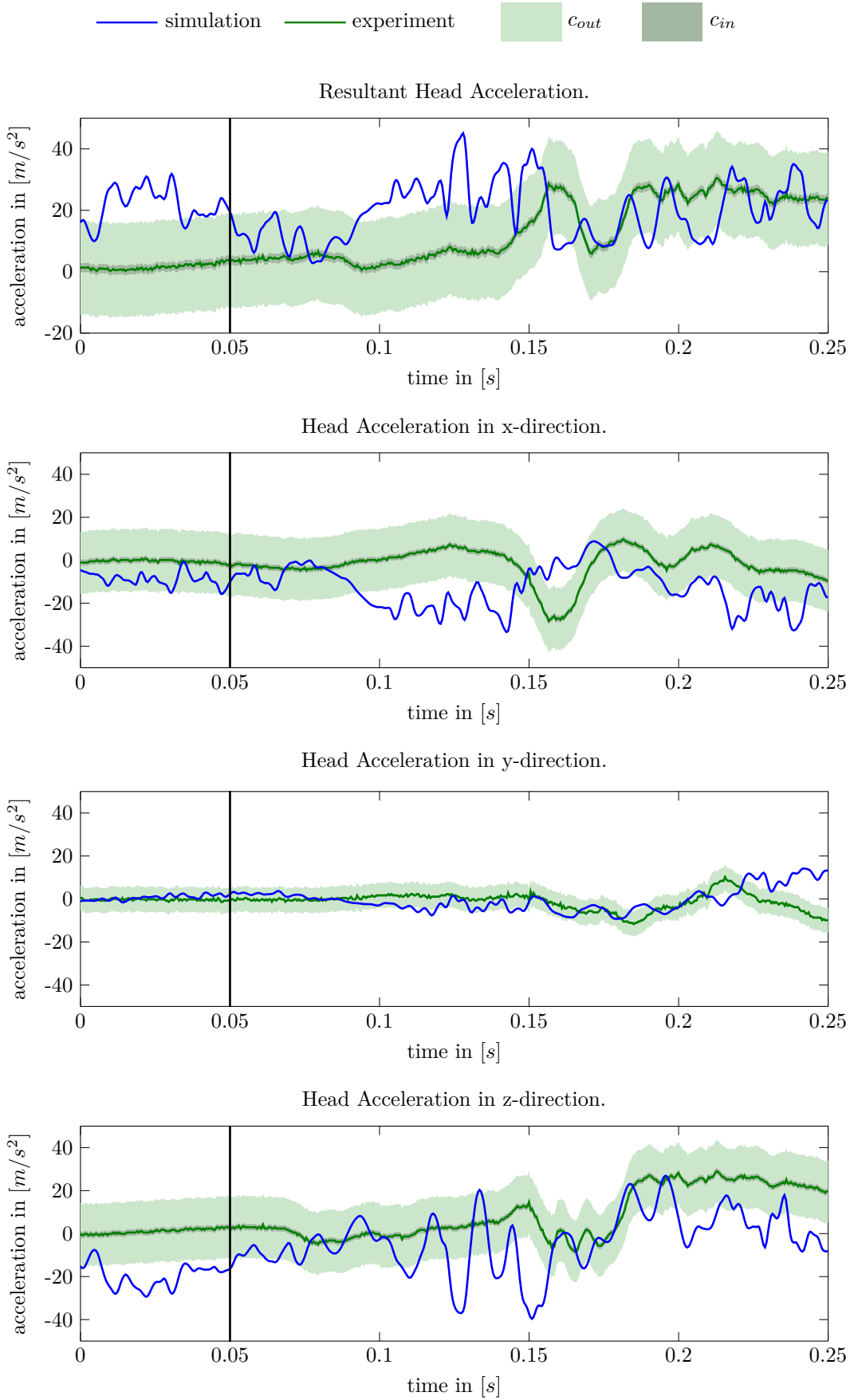
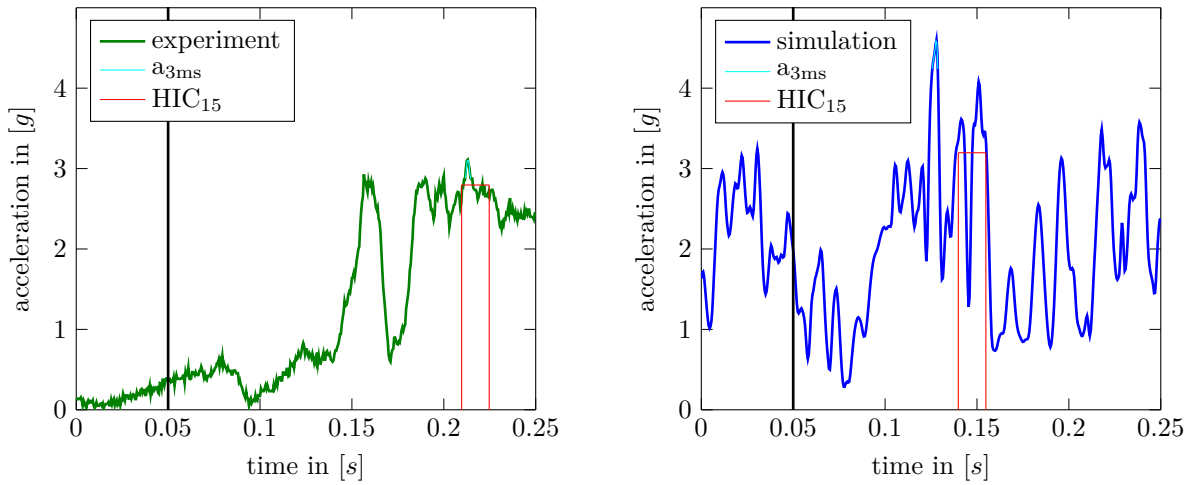


Figure 5.15: Head Acceleration at $9.5 \frac{km}{h}$.

Since the crash took place after 50 ms, it is obvious, that the deceleration of the head is delayed in the simulation and the experimental data. The simulation data is mostly placed outside the inner corridor, which is reflected by the corridor rates in the second column of table 5.1. The course of the x-curve, is almost similar to the experimental curve. But the simulation data is shifted and stretched with an earlier and longer deceleration phase. The minimum values of the deceleration are in the same dimension at about $-30 \frac{m}{s^2}$. In y-direction the two curves fit better. The decreasing starts earlier in the simulation data and the experimental data decelerates faster. Also, the values of the y-acceleration are smaller than the ones for the other directions, as expected, since the motorcycle is driving in x-direction. After 220 ms, the course of the two curves is different. The simulation curve in z-direction shows greater oscillations than in the other directions. But, when only the main progress is considered, the signal is also dropping and raising as in the experimental data. The minima of the deceleration differ around $30 \frac{m}{s^2}$. Thus, in the simulation, there is a higher deceleration on the head than in the experiment.



(a) *Experiment: resultant acceleration in [g] with $HIC_{15,e} = 0.196$.* (b) *Simulation: resultant acceleration in [g] with $HIC_{15,s} = 0.274$*

Figure 5.16: Head Injury Criteria (HIC) at $9.5 \frac{km}{h}$

The HIC_{15} was calculated with the resultant acceleration (figure 5.16). On the left side, the experimental data and on the right side the simulation curve is presented. The red lines are demonstrating the time phase of 15 ms for the maximal HIC. The HIC value for the experimental data is calculated as $HIC_{15,e} = 0.196$ and for the simulation as $HIC_{15,s} = 0.274$. As expected, the threshold of $HIC_{15,max} = 700$ was not reached. The injury criterion correlates with 71 %, which is an acceptable result. The time interval of the HIC calculation is earlier in the simulation, because of the greater deceleration in z-direction.

The a_{3ms} criterion was also calculated for the two compared signals. The maximal acceleration for 3 ms is also shown in figure 5.16 by the traced signal in bright blue colour. The values of the a_{3ms} criterion vary about 32 %. Thus, for the simulation data it was calculated with $a_{3ms,s} = 4.44 g$ and for the experimental data with $a_{3ms,e} = 3.02 g$.

Neck Force

The simulated neck forces are also compared with the experimental crash signals and the corridors (plots in figure 5.17).

By observing the force in x-direction, it is clearly visible, that the simulation data is shifted, so that the decreasing of the force takes place earlier. But the course of the data looks similar.

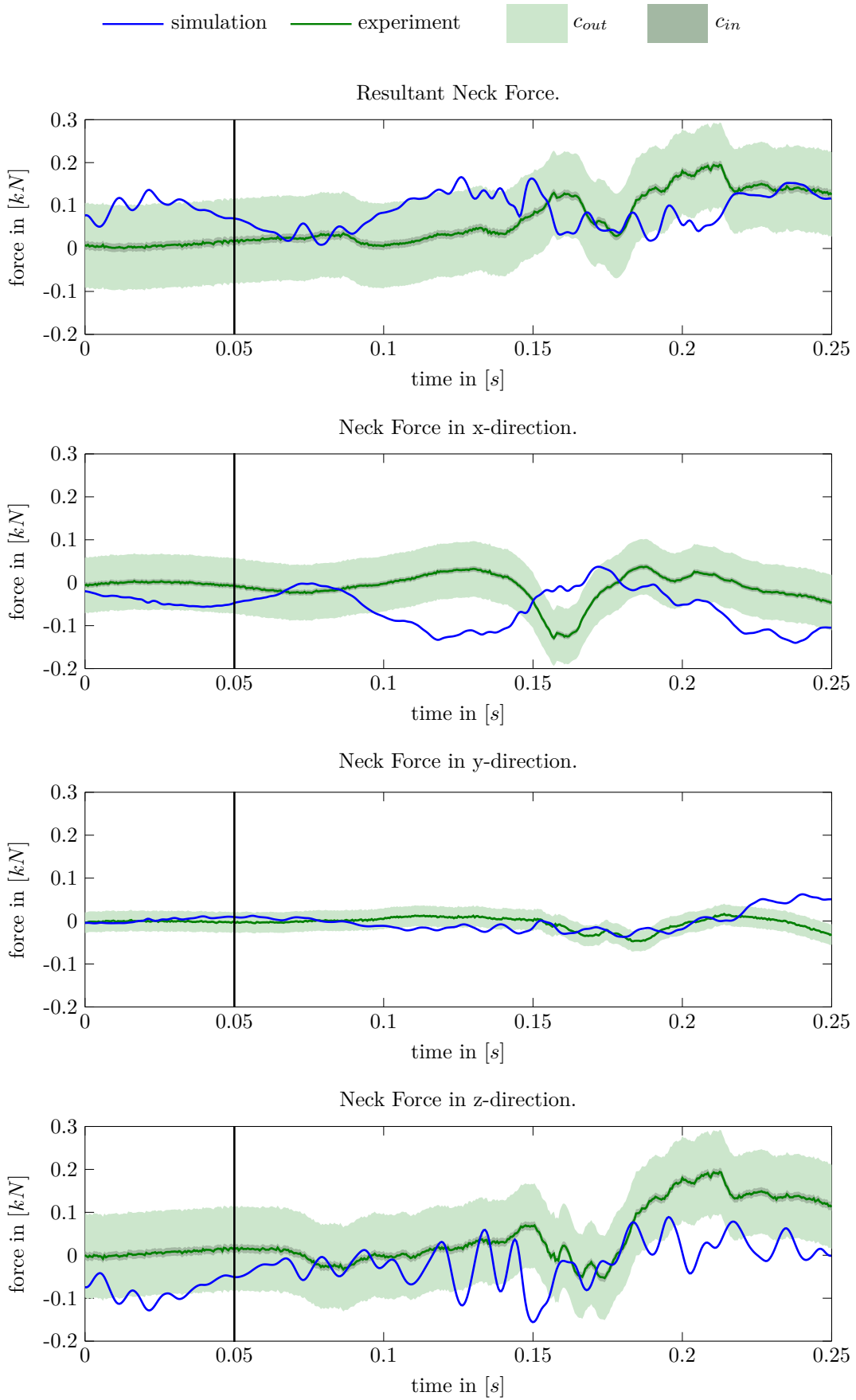


Figure 5.17: Neck Force at $9.5 \frac{km}{h}$.

Table 5.1: Corridor Rate of the $9.5 \frac{km}{h}$ Crash

Direction	Head Acceleration	Neck Force	Neck Moment
X	0.222	0.190	0.435
Y	0.421	0.406	0.194
Z	0.220	0.321	0.551
Resultant	0.256	0.380	0.537

Also the maximum values are barely different with 7.2 %. The force in y-direction is smaller than the other forces. Also the curves present a decreasing and increasing behaviour. However this cannot be seen as clearly as in the experimental data. For the z-force applies the same as for the acceleration. The shape of the course correlates with the sensor signals. And the maximum values show 20.5 % difference. Though, the simulation data does not fit the inner corridors well, the corridor rate is between 0.406 and 0.190 for the force comparison (see column three in table 5.1).

When the neck injury criterion (NIC) is considered, the load is plotted with its duration time (figure 5.18 and 5.19). The shear and tensile force curve are compared to the threshold values which are given in the occupant protection regulations (like ECE-R 94). The maximal values for the corner points are calculated, they do not exceed the boundary at any time. And also the experiment values and the simulation values are in the same dimensional range (see table 5.2).

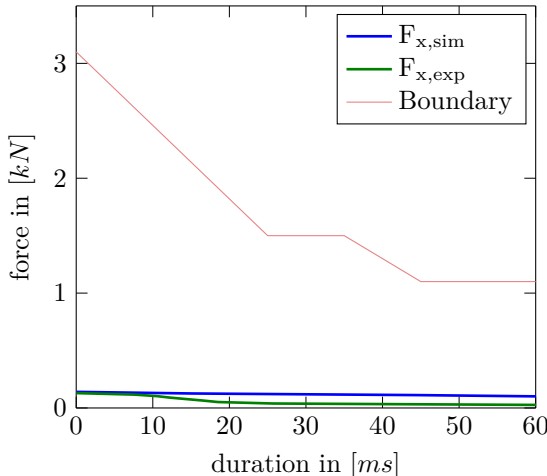


Figure 5.18: Neck Shear Force F_x at $9.5 \frac{km}{h}$ with Threshold.

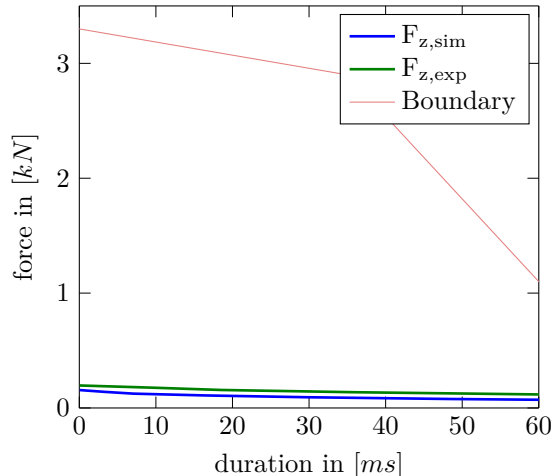


Figure 5.19: Neck Tensile Force F_z at $9.5 \frac{km}{h}$ with Threshold.

Neck Moments

The moments, which act upon the neck, are displayed in figure 5.20. For the different directions, all the plot axes have the same limits. Thereby, the dimensional difference can be clearly observed. The moment in y-direction is the greatest, because as a consequence of the crash, the dummy bends his neck to the front and back. The course of the moment in x- and z-direction are minimal and closely the same to the experimental data. For the y-moment, the shape of the course is also correlating with the experimental data. However, the simulation data is shifted to an earlier decrease and increase of the signal. Though, the dummy neck is moving more in the simulation than in the experiment. The corridor rating for the resultant

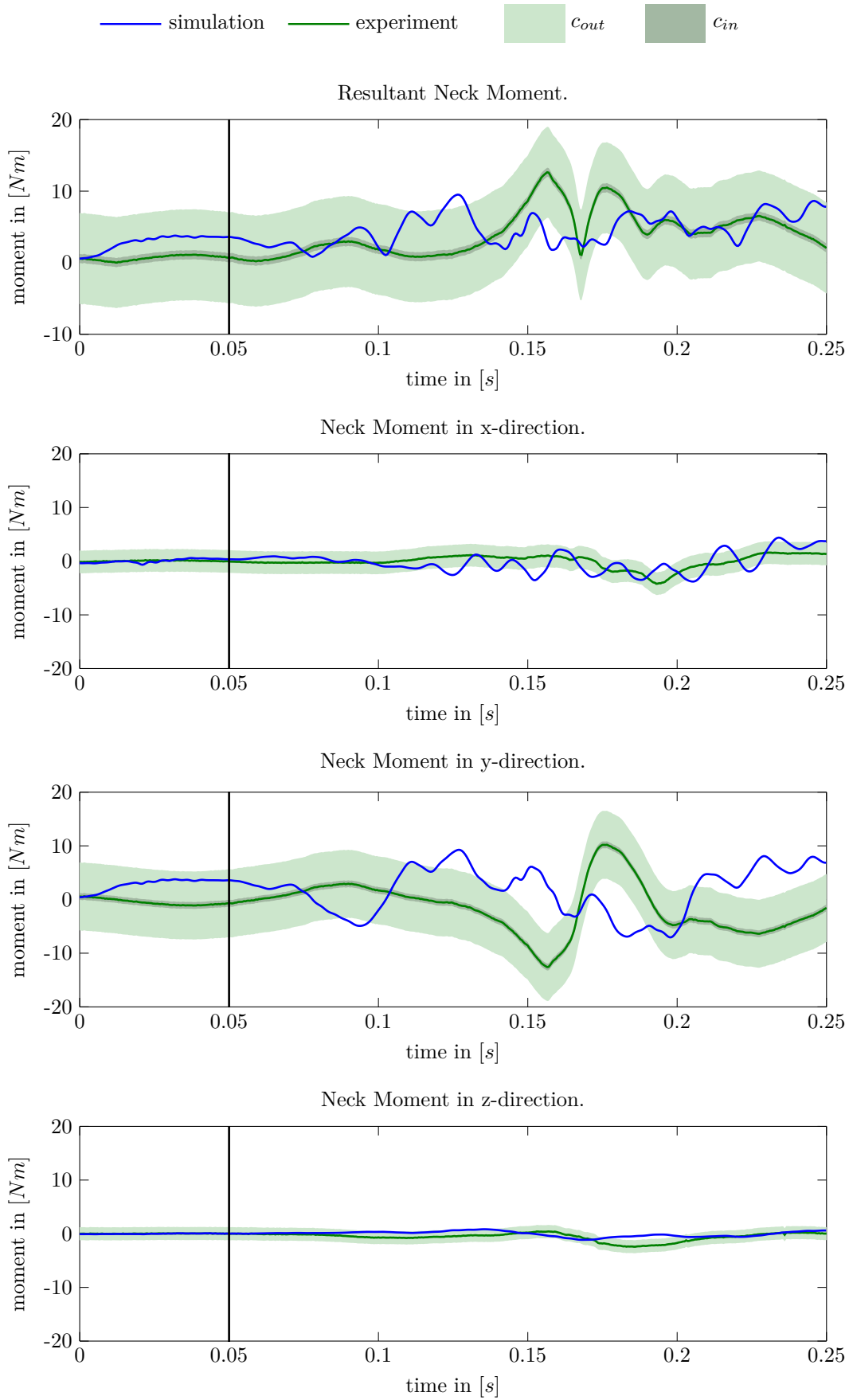


Figure 5.20: Neck Moment at $9.5 \frac{km}{h}$.

Table 5.2: NIC values of the $9.5 \frac{km}{h}$ Crash (check marks show, whether the values are below the threshold values)

	Threshold	Experiment + Check	Simulation + Check
F_x for 0ms [kN]	3.1	0.130 ✓	0.140 ✓
F_x for 25-35ms [kN]	1.5	0.084 ✓	0.123 ✓
F_x for 45ms [kN]	1.1	0.046 ✓	0.109 ✓
F_z for 0ms [kN]	3.3	0.196 ✓	0.156 ✓
F_z for 35ms [kN]	2.9	0.162 ✓	0.094 ✓
F_z for 60ms [kN]	1.1	0.150 ✓	0.075 ✓
M_y [Nm]	57	12.657 ✓	9.268 ✓

moment signal is the best. More than 53 % of the resultant moment lies within the inner corridor (compare with the forth column of table 5.1).

The bending moment around the y-axis is compared to the boundary value (see the last row of table 5.2). The results show, that the moment at $9.5 \frac{km}{h}$ doesn't reach the maximal load condition with $M_{y,max} = 57 \text{ Nm}$. The maximum value of the simulation data is calculated with 9.268 Nm and for the experimental data with 12.657 Nm. Thus, the simulation and the experiment correlate for 73.2 %.

Furthermore, the N_{ij} criterion is calculated with the tensile force F_z and the bending moment M_y , which are normed by the reference values of chapter 2. The boundary condition with a maximum of 1 is kept for this crash test scenario, which is evinced in table 5.3.

Table 5.3: N_{ij} values of the $9.5 \frac{km}{h}$ Crash (check marks show, whether the values are below the threshold value $N_{ij} < 1$)

N_{ij}	Loads	Experiment + Check	Simulation + Check
N_{te}	Tension + Extension	0.123 ✓	0.065 ✓
N_{tf}	Tension + Flexion	0.062 ✓	0.043 ✓
N_{ce}	Compression + Extension	0.103 ✓	0.078 ✓
N_{cf}	Compression + Flexion	0.042 ✓	0.055 ✓

To summarize the load results of the crash test with $9.5 \frac{km}{h}$, it can be said, that the load of the simulation correlates partly with the experimental data. Additionally, it can be retained, that there aren't any injury predictions to the dummy above the boundary conditions, in the experiment as well as in the simulation.

Load at $12.8 \frac{km}{h}$

The load results of the crash test with $12.8 \frac{km}{h}$ are also shown and validated. Since the velocities from the first and the second crash scenario differ only with a speed difference of $3.3 \frac{km}{h}$, there aren't many different results expected.

Head Acceleration

The acceleration of the head is shown for the resultant and the three directions in figure 5.21. In x-direction, there is a deceleration in the simulation after the crash, which isn't seen in the experiment. Afterwards, the acceleration increases and correlates with the experimental signal.

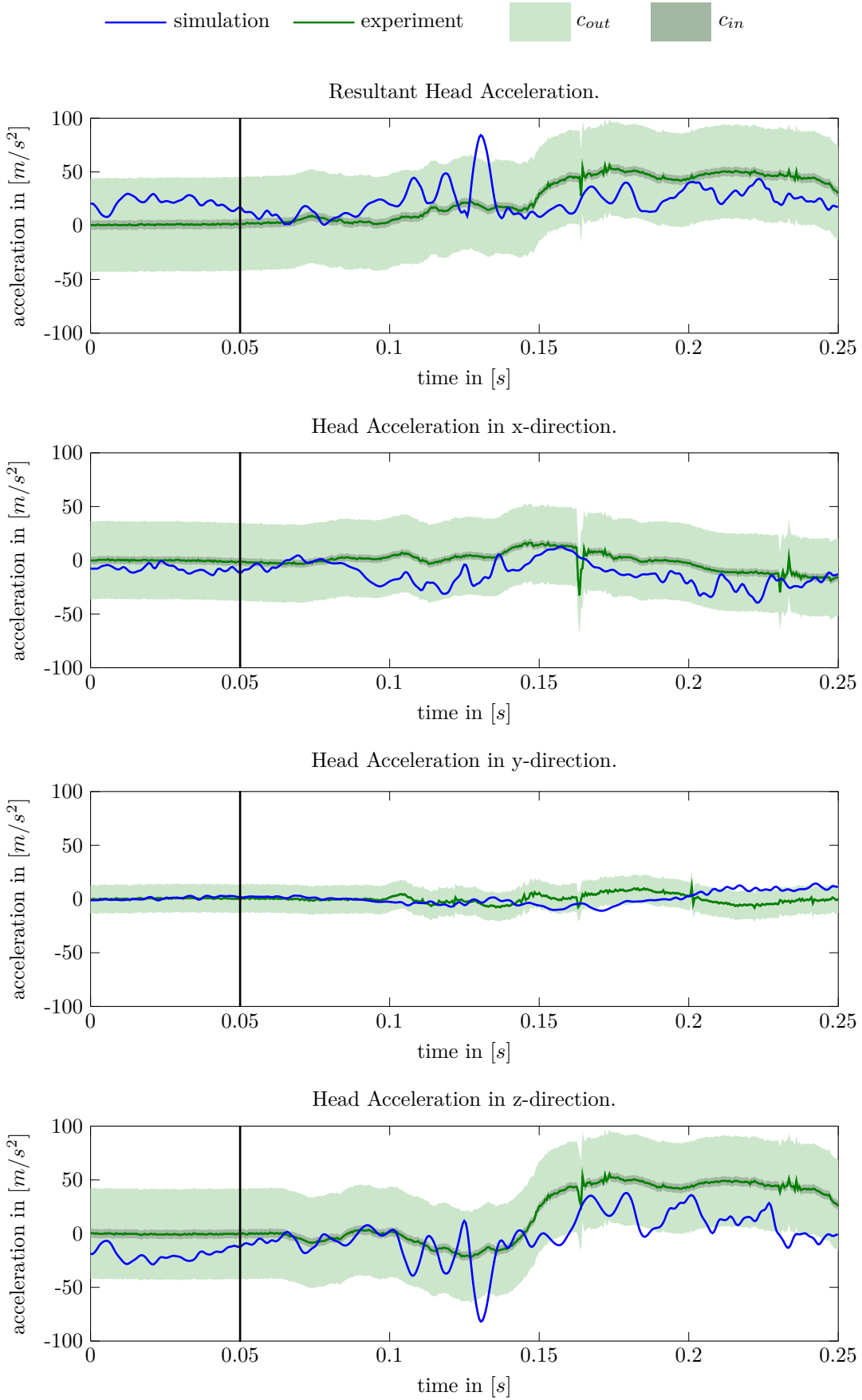
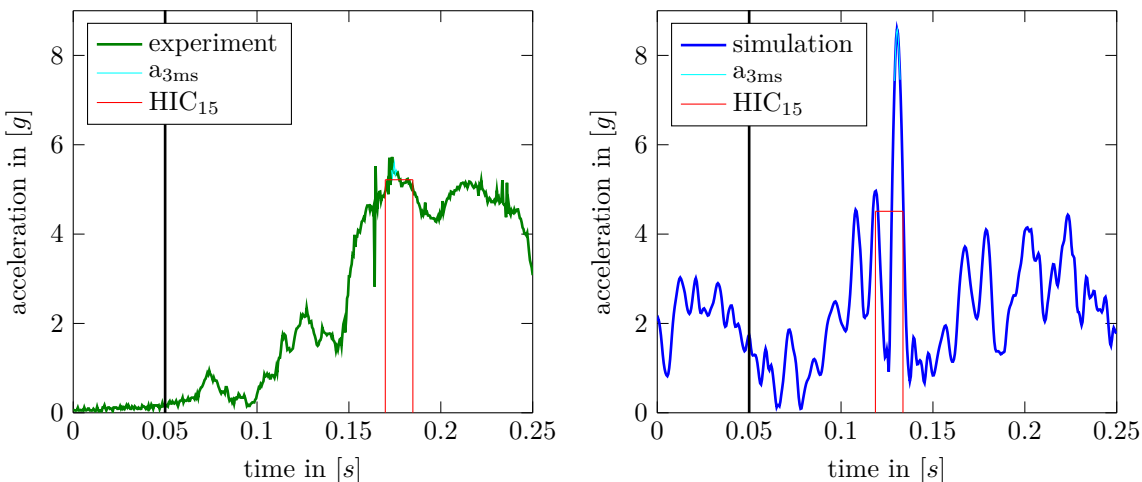


Figure 5.21: Head Acceleration at $12.8 \frac{km}{h}$.

As expected, the acceleration in y-direction is small, but the peaks don't correlate with each other. For the z-acceleration, there are again oscillations. But the shape of the simulation curve matches with the experiment with a deceleration at 100 ms and an acceleration afterwards. Also the dimensions of the curves are consistent. In this direction, the greatest acceleration values are recorded, which is caused by the lifting of the dummy pelvis.

The corridor rate for the resultant acceleration data is 0.503, which means 50.3 % of the signal is close to the inner corridor. The values for the z-acceleration are smaller, because of the oscillations (see table 5.4).

The head injury criterion was determined with the resultant acceleration (figure 5.22). Hereby, the HIC_{15} of the simulation data was computed to $HIC_{15,s} = 0.648$, the experimental HIC_{15} however to $HIC_{15,e} = 0.932$. The difference between the two values is 30.5 %. Also the time interval of the HIC calculation does not agree. The peak of the simulation data is earlier than the one in the experiment. For the a_{3ms} criterion, the maximal acceleration with a duration of 3 ms is calculated. In the simulation the value amounts to $a_{3ms,s} = 8.179 g$ and in the experiment to $a_{3ms,e} = 5.408 g$ (shown in bright blue colour in figure 5.22).



(a) *Experiment: resultant acceleration in [g] with $HIC_{15,e} = 0.932$.* (b) *Simulation: resultant acceleration in [g] with $HIC_{15,s} = 0.648$.*

Figure 5.22: Head Injury Criteria (HIC) at $12.8 \frac{km}{h}$

Table 5.4: Corridor Rate of the $12.8 \frac{km}{h}$ Crash

Direction	Head Acceleration	Neck Force	Neck Moment
X	0.604	0.240	0.579
Y	0.554	0.380	0.302
Z	0.431	0.345	0.599
Resultant	0.503	0.336	0.513

Neck Force

The forces that act on the neck are shown in figure 5.23. The course of the curves are fitting with a minor corridor rate of 33.6 % (third column in table 5.4).

In x-direction, there is a decrease of the force which isn't measured in the experiment. But the maximum force after 0.157 s is coincident, only the value of the simulation signal is minimally

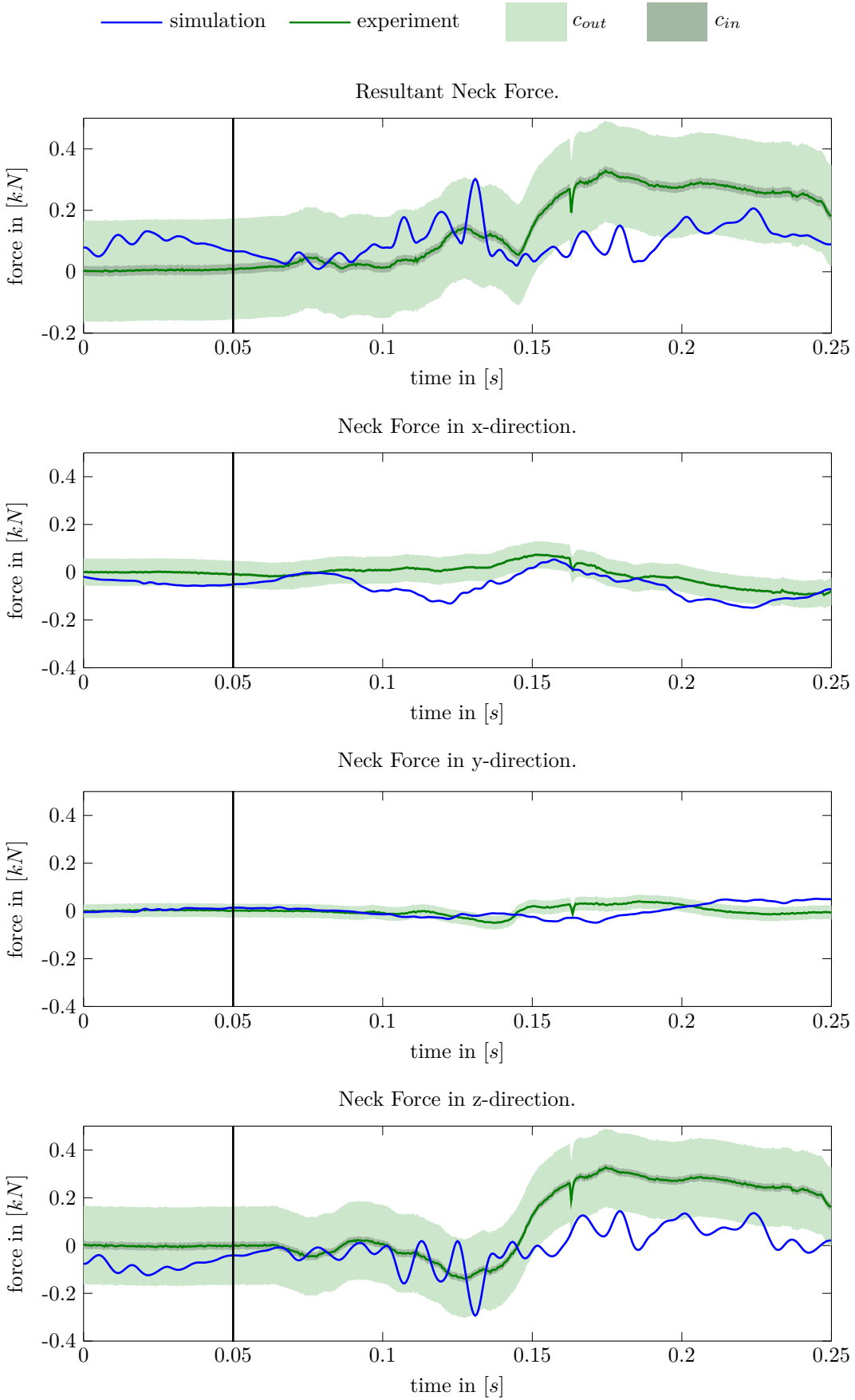


Figure 5.23: Neck Force at $12.8 \frac{km}{h}$.

smaller than the one from the experiment. If the simulation data of the y-force is inverted, it correlates good with the experimental data. This can be explained with the position of the FE dummy after the gravity simulation, where the dummy model was leaning to the opposite side than the reference dummy. Because the motion in this direction is less, there is only a small force. The force in z-direction is the greatest. Without the oscillations, the course of the curve would fit with the decreasing and increasing force. But the maximum value of the simulation is smaller than in the experiment.

The neck injury criteria for the forces is calculated and compared to the thresholds (figure 5.24 and 5.25). The axial tension and the shear force are very small in the experiment and also in the simulation. Thereby, the boundary conditions are kept. The values for the force in x-direction are laying close to each other. Whereas, there is a bigger difference in the z-force (5.5).

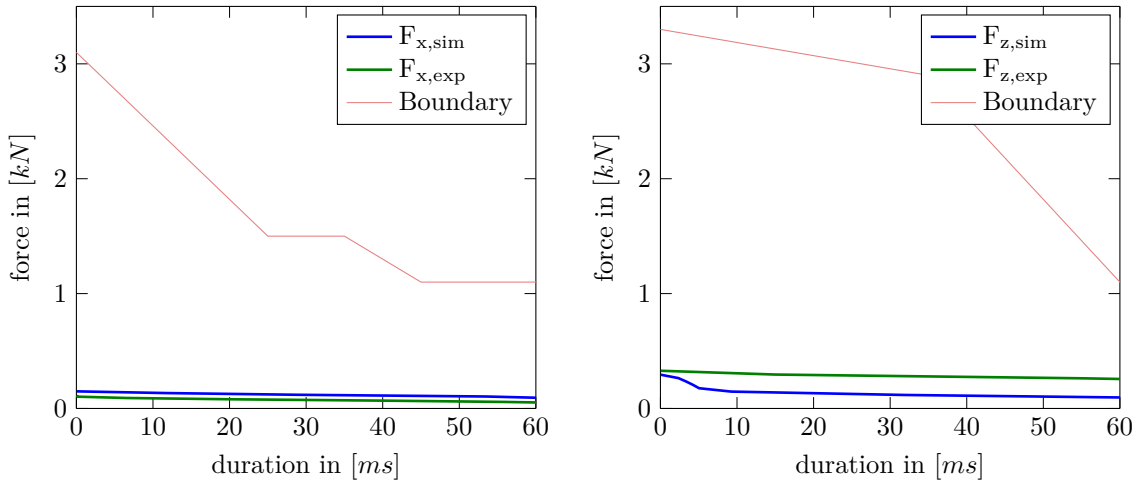


Figure 5.24: Neck Shear Force F_x at $12.8 \frac{km}{h}$ with Threshold. **Figure 5.25:** Neck Tensile Force F_z at $12.8 \frac{km}{h}$ with Threshold.

Table 5.5: NIC values of the $12.8 \frac{km}{h}$ Crash (check marks show, whether the values are below the threshold values)

	Threshold	Experiment + Check	Simulation + Check
F_x for 0ms [kN]	3.1	0.114 ✓	0.149 ✓
F_x for 25-35ms [kN]	1.5	0.086 ✓	0.131 ✓
F_x for 45ms [kN]	1.1	0.075 ✓	0.122 ✓
F_z for 0ms [kN]	3.3	0.328 ✓	0.294 ✓
F_z for 35ms [kN]	2.9	0.293 ✓	0.100 ✓
F_z for 60ms [kN]	1.1	0.285 ✓	0.079 ✓
M_y [Nm]	57	14.020 ✓	10.287 ✓

Neck Moments

The comparison of the neck moments in the simulation and in the experiment can be found in figure 5.26. The resultant moment course fits, with an exception of the peak. The maximum of the experimental data, is not reflected in the simulation data. The corridor rate of the resultant moment is calculated with 0.513 (see column four in table 5.4). In x-direction, the

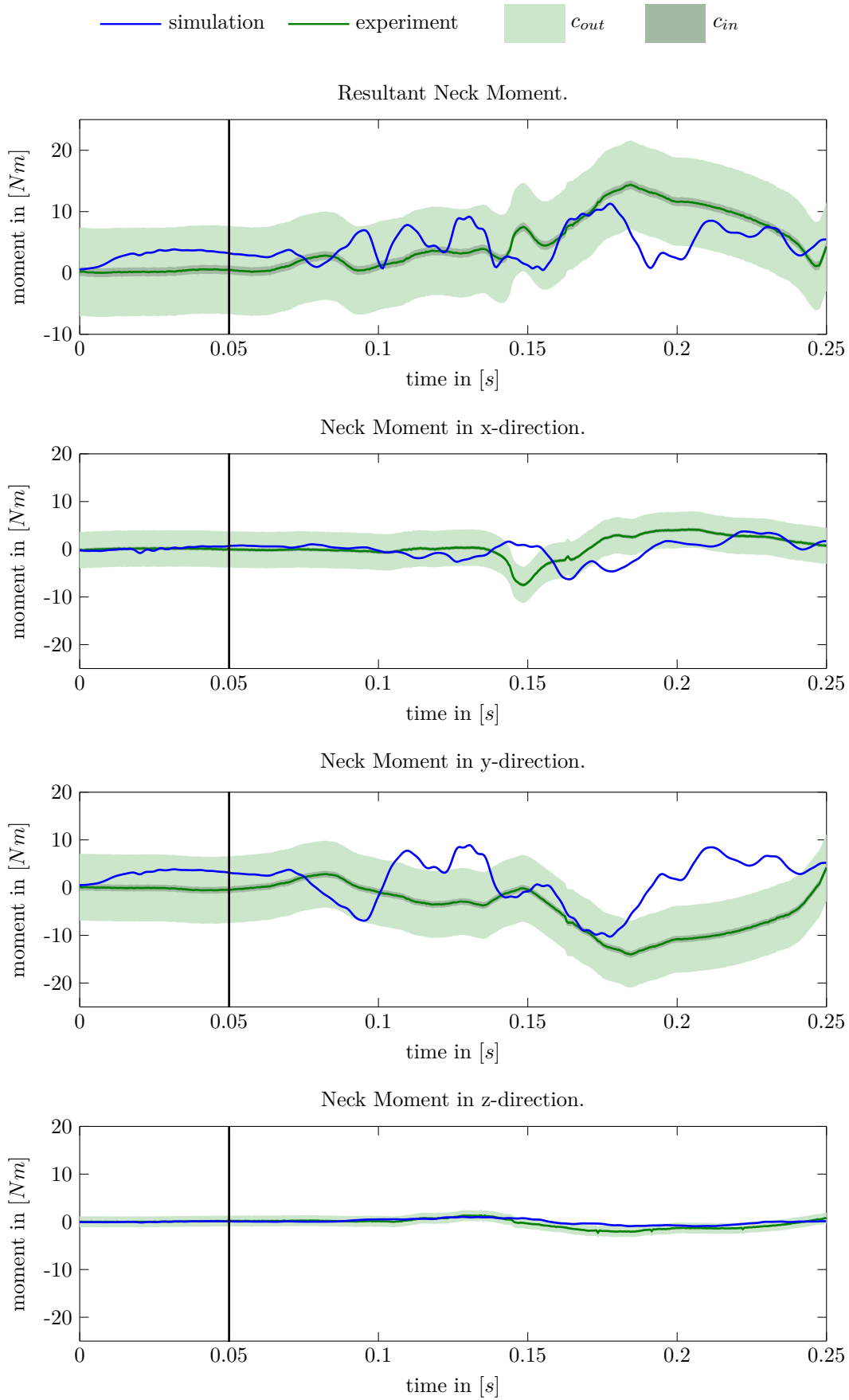


Figure 5.26: Neck Moment at $12.8 \frac{km}{h}$.

extreme values of the curve don't fit. But the simulation data might be delayed. It is obvious, that the moment in y-direction has the greatest peaks. But the time points of the peaks and the dimensions do not correlate to each other. In the simulation, the dummy neck is bending back and forth faster and more often. In z-direction, the moment is very small and the course correlates between the simulation and the experimental data.

Additionally, the neck injury criteria is considered and validated. The moment around the y-axis is within the boundary value (compare last row of table 5.5). The difference of the maximal moment in y-direction amounts to 26.7 %. And also the N_{ij} criteria is fulfilled in every load condition. However, the values of the experiment and the simulation are different.

Table 5.6: N_{ij} values of the $12.8 \frac{km}{h}$ Crash (check marks show, whether the values are below the threshold value $N_{ij} < 1$)

N_{ij}	Loads	Experiment + Check	Simulation + Check
N_{te}	Tension + Extension	0.152 ✓	0.097 ✓
N_{tf}	Tension + Flexion	0.062 ✓	0.050 ✓
N_{ce}	Compression + Extension	0.127 ✓	0.124 ✓
N_{cf}	Compression + Flexion	0.036 ✓	0.076 ✓

All in all, the second crash scenario is valid to the injury criteria. The signals of the simulation have partly different courses and the corridor rate is calculated with a minimum of 0.260 for the force in x-direction and a maximum of 0.655 for the moment in z-direction.

Load at $47.8 \frac{km}{h}$

The results for the fast crash scenario with $47.8 \frac{km}{h}$, show clearly, that the impact on the dummy was greater than in the other crashes. The calculation of the simulation ended 82.5 ms after the crash because of numerically instabilities. Hence, the available simulation data is compared to the corresponding experimental signals, again with 50 ms before the crash. In total 132.5 ms of the signals are compared.

Head Acceleration

In figure 5.27, the head accelerations are plotted. The signals are almost within the defined corridors, even though, the peak values don't fit the experimental course. This also represents the good corridor rate with values above 60 % (see table 5.7, second column). In x-direction, there is more acceleration in the simulation data than in the experimental signal. After the increasing accelerations of the simulation data, the signal declines. However, the course before and after the movements correlate good with the experiment. For the acceleration in y-direction, there is an increasing part at the end of the simulation. Whereas the experimental data lays in a smaller range. But the two curves fit very good. The z-acceleration is oscillating, while the experimental data shows a slight decrease and increase. The absolute maximum of this curve is with $525 \frac{m}{s^2}$ 32.8 % greater than the compared experimental value. In this direction, the greatest acceleration was measured and calculated, because the dummy was rising up as a consequence of the crash.

The HIC calculation shows, that the crash test with $47.8 \frac{km}{h}$ still doesn't exceed the threshold values. The HIC_{15} of the simulation data is extremely higher with $HIC_{15,s} = 119.57$ than the same calculated HIC of the experimental data $HIC_{15,e} = 18.80$. Also the time intervals don't match. The a_{3ms} criterion satisfies the boundary condition with $a_{3ms,max} = 80 g$. But with $a_{3ms,s} = 53.93 g$ the criterion for the simulation signal is greater than for the experimental signals, which amounts to $a_{3ms,e} = 23.29 g$.

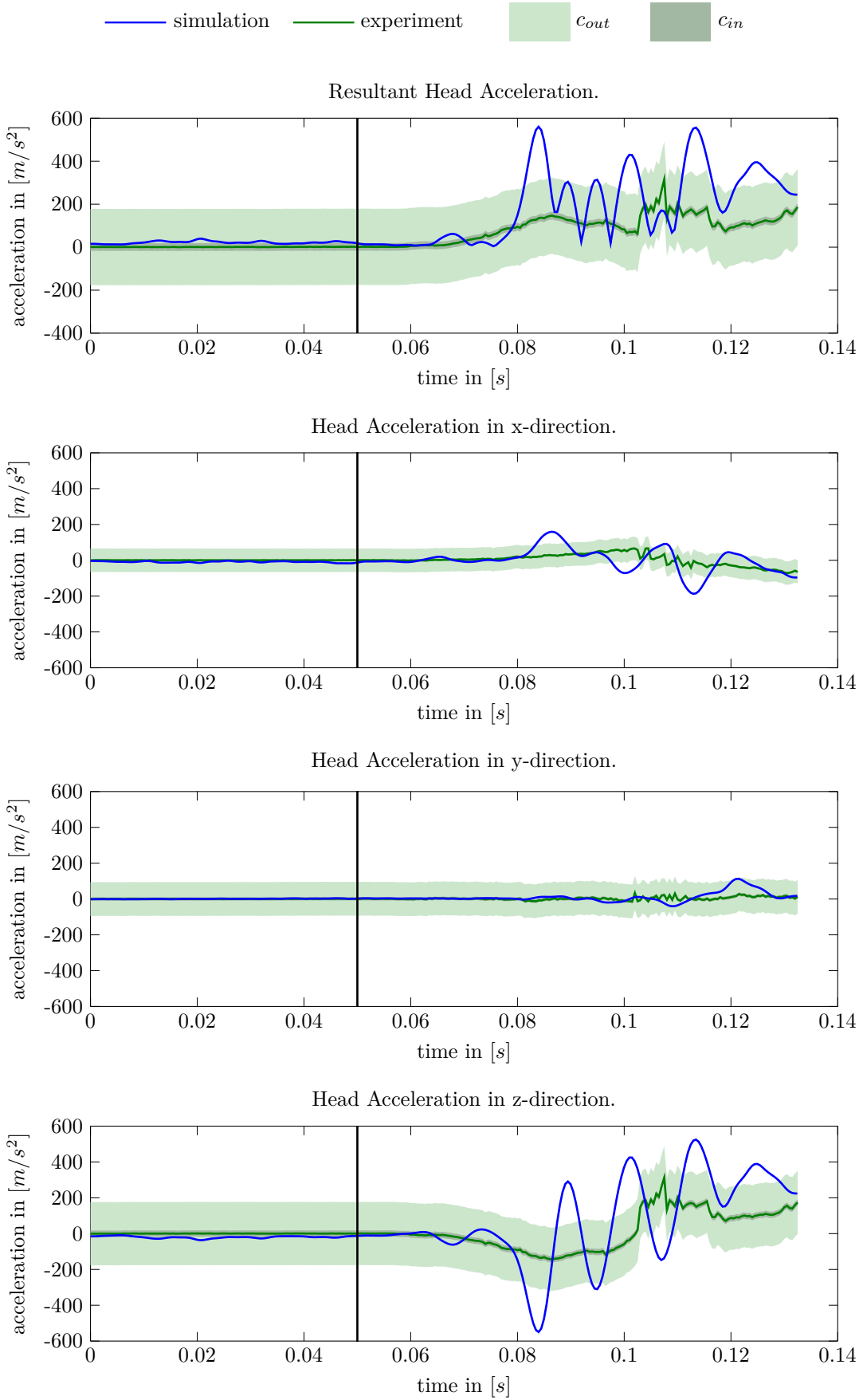
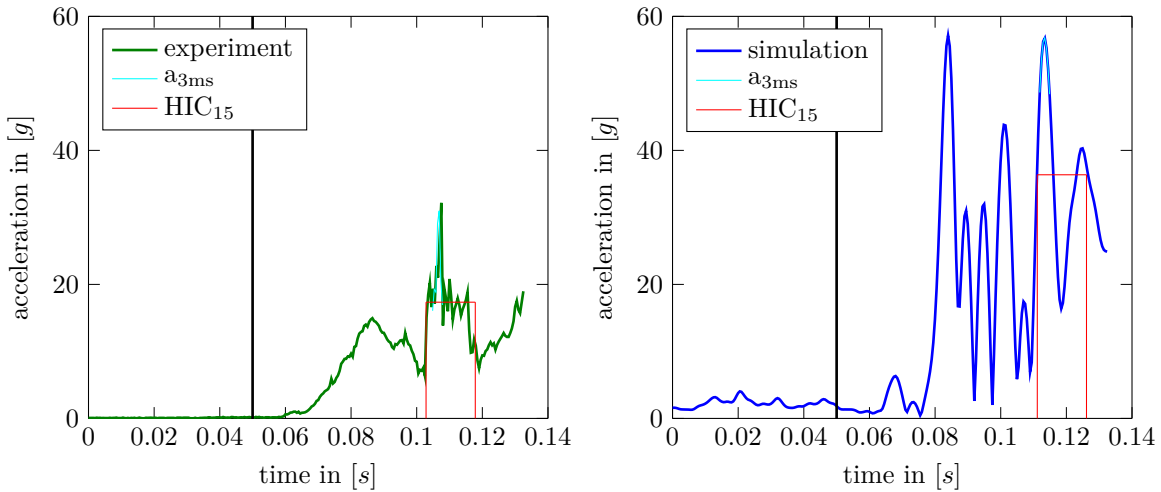


Figure 5.27: Head Acceleration at $47.8 \frac{km}{h}$.

Table 5.7: Corridor Rate of the $47.8 \frac{km}{h}$ Crash

Direction	Head Acceleration	Neck Force	Neck Moment
X	0.685	0.534	0.654
Y	0.889	0.659	0.606
Z	0.603	0.634	0.660
Resultant	0.641	0.674	0.678



(a) *Experiment: resultant acceleration in [g] with $HIC_{15,e} = 18.8$.* (b) *Simulation: resultant acceleration in [g] with $HIC_{15,s} = 119.57$.*

Figure 5.28: Head Injury Criteria (HIC) at $47.8 \frac{km}{h}$

Neck Force

In the plots of figure 5.29 the forces on the dummy neck are demonstrated.

The neck force of the simulation has a good correlation to the experimental data according to the corridor rates (table 5.7). For the resultant, there is an accordance of 67.4 %.

The shapes of the simulation data are fitting to the ones of the experimental data. The decreasing of the x-force correlates to each other, with a few exceptions. In the simulation, there is more change in the force than in the experimental data. Also the y-force curves lay close and distinguish barely. Again, there is more force in the z-direction of the simulation than in the z-direction of the experiment. The z-force is also the greatest force, which appeals on the neck. In the simulation it ranges from 2.26 kN unto -2.27 kN and in the experiment from 1.47 to -0.85 kN. Thus, the minimum and the maximum of the simulation are greater than in the experiment.

Upon closer inspection, it can be determined, that in all crash scenarios, the course of the acceleration and the course of the force is nearly the same in every direction. This is as expected, because, the forces act on the neck as a result of the deceleration and acceleration of the head.

The observation of the neck injury criterion shows, that during the scenario, all signals are within the defined thresholds (figure 5.30 and 5.31). The shear force and the tensile force, calculated depending on the duration of the load, have almost the same course in the experiment and the simulation. The simulation values of the forces are greater than the experimental ones for the most durations. The maximum shear force of the simulation is calculated as

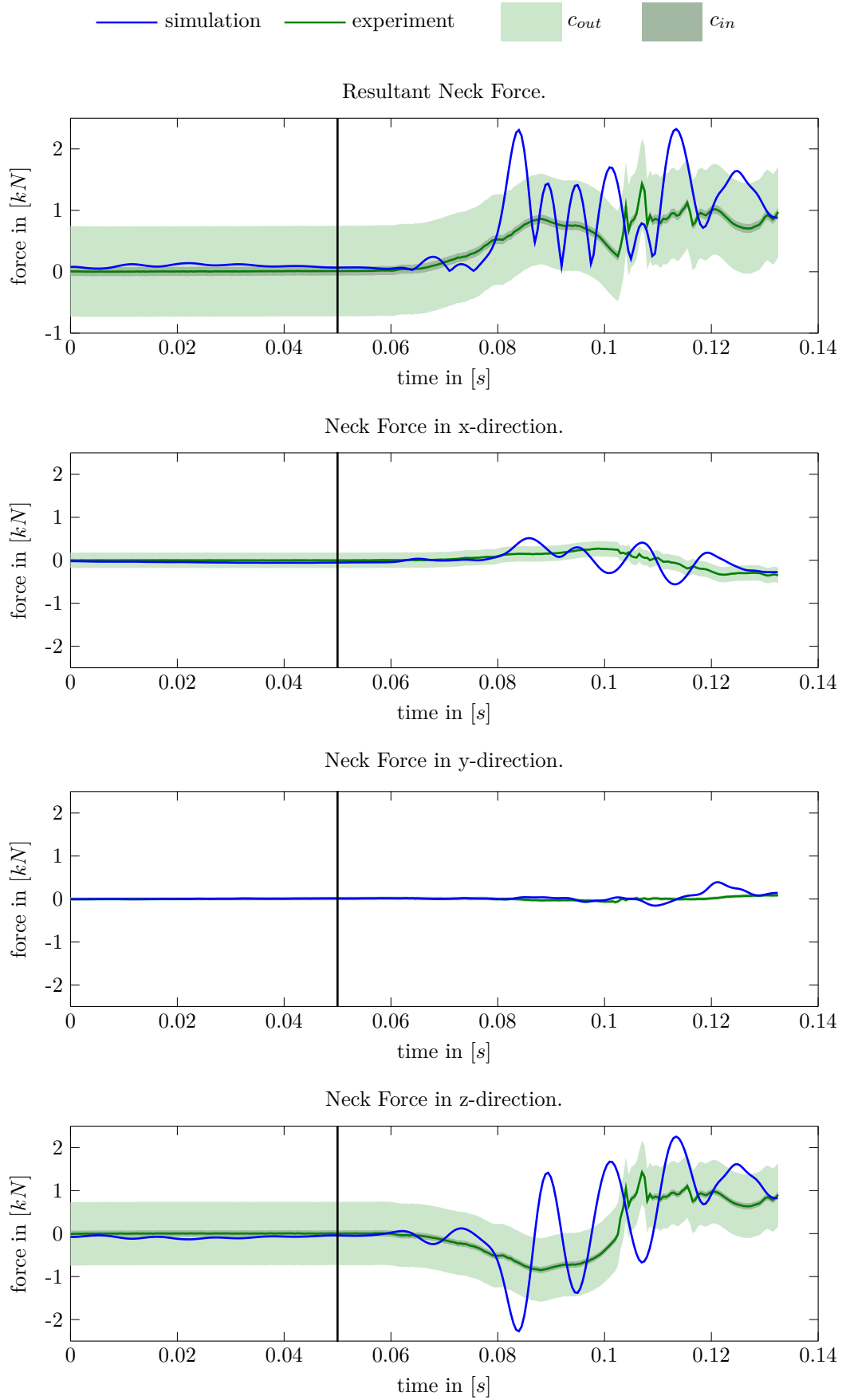


Figure 5.29: Neck Force at $47.8 \frac{km}{h}$.

$F_{x,max,s} = 0.561 \text{ kN}$ and the experimental maximum amounts $F_{x,max,e} = 0.358 \text{ kN}$. The difference between these values amounts to 36.2 %. For the tensile force, the higher value at the beginning and the decrease afterwards are clearly visible. The maximal values have a difference of 35.3 %, which was also visible by comparing the peak values in figure 5.29. The forces at the corner points of the boundary conditions are calculated and presented in table 5.8.

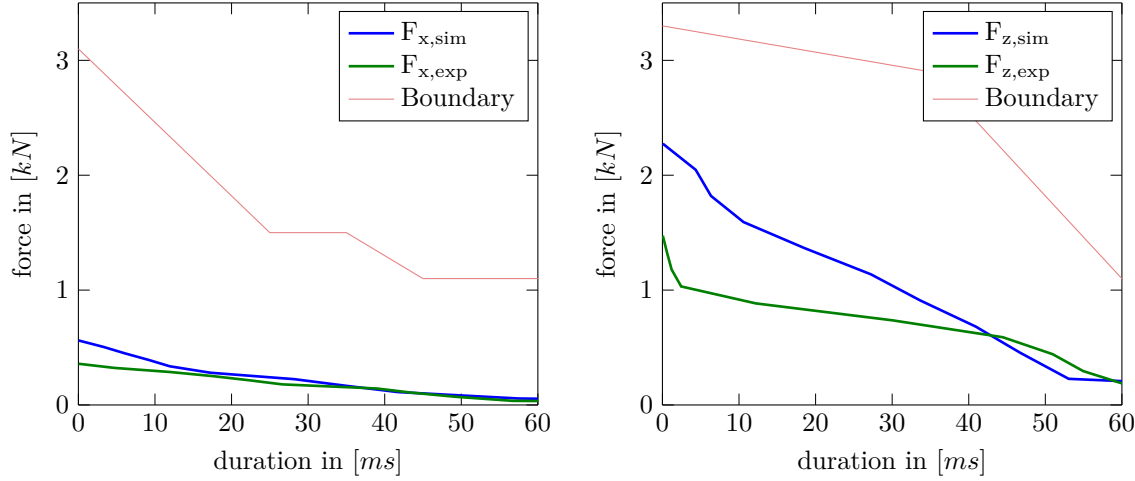


Figure 5.30: Neck Shear Force F_x at $47.8 \frac{\text{km}}{\text{h}}$ with Threshold **Figure 5.31:** Neck Tensile Force F_z at $47.8 \frac{\text{km}}{\text{h}}$ with Threshold

Table 5.8: NIC values of the $47.8 \frac{\text{km}}{\text{h}}$ Crash (check marks show, whether the values are below the threshold values)

	Threshold	Experiment + Check	Simulation + Check
F_x for 0ms [kN]	3.1	0.358 ✓	0.561 ✓
F_x for 25-35ms [kN]	1.5	0.203 ✓	0.196 ✓
F_x for 45ms [kN]	1.1	0.124 ✓	0.119 ✓
F_z for 0ms [kN]	3.3	1.474 ✓	2.275 ✓
F_z for 35ms [kN]	2.9	0.674 ✓	1.041 ✓
F_z for 60ms [kN]	1.1	0.299 ✓	0.414 ✓
M_y [Nm]	57	46.990 ✓	56.09 ✓

Neck Moments

The moments measured in the neck section, are compared in figure 5.32. It is obvious, that in the simulation data, there are more and greater peaks than in the experiment. The values of the peaks in the simulation signal in x-direction are higher. In the experiment, there is less motion. The bending to the left and right side around the x-axis of the dummy neck in the simulation animation is shown in figure 5.33 for the initial position (0 s) and the two peaks at 0.12 s and 0.13 s. The highest moment is measured in y-direction. A look on the y-moment leads to the assumption, that the simulation data is shifted to an earlier and faster decrease. There is also more movement in the simulation than in the experiment, especially the increase of the moment at 0.08 s. However, the dimensions of the minima correlate in a range between -46 Nm and -56 Nm. In z-direction, the moment is very small and close to 0. Thus, there is

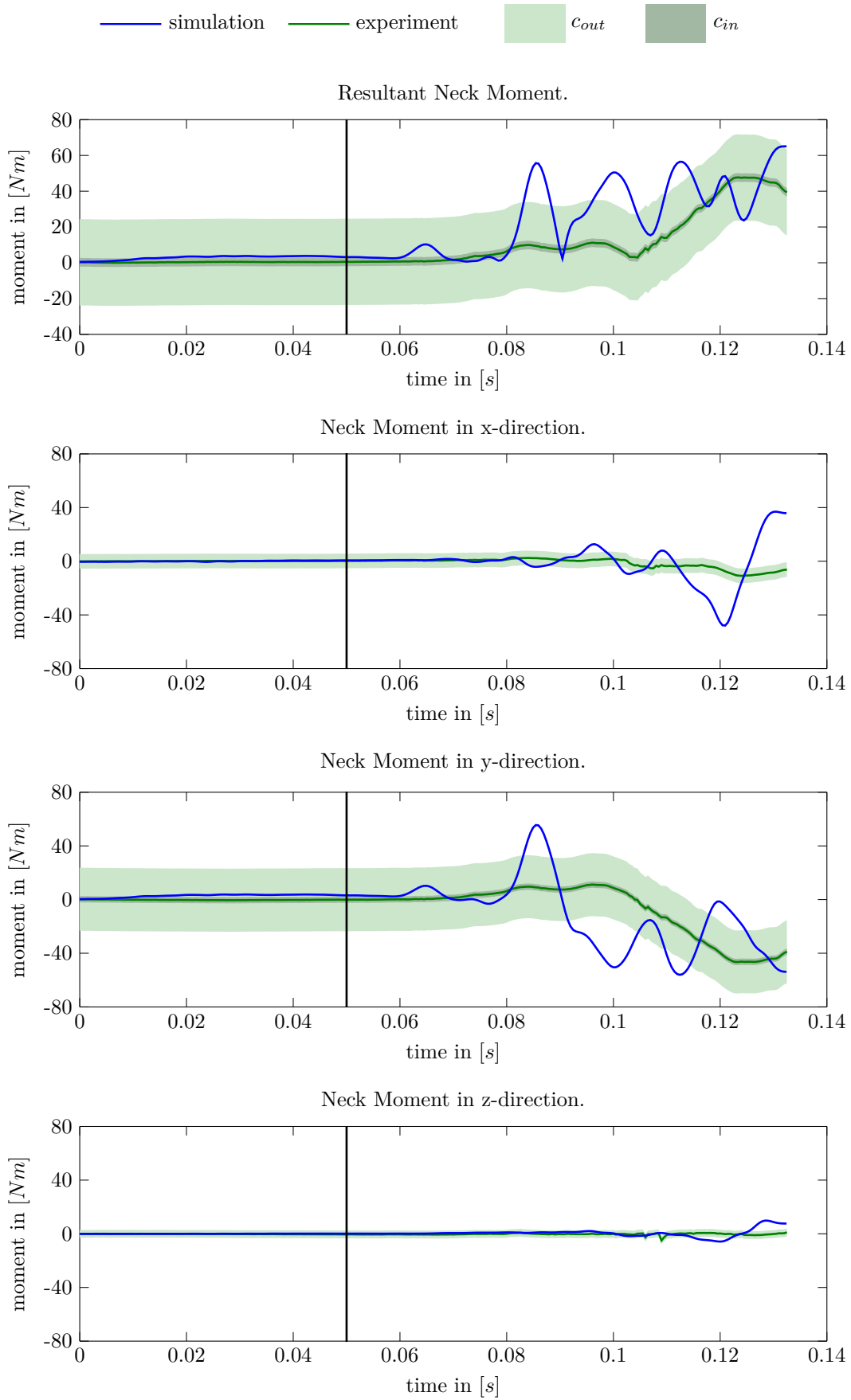


Figure 5.32: Neck Moment at $47.8 \frac{km}{h}$.

only a minimal turning of the neck around the vertical axis.

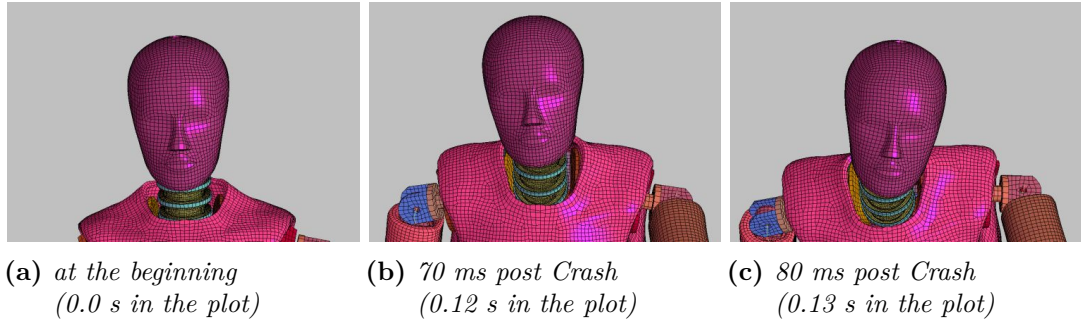


Figure 5.33: Neck Movement at Crash with $47.8 \frac{\text{km}}{\text{h}}$ in a frontal view.

For the analysis of the neck injuries, a closer look at the moment around the y-axis has to be taken. In figure 5.34 the experimental and simulation data with the boundary at 57 Nm is shown. Thereby it is obvious, that the simulation moment is close to the threshold in the positive and negative range, but does not exceed. Thus, for the simulation and the experiment there are still no heavy injury estimations for the dummy.

Additionally, the N_{ij} was calculated and listed in table 5.9. In no direction, the maximal acceptable value of 1 is reached or overstepped. But the values of the experiment and the simulation are different with a maximum of 69 % for the compression and flexion.

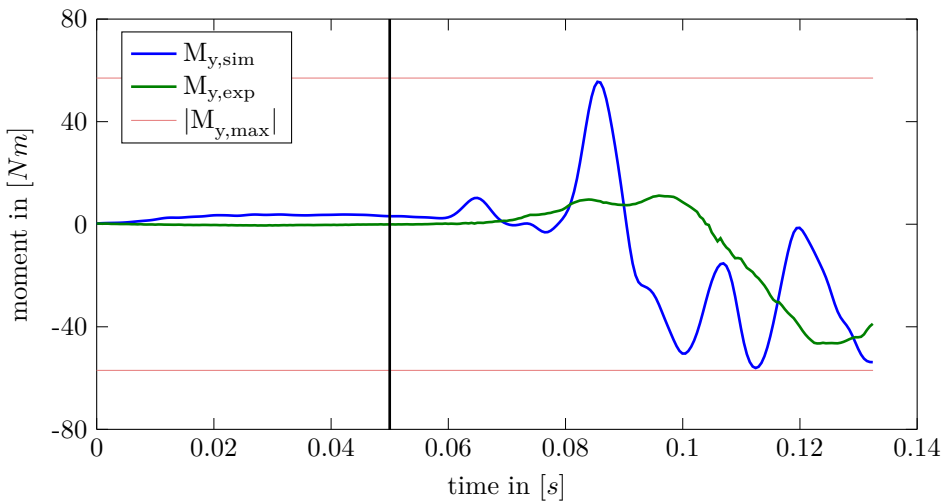


Figure 5.34: Experiment and Simulation Neck Moment at $47.8 \frac{\text{km}}{\text{h}}$.

Table 5.9: N_{ij} values of the $47.8 \frac{\text{km}}{\text{h}}$ Crash (check marks show, whether the values are below the threshold value $N_{ij} < 1$)

N_{ij}	Loads	Experiment + Check	Simulation + Check
N_{te}	Tension + Extension	0.565 ✓	0.747 ✓
N_{tf}	Tension + Flexion	0.253 ✓	0.511 ✓
N_{ce}	Compression + Extension	0.486 ✓	0.785 ✓
N_{cf}	Compression + Flexion	0.174 ✓	0.549 ✓

To summarize the third crash simulation, it can be said, that the acceleration and forces are valid to the experimental data. The values of the load maximum have partly different dimensions. By considering the moment signals, the simulation shows extremely high peaks. For the simulation, even the boundary value of the bending moment could be kept. However, the simulation didn't have a normal termination and therefore, the statements should be considered with caution.

Compared to the other crash test scenarios, the curves of the $47.8 \frac{km}{h}$ test correlate partly about 20 % better.

6 Discussion

The dummy position and the validation results are interpreted and discussed in this chapter. Thereby the used models are observed and argued. Furthermore, the validation aspects of chapter 5 are discussed by considering three points: position, kinematics and load.

6.1 Model

In this section, the used motorcycle and dummy model are discussed. Additionally, the contact specifications, which were made in this work, are analysed. Therefore, the used friction values and tiebreak values are considered.

6.1.1 Dummy Model

The FE dummy model, which is used in this work, was the 50th percentile sitting Hybrid III dummy from LSTC. This dummy is normally used for automotive crash tests, thus its pelvis has a pre-formed sitting structure. Since this model is a free accessible model with the LS-DYNA licence, it is kept simple and is mostly modified by the user for the actual purpose. There aren't any tests with this dummy on motorcycles, therefore, the dummy wasn't optimized for this use case.

In the ISO 13232-3, the special dummy model for motorcycle crash tests is described. This dummy has several modifications, like a more detailed neck, because in this region more load acts on a motorcyclist than on a car occupant. Also the head should be modified, to suit a helmet [37].

Thus, the used dummy model wasn't specific for a motorcycle crash test scenario. The material of the dummy model is mainly elastic and rubber like. However, the dummy has no bones or comparable parts in his hands and feet. Therefore, the hands and feet make strange movements within the simulations. In the gravity simulation, the fingers are moving randomly. Also the shoes behave elastic, which also led to difficulties within the gravity simulation.

Furthermore, the validity of the dummy could be questioned, when the load results are regarded. However, the dummy was calibrated by LSTC with a neck extension and flexion test and a thorax impact procedure. Thus, it is assumed, that the dummy is valid.

6.1.2 Motorcycle Model

Additionally, the motorcycle model can be discussed. The used motorcycle is a new model. It is only validated by comparing the x acceleration. The fork and tire behaviour isn't valid compared to the real motorcycle. At the beginning of the gravity simulation, the motorcycle lifts its front wheel. The springs which are defined in the fork might not be implemented correctly. Also the rotation of the tires is not implemented yet. In the real test case, the motorcycle parts are deformable and breakable, this is not yet implemented in the simulation model. Thus, this model might need further investigation itself.

6.1.3 Contact Specifications

The contacts play an important role in this work. That's why the contact specifications are also discussed.

Used Friction Values

The friction values, which are used in this work, are adjusted amounts of the literature and the experience of the DYNAmore support. But it is stated, that the friction and damping has a large influence on the dummy behaviour [62]. Therefore, the parameters need to fit the used material. Thus, the friction of the protective clothing with the seat and the fairing, the friction of the leather gloves with the handlebar and the friction of the boot sole with the footrest have to be determined. The coefficient for PTFE, the Gore-Tex material, is defined as $\mu_{gore} = 0.09$, but the value for the PTFE friction on the motorcycle material can differ [47]. Therefore, further investigations and research have to be done.

Used Tiebreak Value

The implementation of the tiebreak contact also gives occasion for discussion.

The contact definition isn't initially thought for a holding force. Actually, with this contact the release of sticking can be realized in a good way. If the force and the area of the combined parts are known, the necessary failure stress can be calculated. Though it wasn't possible to measure the force which was acting on the hands within a crash test, the parameters are set to empirical values.

In this work, the holding of the dummy hands to the handlebar was recreated. Therefore, it was tried to reproduce the behaviour of the gaffer tape in the crash tests. This does not reflect the behaviour of the real accidents.

For crash simulations which are comparable to the reality, the grip force of a motorcyclist has to be implemented. However, this might be difficult, because many different factors are playing a role and may distribute the actual behaviour. The reaction time of the rider is important and also the muscle strength defines the point of release, just to name a few. For this purpose a whole study could be made, wherein the holding force or stress would be measured and analysed for different riding conditions.

In the literature, studies to the braking behaviour of motorcyclist can be found. Savino et al. [70] researched the parameter of an Autonomous Braking System (AEB). Thereby, the rider didn't loose control in unaware situations with a maximum deceleration of $2.5 \frac{m}{s^2}$ by the AEB. With a pre-warning of 0.2 s before crash, the possible deceleration could be increased to $4.0 \frac{m}{s^2}$ [70]. In other studies the deceleration for the AEB was assumed to be 0.35 g, without loosing the grip at the handles.

There are also publications on the values of the maximal produced hand force of the human available. Thus, the maximum force of the hand is stated with 488 N [54] or 419.67 N [48]. The parameters ($NFLS = 0.05 \frac{kN}{mm^2}$ and $SFLS = 0.0035 \frac{kN}{mm^2}$) set in the tiebreak contact have a maximum tied area of $733 mm^2$. Thus, it sets the failure forces to 36.65 kN in normal direction and to 2.57 kN for shear loads.

The comparison between the gaffer tape specifications ($4.6 \cdot 10^{-6} \frac{kN}{mm^2}$) and the tiebreak parameters, showed that the parameters are more than 100 times greater. Also comparing the measured hand force (488 N) and the calculated tiebreak force lead only to an accordance of less than 20 %. In conclusion, it can be said, that the empirical tested parameters aren't correlating to any literature value.

But in this work, the aim was to rebuilt the behaviour of the dummy within a crash test. The simulations with these tiebreak failure values are reflecting the dummy behaviour of the experimental crash tests in a good way.

6.2 Validation Aspects

In this section the position, kinematics and load of the dummy are regarded with the aspect of validity. Therefore, the results are considered and discussed. The gained knowledge and the fitting postures and motions are mentioned as well as the challenges and disadvantages of the validation. Furthermore some improvement suggestions are listed.

6.2.1 Position

It was established, that the position of the dummy has a great influence on its behaviour. Also the kinematics and load are depending on the position of the dummy model. Therefore, the right position of the dummy is decisive for the results. In this work, the dummy was positioned in a way, that was approaching the reference position, but also fits the motorcycle model and the crash test scenarios. After the gravity simulation, the position wasn't symmetric anymore, this posture correlated more to the mirrored reference picture. Also the leg position and the foot angle observed from a side view, correlate more with the real dummy.

For a more precise positioning and a better validation, pictures with a normed perspective would be helpful. Also markers placed on significant points, like the joints could improve the positioning process.

6.2.2 Kinematics and Load

Since kinematics and load depend on each other, they are discussed together.

In the analysis of the animation kinematics, the differences were small. Some postures were different, but the behaviour after the crash was similar.

The load validation showed differences in the dimension and course of the signals. But in total, the behaviour of the signals was related. However, the oscillations in z-direction are disturbing the signal process. To analyse the reasons, the neck has to be regarded more precise. The boundaries of the injury criteria were kept for all crash scenarios.

Besides the position of the dummy, also the motorcycle position is important for the results. The angle of impact has an influence on the load signals.

For a better validation of the kinematics and load, more crash tests with the same conditions are needed. Since every crash is different, also the results are varying. To gain a valid model for different crash conditions, the reference signals need to represent the average behaviour. In the real crash tests, the dummy was wearing protection clothes. Thereby, the model has more weight and also the kinematics might be influenced. Moreover, the dummy was wearing a helmet. This might damp the loads on the head and neck. By wearing a helmet, the risk of suffering injuries on the head and neck is reduced [34]. Therefore, the load signals of the experimental crash tests aren't directly comparable to the simulation data.

More investigations are necessary, to call the model valid for further research.

7 Conclusion and Outlook

By positioning the Hybrid III FE dummy model on the KTM 125 Duke motorcycle FE model, crash simulations considering the dummy kinematics and loads were realized. Real crash tests were rebuilt. They serve as a reference for the positioning and validation of the dummy in this work.

First of all, the two finite element models, were combined into one model. Therefore, the dummy angles were adjusted to reflect the experimental crash tests and to fit on the motorcycle in a seating position. Additionally, the contacts between the dummy and the motorcycle were implemented. An extra investigation was made for the holding contact of the dummy hands to the motorcycle handlebar, because the grip behaviour differed in the experiment depending on the velocity. With a certain deceleration, the hand was released from the handlebar. For the realization of this contact behaviour a tiebreak contact definition was used.

With the defined posture, the gravity simulation was calculated. Thereby, the equilibrium state was aimed at. The resultant position and displacements of the dummy and the motorcycle were saved for further simulations. However, because of numerical instabilities and extraordinary dummy behaviour, finding the right position for further investigations was challenging. The positions before and after the gravity simulation were validated by comparing them with the reference specifications and pictures.

The crash simulations were made with the pre-positioned models. The motorcycle was driven with three different velocities frontal against a wall. Afterwards, the results of the crash simulations were validated. On the one hand, the kinematics of the simulation was compared to the video data of the experiment. The dummy kinematics was correlating to the reference for all three velocities. Also the contact behaviour of the hands was rebuilt analogous to the experiment. By simulating the different crash scenarios, the contact failure parameters for the dummy hands were adapted. The load signals of the dummy head and neck were validated with the experimental signals and evaluated for the injury criteria. Hence, it can be said, that the courses of the loads were qualitatively the same, since they were fitting mostly and were reflecting the crash test scenarios. However, in some cases the dimensions and the maxima of the signals were not quantitatively similar. Moreover, the FE dummy in the simulation was moving more than the dummy in the real crash tests. Especially in z-direction, there was more motion measured in the simulation than in the experimental data. The injury criteria could be kept for every scenario, load and direction. Nevertheless, the simulation load data was comparable to the experimental data as well as the injury criteria, but further investigations are necessary to call the model valid.

In summary, the motorcycle crash scenarios with the included dummy model in the FE simulation, rebuilt the crash tests recorded by the DEKRA in a good way.

To improve the simulation results and the validation, more research and analysis is required. For a better validation, more crash tests with the same conditions are necessary. Using the mean data and mean position conditions as reference might improve the initial models and values as well as the validation results of the simulation.

Furthermore, the sensors from the BHCS, which were used in the reference tests on the dummy's wrists, chest and on the helmet, could be considered. Thereby, more produced

signals of the FE simulation could be compared to the experimental tests and by that the validation of the FE model could be extended.

The addition of a helmet and protective clothing to the dummy model could further optimize the model. Thereby, the loads on the head and neck are damped and especially the bending of the neck is constrained. Modifying the dummy head and neck is also a possibility to enhance the simulation results. Moreover, simulations with the advanced dummy for motorcycle crashes, the MATD, should be considered to gain more realistic signals.

Another topic are further investigations on the motorcycle model. In this work, the focus was laid on the behaviour and validation of the dummy. But also the motorcycle model has to be validated and the kinematics have to be improved.

Nevertheless, the model can be further improved and validated and then it can be used for more simulations. Additionally, other crash conditions and scenarios could be tested, like different velocities, impact angles or crash objects. It is also possible to use the improved model to research safety features. For this, airbags, seatbelts or other parts could be added.

A Appendix I: Extended Validation

Position Validation right side



Figure A.2: Motorcycle and Dummy models before the gravity simulation (0 ms) with reference lines, right side.

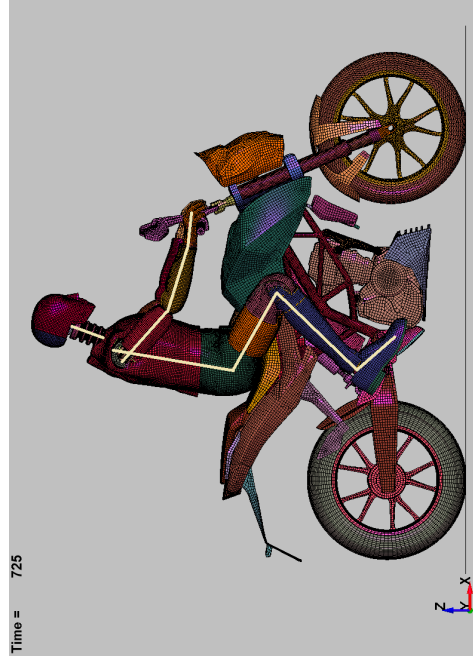


Figure A.3: Motorcycle and Dummy models after the gravity simulation (725 ms) with reference lines, right side.

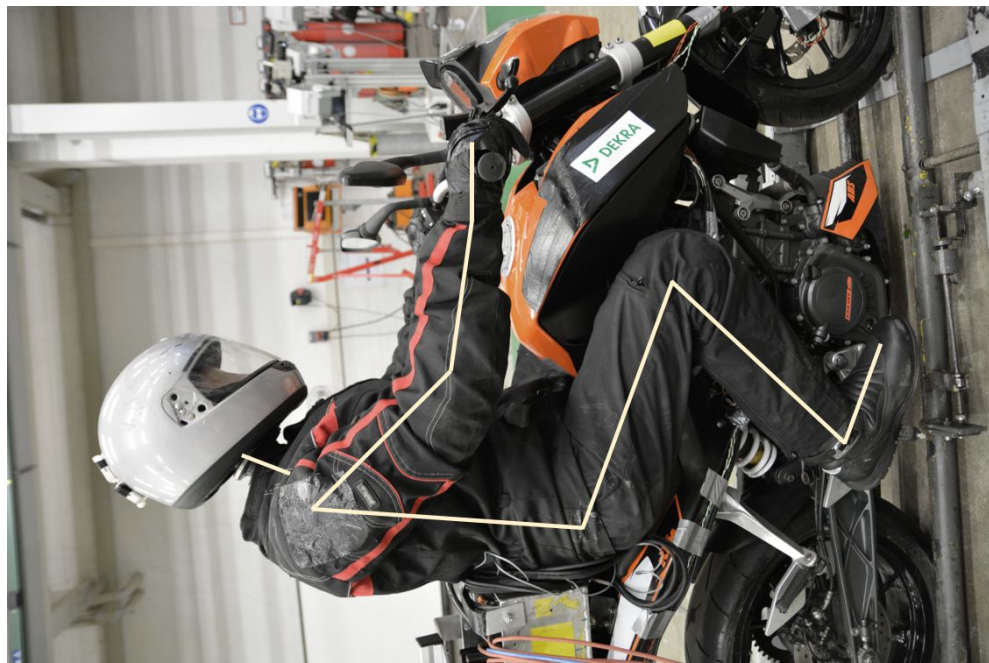


Figure A.1: Reference position of the dummy with lines, right side.

Bibliography

- [1] Bacchetti, A. & Maltha, J.: MADYMO: a general purpose mathematical dynamical model for crash victim simulation. *Delft, Research Institute for Road Vehicles IW TNO/Voorburg, SWOV Institute for Road Safety Research, 1978, 72 p., fig., graph., tab., ref.; Rapport No. 753012-C 72* (1978).
- [2] Bala, S.: Tiebreak Contact in LS-DYNA (2007), URL <https://www.d3view.com/2007/09/tiebreak-contact-in-ls-dyna/>.
- [3] Bala, S.: H-point (2018), URL <https://en.wikipedia.org/wiki/H-point>.
- [4] Barbani, D.; Baldanzini, N. & Pierini, M.: Development and Validation of an FE Model for Motorcycle–Car Crash Test Simulations. *International Journal of Crashworthiness* **19** (2014), 244–263.
- [5] BETA CAE Systems International AG: Dummy Positioning and Restraining. *ANSA version 13.2.1 User's Guide* (2011).
- [6] Blausen Medical: Layers Covering the Brain (2014), URL https://commons.wikimedia.org/wiki/File:Blausen_0110_BrainLayers.png.
- [7] Bulla, M.: Latest Development of the GHBMC Human Body Model in RADIOSS. *5th International Symposium: Human Modeling and Simulation in Automotive Engineering* (2014).
- [8] carhs GmbH: cahrs: Empowering Engineers (2017), URL <https://www.carhs.de>.
- [9] Conrad Electronics: Bühnen-Klebeband Advance AT 170 Gaffer (2016), URL https://www.conrad.de/de/buehnen-klebeband-advance-at-170-gaffer-1268290.html?WT.mc_id=google_pla&WT.srch=1&ef_id=WpgD9gAABQm8rhpj:20180301134526:s&gclid=EAIAIQobChMI2_GjjqHL2QIVU5kbCh0mbgd3EAYYASABEgLPRvD_BwE&hk=SEM&insert_kz=VQ&s_kwcid=AL!222!3!231682502312!!!g!!
- [10] crashtest.org: Vehicle Safety and Accident Prevention: Crash Test (), URL <http://www.crashtest.org/>.
- [11] DAIMLER AG: Tough Test. The Technology Centre for Vehicle Safety in Sindelfingen (), URL <https://www.daimler.com/innovation/specials/crashtest-2.html>.
- [12] Deguchi, M.: Modeling of a Motorcycle for Collision Simulation. *Proceedings of the 18th International Technical Conference on the Enhanced Safety of Vehicle (ESV), Nagoya, Japan* (2003).
- [13] Desai, C.; Sharma, G.; Shah, P.; Ageorges, C.; Mayer, C. & Fressmann, D.: A generic Positioning Tool for Human Body FE Models. *International Research Council on the Biomechanics of Injury (IRCOBI), Dublin, Ireland* (2012).
- [14] Dictionary.com: Anthropometric (2017), URL <https://www.dictionary.com/browse/anthropometric>.

- [15] DIN 33402-2: Ergonomics - human body dimensions - part 2: Values (2005).
- [16] DYNAmore: Human Model (2017), URL https://www.dynamore.de/en/products/models/human?set_language=en.
- [17] DYNAmore: LS-Dyna Einführung (2017), URL <https://www.dynamore.de/de>.
- [18] ECE-R 94: Concerning the adoption of uniform technical prescriptions for wheeled vehicles, equipment and parts which can be fitted and/or be used on wheeled vehicles and the conditions for reciprocal recognition of approvals granted on the basis of these prescriptions (2016).
- [19] Fasanella, E. & Jackson, K.: Best Practices for Crash Modeling and Simulation. *CiteSeer* (2002).
- [20] Flash, T. & Mussa-Ivaldi, F.: Human arm stiffness characteristics during the maintenance of posture. *Experimental Brain Research* **82** (1990).
- [21] FMVSS 208: Federal motor vehicle safety standard no. 208 occupant crash protection (2018), URL https://www.ecfr.gov/cgi-bin/text-idx?node=se49.6.571_1208.
- [22] Formelsammlung und Berechnungsprogramme, Anlagenbau: Reibwerte von verschiedenen Materialien (2017), URL <https://www.schweizer-fn.de/stoff/reibwerte/reibwerte.php>.
- [23] Fressmann, D.: Positioning and Scaling of Human Models using geometric modification Techniques. *6th International Symposium: Human Modeling and Simulation in Automotive Engineering* (2014).
- [24] Frisbee, J.: The Track to Survival. *Air Force Magazine* (1983).
- [25] Ghajari, M.; Deck, C.; Galvanetto, U.; Iannucci, L. & Willinger, R.: Development of numerical Models for the investigation of Motorcyclists Accidents. In *Proceedings of the 7th European LS-DYNA Conference, May*, 2009, pp. 14–15.
- [26] Gilchrist, M.: *IUTAM Symposium on Impact Biomechanics: From Fundamental Insights to Applications*. Solid Mechanics and Its Applications, Springer Netherlands 2005, ISBN 9781402037955.
- [27] Graf, T.: Contact modelling part i-iii. workshop document (2017).
- [28] Gromer, A.: Workshop: Dummy Positioning. *DYNAmore* (2014).
- [29] Haasper, C.; Junge, M.; Ernstberger, A.; Brehme, H.; Hannawald, L.; Langer, C.; Nehmzow, J.; Otte, D.; Sander, U.; Krettek, C. & Zwipp, H.: Die Abbreviated Injury Scale (AIS). *Der Unfallchirurg* **113** (2010), 366–372.
- [30] Haug, E.: Engineering safety analysis via destructive numerical experiments. *Engineering Transactions* **29** (1981), 39–49.
- [31] Haug, E.; Schamhorst, T. & Du Bois, P.: FEM-Crash Simulation of a Frontal Impact (VW-POLO). *Translated From German, VDI Report* **613** (1986), 479–505.
- [32] Hirth, A.; Gromer, A. & Borrrell, T.: DUMMY Positioning Using LS-DYNA Implicit. *10th European LS-DYNA Conference* (2009).

- [33] Humanetics Innovative Solutions: Crash Test Dummies (2017), URL <https://www.humaneticsatd.com>.
- [34] IIHS: Insurance Institute for Highway Safety: Motorcycles (2017), URL www.iihs.org/iihs/topics/t/motorcycles/fatalityfacts/motorcycles.
- [35] IRCOBI: IRCOBI: International Research Council on Biomechanics of Injury (2017), URL <http://ircobi.org>.
- [36] ISO 13232: Motorcycles - test and analysis procedures for research evaluation of rider crash protective devices fitted to motorcycles (2005).
- [37] ISO 13232-3: Motorcycles - test and analysis procedures for research evaluation of rider crash protective devices fitted to motorcycles - motorcyclist anthropometric impact dummy (2005).
- [38] ISO 18571: Road vehicles – objective rating metric for non-ambiguous signals (2014).
- [39] Jackson, K. E.; Fasanella, E. L.; Littell, J. D.; Annett, M. S. & Stimson, C. M.: Simulating the Impact Response of Three Full-scale Crash Tests of Cessna 172 Aircraft. *NASA* (2017).
- [40] JASTI CO. LTD: Antropomorphic Test Devices Dummy (2017), URL <http://www.jasti.co.jp/en/product/dummy.html>.
- [41] Jolivet, E.: Positioning and Personalization Methods and Tools. *PIPER Workshop* (2015).
- [42] Kirsch, J.; May, C.; Lorke, D.; Winkelmann, A.; Schwab, W.; Herrmann, G. & Funk, R.: *Taschenlehrbuch: Anatomie*. Georg Thieme Verlag KG, Stuttgart 2011.
- [43] KISTLER: Saving Lives Day after Day – Vehicle Safety Tests with Kistler (), URL <https://www.kistler.com/en/applications/automotive-research-test/vehicle-safety/>.
- [44] Klein, B.: *FEM: Grundlagen und Anwendungen der Finite-Element-Methode im Maschinen- und Fahrzeugbau*. Springer Fachmedien Wiesbaden 2015.
- [45] Kramer, F.: *Integrale Sicherheit von Kraftfahrzeugen: Biomechanik - Simulation - Sicherheit im Entwicklungsprozess*. Springer Vieweg, Wiesbaden 2013, 4., erw. und korrig. Aufl. edn., URL <http://swbplus.bsz-bw.de/bsz383532205cov.htm>.
- [46] Kummer, B.: *Biomechanik, Form und Funktion des Bewegungsapparats*. Deutscher Ärzte Verlag 2005.
- [47] Kunststoffhandel Merk & Partner GmbH: PTFE Polytetrafluorethylen (2017), URL <http://www.merk-partner.de/index.php/ptfe-polytetrafluorethylen>.
- [48] Lenkeit, J.; Hagoski, B. & Bakker, A.: A study of motorcycle rider braking control behavior. *National Highway Traffic Safety Administration* (2011).
- [49] Lin, M.-P.; Chang, C.-M.; Cho-Hsuan, T.; Tai, C.-H. & Lee, C.-T.: Usage of LSTC_NCAC Hybrid III 50th Dummy in frontal Occupant Simulation. *13th International LS-DYNA Users Conference* (2014).

- [50] Livermode Software Technology Corporation (LSTC): Tutorial 9: Calculate occupant injury criterion. (2012), URL <http://www.lstc.com/lstpp/content/tutorials/9/t9p5.shtml>.
- [51] Livermode Software Technology Corporation (LSTC): LS-DYNA Keyword User's Manual Volume I-III (LS-DYNA R8.0). LSTC (2015).
- [52] LS-DYNA Support: Contact modeling in LS-DYNA (2017), URL <http://www.dynasupport.com/tutorial/ls-dyna-users-guide/contact-modeling-in-ls-dyna>.
- [53] LS-DYNA Support: Mass scaling (2017), URL <http://www.dynasupport.com/howtos/general/mass-scaling>.
- [54] Mathiowetz, V.; Kashman, N.; Volland, G.; Weber, K.; Dowe, M. & Rogers, S.: Grip and Pinch Strength: Normative data for adults. *Archives of physical medicine and rehabilitation* (1985).
- [55] MILLBROOK: State-of-the-art ServoSled facility is the first of its kind in the UK. (), URL <http://www.millbrook.co.uk/services/safety/servosled-crash-test-facilities/>.
- [56] Mohan, P.; Park, C.-K.; Marzougui, D.; Kan, C.-D.; Guha, S.; Maurath, C. & Bhalsod, D.: LSTC/NCAC Dummy Model Development. *11th International LS-Dyna Users Conference* (2010).
- [57] Motorcyvle Specs: KTM 125 Duke (2017), URL http://www.motorcyclespecs.co.za/model/ktm/ktm_125_duke.htm.
- [58] Mukherjee, S.; Chawla, A. & Iyer, S.: Positioning of Motorcyclist Dummies in Crash Simulations. *International Journal of Crashworthiness* **11** (2006), 337–343.
- [59] Mukherjee, S.; Chawla, A.; Mohan, D.; Singh, M.; Sakurai, M. & Tamura, Y.: Motorcycle-Car Side Impact Simulation. *Proc. IRCOBI,(Isle of Man, UK)* (2001).
- [60] Namiki, H.; Nakamura, T. & Iijima, S.: A Computer Simulation for Motorcycle Rider Injury Evaluation in Collision. *HONDA R AND D TECHNICAL REVIEW* **17** (2005), 153.
- [61] NHTSA: National Highway Traffic Safety Administration: Ratings, Biomechanics and Trauma, Motorcycle Safety (), URL <https://www.nhtsa.gov>.
- [62] Nieboer, J.; Wismans, J.; Versmissen, A.; Van Slagmaat, M.; Kurawaki, I. & Ohara, N.: Motorcycle Crash Test Modelling. *SAE Technical Paper* (1993).
- [63] Noureddine, A.; Eskandarian, A. & Digges, K.: Computer Modeling and Validation of a Hybrid III Dummy for Crashworthiness Simulation. *Mathematical and Computer Modelling* **35** (2002), 885 – 893.
- [64] safety Observatory, E. R.: Traffic Safety Basic Facts 2016: Motorcycles and Mopeds. *European Commission Directorate General for Mobility and Transport* (2016).
- [65] pdb: CORA (2017), URL <http://www.pdb-org.com/de/information/18-cora-download.html>.

- [66] Pearlman, M. D.; Viano, D. et al.: Automobile Crash Simulation with the first pregnant Crash Test Dummy. *American Journal of Obstetrics and Gynecology* **175** (1996), 977–981.
- [67] Prasad, P. & Daniel, R.: *A biomechanical analysis of head, neck, and torso injuries to child surrogates due to sudden torso acceleration*. Tech. rep., SAE Technical Paper 1984.
- [68] Richard, H. & Kullmer, G.: *Biomechanik: Grundlagen und Anwendungen auf den menschlichen Bewegungsapparat*. Springer Fachmedien Wiesbaden 2013.
- [69] SAE-J1733: Sign convention for vehicle crash testing (2007).
- [70] Savino, G.; Pierini, M. & Baldanzini, N.: Decision logic of an active braking system for powered two wheelers. *Proceedings of the Institution of Mechanical Engineers, Part D: Journal of Automobile Engineering* **226** (2012), 1026–1036.
- [71] Schmitt, K.; Niederer, P.; Cronin, D.; Muser, M. & Walz, F.: *Trauma-Biomechanik: Einführung in die Biomechanik von Verletzungen*. VDI-Buch, Springer Berlin Heidelberg 2014.
- [72] Schuessler, F.: Dummy Models General Update. *Humanetics Innovative Solutions* (2016).
- [73] Spine-Concept-Sobernheim: Body planes and directional terms (2016), URL <https://www.scoliosis-rehabilitation.com/slika-1/>.
- [74] St Laurent, A.; Szabo, T.; Shewchenko, N. & Newman, J.: Design of a Motorcyclist Anthropometric Test Device. In *proceedings of the Twelfth International Conference on Experimental Safety Vehicles, Göteborg, Sweden, National Highway Traffic Safety Administration, Washington DC*, 1989, pp. 1308–1316.
- [75] TASS International: MADYMO dummy models (2017), URL <https://www.tassinternational.com/madymo-dummy-models>.
- [76] The Stapp Association: Stapp Car Crash Conference (2017), URL <http://www.stapp.org>.
- [77] Walsh, M.J. and Calspan Corporation and United States.: *Sled Test Comparisons Between Three Types of Human Surrogates*. Department of Transportation, National Highway Traffic Safety Administration, Office of Vehicle Structures 1976.
- [78] Wayne State University: Larry Patrick, pioneer auto safety researcher (2006), URL <https://wayne.edu/newsroom/release/2006/05/02/larry-patrick-pioneer-auto-safety-researcher-85-2282>.
- [79] Wiley, K.; Zellner, J.; Laurent, A.; Newman, J.; Szabo, T. & Shewchenko, N.: Motorcycle Accident Simulation Test Dummy. United States Patent (1991).
- [80] Young, W.; Sobhani, A.; Lenné, M. G. & Sarvi, M.: Simulation of Safety: A review of the state of the art in road safety simulation modelling. *Accident Analysis & Prevention* **66** (2014), 89–103.